

**PURDUE UNIVERSITY**  
**GRADUATE SCHOOL**  
**Thesis/Dissertation Acceptance**

This is to certify that the thesis/dissertation prepared

By Smita Pravin Soni

Entitled The Effect of Acyl Chain Unsaturation on Phospholipid Bilayer

For the degree of Doctor of Philosophy

Is approved by the final examining committee:

Stephen R. Wassall

Chair

Ken Ritchie

Horia Petrache

Marvin Kemple

Andrew J. Rader

To the best of my knowledge and as understood by the student in the *Research Integrity and Copyright Disclaimer (Graduate School Form 20)*, this thesis/dissertation adheres to the provisions of Purdue University's "Policy on Integrity in Research" and the use of copyrighted material.

Approved by Major Professor(s): Stephen R. Wassall

Approved by: Ricardo Decca

Head of the Graduate Program

January 22, 2010

Date

**PURDUE UNIVERSITY  
GRADUATE SCHOOL**

**Research Integrity and Copyright Disclaimer**

Title of Thesis/Dissertation:

The Effect of Acyl Chain Unsaturation on Phospholipid Bilayer

For the degree of Doctor of Philosophy

I certify that in the preparation of this thesis, I have observed the provisions of *Purdue University Teaching, Research, and Outreach Policy on Research Misconduct (VIII.3.1)*, October 1, 2008.\*

Further, I certify that this work is free of plagiarism and all materials appearing in this thesis/dissertation have been properly quoted and attributed.

I certify that all copyrighted material incorporated into this thesis/dissertation is in compliance with the United States' copyright law and that I have received written permission from the copyright owners for my use of their work, which is beyond the scope of the law. I agree to indemnify and save harmless Purdue University from any and all claims that may be asserted or that may arise from any copyright violation.

Smita Pravin Soni

Printed Name and Signature of Candidate

01/22/2010

Date (month/day/year)

\*Located at [http://www.purdue.edu/policies/pages/teach\\_res\\_outreach/viii\\_3\\_1.html](http://www.purdue.edu/policies/pages/teach_res_outreach/viii_3_1.html)

THE EFFECT OF ACYL CHAIN UNSATURATION ON PHOSPHOLIPID BILAYER

A Dissertation

Submitted to the Faculty

of

Purdue University

by

Smita Pravin Soni

In Partial Fulfillment of the

Requirements for the Degree

of

Doctor of Philosophy

May 2010

Purdue University

Indianapolis, Indiana

To my parents, Pravin and Shakuntala Soni,  
my godfather, Jayantilal Shah,  
my younger sister and brother,  
but most of all to  
my sister, Rina and brother-in-law, Abdul Mohammed.

## ACKNOWLEDGMENTS

I would like this opportunity to express my heartfelt gratitude and acknowledgement to my advisor Dr. Stephen R. Wassall for his time, expertise as well as for being such a supportive mentor. I am very grateful for all his help towards my achievements. I also wish to extend my thanks to the entire Department of Physics, especially to Dr. Marvin Kemple, Dr. Horia Petrache, Dr. Riccardo Decca, Dr. Gautam Vemuri, and Dr. Andy Gavrin for providing unlimited support, encouragement and guidance throughout my project.

I would also like to acknowledge Dr. William Stillwell not only for his collaboration but also for his constant support and encouragement. I would like to extend my gratitude to Dr. Stephanie Sen for her collaboration. I would also like to acknowledge Dr Scott Feller and Jesse Ward for their help, collaboration and support every step of the way. I'm very grateful to Dr Robert Bittman for without his help some of our work would have been very difficult. Very special thanks to Dr. Bruce Ray, for sharing his vast knowledge and assisting during the execution of my project.

All these years of work would not have been possible without my friends and colleagues. Drs. Alan McCabe and Raza Shaikh helped me out to understand the basic concepts of my work and I'm really thankful for their help and friendship. I would

specially like to thank my best friend and well wisher, Cynthia Wassall, for making me smile and helped getting through rough days. I cannot thank enough to my parents, Pravinkumar Soni and Shakuntala Soni, and my godfather, Jayantilal M. Shan for their love and support. Lastly, but not the least, my elder sister, Rina and brother-in-law, Abdul Nayeem Mohammed, with their help, support and constant encouragement, made the pursuit of my education possible. Without them none of my achievement would have been complete.

## TABLE OF CONTENTS

	Page
LIST OF TABLES .....	viii
LIST OF FIGURES .....	ix
LIST OF ABBREVIATIONS .....	xvi
ABSTRACT .....	xviii
CHAPTER 1: LIPID MEMBRANES .....	1
Membrane structure .....	2
Lipids .....	3
Molecular organization in model membrane .....	5
Membrane phase behavior .....	5
Acyl chain order .....	7
CHAPTER 2: SOLID STATE <sup>2</sup> H NMR OF MEMBRANES .....	18
Basic theory .....	19
Lipid bilayers .....	20
Lineshape analysis .....	22
Moments .....	22
Depacking .....	24

	Page
CHAPTER 3: THE EFFECT OF TRANS UNSATURATION ON MOLECULAR ORGANIZATION IN A PHOSPHOLIPID MEMBRANE .....	35
Experimental procedure .....	38
<sup>2</sup> H NMR spectroscopy .....	39
MD simulation .....	41
Results .....	42
<sup>2</sup> H NMR .....	42
Phase behavior .....	42
Acyl chain order .....	45
MD Simulation .....	47
Acyl chain order .....	47
Discussion .....	49
EA packs better than OA in the gel phase .....	49
EA disorders almost as much as OA in the liquid crystalline phase .....	52
Conclusion .....	58
CHAPTER 4: DOCOSAHEXANOIC ACID ENHANCES SEGREGATION OF LIPIDS BETWEEN RAFT AND NON-RAFT DOMAINS: <sup>2</sup> H-NMR STUDY .....	78
Materials and methods .....	82
<sup>2</sup> H NMR spectroscopy .....	84
Differential scanning calorimetry .....	85
Results .....	86
Phase behavior .....	86



	Page
Acyl chain order.....	93
Discussion.....	95
Segregation into SM-rich and PE-rich nano-sized domains.....	97
PUFA-cholesterol aversion excludes sterol from DHA-containing PE-rich domains.....	101
Conclusion .....	105
CHAPTER 5: CONCLUSIONS .....	127
PUFA .....	127
TFA.....	129
APPENDICES	
Appendix A.....	141
Appendix B.....	143
VITA.....	147

## LIST OF TABLES

Table	Page
3.1 Temperature $T_m$ for the gel to liquid crystalline phase transition determined by moment analysis of $^2\text{H}$ NMR spectra.....	69
3.2 Average order parameter $\bar{S}_{CD}$ calculated from the first moment $M_1$ for the $[^2\text{H}_{35}]18:0$ <i>sn</i> -2 chain in <i>t</i> 18:1- $[^2\text{H}_{35}]18:0\text{PC}$ and <i>c</i> 18:1- $[^2\text{H}_{35}]18:0\text{PC}$ at 45 °C, and the corresponding value calculated from MD simulations. A temperature of 60 °C applies to the value of $\bar{S}_{CD}$ stated for 18:0- $[^2\text{H}_{35}]18:0\text{PC}$ .....	70
4.1 Average order parameters $\bar{S}_{CD}$ derived from $^2\text{H}$ NMR spectra for POPE/PSM* (1:1 mol) and PDPE/PSM* (1:1 mol) in the absence and presence of cholesterol (1:1:1 mol) at 35 °C. Corresponding values for POPE*/egg SM (1:1 mol) and PDPE*/egg SM (1:1 mol) are included for comparison.....	114
5.1 Average order parameter for <i>t</i> $[^2\text{H}_{33}]18:1$ -18:0PC and <i>c</i> $[^2\text{H}_{33}]18:1$ -18:0PC using solid state $^2\text{H}$ NMR and MD simulation data.....	135

## LIST OF FIGURES

Figure	Page
1.1 Lateral view of a biological membrane schematically depicting lipids, cholesterol and protein.....	13
1.2 Examples of different types of lipids found in membranes.a) Phosphatidylcholine (16:0-16:1PC) b) Phosphatidylethanolamine (16:0-16:1PE) c) Sphingomyelin (16:0SM) d) Cholesterol.....	14
1.3 Examples of common headgroups and fatty acid types, stick intersections represents a carbon atom and hydrogen atoms are implicit. a) Glycerophosphocholine, b) Glycerophosphoethanolamine, c) Palmitic (16:0) acid, d) Stearic (18:0) acid, e) Oleic (18:1) acid, f) Docosahexaenoic (22:6) acid. ....	15
1.4 a) The graph showing the chain melting temperature dependence on the acyl chains of the diacylphospholipids. b) Chain melting dependence on the headgroup for 16:0-16:0 PC and PE. c) Degree of unsaturation present in the <i>sn</i> -2 acyl chain's affect on the phase transition temperature. ....	16

Figure	Page
1.5 a) Average order parameter reduced due to increase in degree of unsaturation for 18:0-XPC lipid <sup>1</sup> . b) Order parameter profile for [ <sup>2</sup> H <sub>31</sub> ]16:0-16:0PC (■) at 43 °C and [ <sup>2</sup> H <sub>31</sub> ]16:0-18:1PC (□) at 42 °C.....	17
2.1 Energy levels for a deuterium nucleus showing the perturbation of the Zeeman energy levels by the quadrupolar interaction with the electric field gradient due to a C- <sup>2</sup> H bond. ....	28
2.2 a) Schematic view of a lipid bilayer illustrating the orientation of a C- <sup>2</sup> H bond. ....	29
b) Doublet and quadrupolar splitting observed for a planar membrane.....	29
2.3 <sup>2</sup> H NMR powder pattern: The dashed lines indicate the transitions between $m = -1$ to $0$ and $m = 0$ to $m = 1$ states while the solid line is the sum of the two components.....	30
2.4 <sup>2</sup> H NMR spectra for [ <sup>2</sup> H <sub>31</sub> ]16:0-16:0PC in the a) gel (20 °C) and b) liquid crystalline (45 °C) state.....	31
2.5 A plot of first moment $M_1$ vs. temperature for [ <sup>2</sup> H <sub>31</sub> ]16:0-16:0PC showing the marked distinction in the value of the moment for gel and liquid crystalline states. The mid-point of the discontinuity identifies the chain melting temperature ( $T_m$ ).....	32
2.6 Depaking : A comparison of a) powder pattern vs. b) FFT depaked spectra for [ <sup>2</sup> H <sub>31</sub> ]16:0-16PC at 45 °C illustrating the enhancement in resolution accomplished by depaking.....	33

Figure	Page
2.7	Order parameter profile: A plot of order parameter $S_{CD}$ vs. carbon number for the $[^2H_{31}]16:0$ <i>sn</i> -1 chain in $[^2H_{31}]16:0-16:0PC$ at 45 °C constructed from depaked data (Figure 6b). The carbon positions in the molecule line up with the abscissa of the plot. ....34
3.1	Molecular structure of (a) <i>t</i> 18:1-18:0PC and (b) <i>c</i> 18:1-18:0PC. The dashed lines used in the figure are to emphasize the distinction in configuration between <i>trans</i> and <i>cis</i> double bonds.....71
3.2	$^2H$ NMR spectra for 50 wt % aqueous dispersions in 50 mM Tris (pH 7.5) of (a-d) 18:0- $[^2H_{35}]18:0PC$ , (e-h) <i>t</i> 18:0- $[^2H_{35}]18:0PC$ and (I-l) <i>c</i> 18:1- $[^2H_{35}]18:0PC$ . The spectra were recorded at (a, e and i) - 5 °C, (b, f and j) 20 °C, (c, g and k) 45 °C and (d, h and l) 60 °C. ....72
3.3	Variation of the first moment ( $M_1$ ) as a function of temperature for 18:0- $[^2H_{35}]18:0PC$ ( $\square$ ), <i>t</i> 18:0- $[^2H_{35}]18:0PC$ ( $\bullet$ ) and <i>c</i> 18:1- $[^2H_{35}]18:0PC$ ( $\diamond$ ). $M_1$ is plotted logarithmically for clarity. The values given for the transition temperature $T_m$ in Table 1 are the midpoint of the sharp drop in moment that accompanies chain melting. ....73
3.4	FFT depaked spectra for (a) <i>t</i> 18:1- $[^2H_{35}]18:0PC$ and (b) <i>c</i> 18:1- $[^2H_{35}]18:0PC$ at 45 °C.....74

Figure	Page	
3.5	Order parameter profiles for <i>t</i> 18:1-18:0PC (●) and <i>c</i> 18:1-18:0PC (◇) at 45 °C generated from FFT depaked spectra for (a) the <i>sn</i> -2 chain and from MD simulations for (b) the <i>sn</i> -2 chain and (c) the <i>sn</i> -1 chain. The continuous line included in (a) is the order parameter profile generated from depaked spectra for the <i>sn</i> -2 chain of 18:0-18:0PC at 60 °C.....	75
3.6	Energy minimized structure for (a) <i>t</i> 18:1-18:0PC and (b) <i>c</i> 18:1-18:0PC.....	76
3.7	Normalized population distribution for the orientation of C-H bonds relative to the bilayer normal calculated from MD simulations for (a) the C9 and C10 positions in the <i>sn</i> -1 chain of <i>t</i> 18:1-18:0PC, (b) the C9 and C10 positions in the <i>sn</i> -1 chain of <i>c</i> 18:1-18:0PC and (c) the C9 position in the <i>sn</i> -2 chain. To the right is a schematic representation of the most probable orientation implied by the maximum in each plot. The arrows indicate where rotations occur between carbons C8 and C11 (H atoms are omitted except on C9 and C10 at the double bond). .....	77
4.1	<sup>2</sup> H NMR spectra for a 50 wt% aqueous dispersion in 50 mM Tris buffer (pH 7.5) of POPE/PSM*(1:1 mol) (left panel) and POPE/PSM*/cholesterol (1:1:1 mol) (right panel). Spectra were recorded at (a and e) -23, (b and f) 12, (c and g) 27 and (d and h) 52 °C.....	116

Figure	Page
4.2 $^2\text{H}$ NMR spectra for a 50 wt% aqueous dispersion in 50 mM Tris buffer (pH 7.5) of PDPE/PSM* (1:1 mol) (left panel) and PDPE/PSM*/cholesterol (1:1:1 mol) (right panel). Spectra were recorded at (a and e) -23, (b and f) 12, (c and g) 27 and (d and h) 52 °C.....	118
4.3 Variation of the first moment $M_1$ as a function of temperature for (a) POPE/PSM* (1:1 mol) in the absence (■) and presence (□) of cholesterol (1:1:1 mol), and (b) POPE/PSM* (1:1 mol) in the absence (■) and presence (□) of cholesterol (1:1:1 mol). $M_1$ is plotted logarithmically for clarity and X designates the midpoint of the sharp drop in moment observed when the sterol is absent. DSC cooling scans for (c) POPE/PSM (1:1 mol) and (d) PDPE/PSM (1:1 mol). The scans are inverted so that transitions appear as positive peaks. ....	120
4.4 FFT depaked spectra for POPE/PSM* (1:1 mol) in the absence (a) and presence (b) of cholesterol (1:1:1 mol), and for PDPE/PSM* (1:1 mol) in the absence (c) and presence (d) of cholesterol (1:1:1 mol) at 43 °C. The arrows specify assignment of the C2 position.....	122

Figure	Page
4.5	Order parameter profiles generated from depaked spectra for (a) POPE/PSM* (1:1 mol) in absence (■) and presence (●) of cholesterol (1:1:1 mol), and for (b) PDPE/PSM* (1:1 mol) in absence (■) and presence (●) of cholesterol (1:1:1 mol) at 43 °C. ....124
4.6	A cartoon depiction of DHA vs. OA-induced lateral segregation of lipid molecules in PE/SM/cholesterol (1:1:1 mol) membranes. PE-rich and SM-rich domains coexist in PDPE/SM (top left) and POPE/SM (bottom left) membranes in the absence of sterol. Upon addition of cholesterol to PDPE/SM, the sterol is preferentially taken up into SM-rich domains for which it has high affinity and further displaces DHA for which it has low affinity. The formation of DHA-containing PE-rich/cholesterol-poor non-raft and SM-rich/cholesterol-rich raft domains is the result (top right). Upon addition of cholesterol to POPE/SM, in contrast, the sterol incorporates into OA-containing PE-rich, albeit to less extent, as well as SM-rich domains (bottom right). The tremendous aversion of cholesterol for DHA is not possessed by OA. ....126
5.1	Molecular Structure of $t[{}^2\text{H}_{33}]18:1-18:0\text{PC}$ and $c[{}^2\text{H}_{33}]18:1-18:0\text{PC}$ with the perdeuterated unsaturated chain. ....136



Figure	Page
5.2 $^2\text{H}$ NMR spectra for 50 wt% aqueous dispersions in 50 mM Tris (pH 7.5) of (a-d) $t[{}^2\text{H}_{33}]18:1-18:0\text{PC}$ and (e-h) $c[{}^2\text{H}_{33}]18:1-18:0\text{PC}$ . The spectra were recorded at (a and e) $-5\text{ }^\circ\text{C}$ , (b and f) $5\text{ }^\circ\text{C}$ , (c and g) $20\text{ }^\circ\text{C}$ and (d and e) $45\text{ }^\circ\text{C}$ . .....	137
5.3 Variation of the first moment ( $M_1$ ) as a function of temperature for a) $t[{}^2\text{H}_{33}]18:1-18:0\text{PC}$ (■) and $t18:1-[]^2\text{H}_{35}]18:0\text{PC}$ (□) b) $c[{}^2\text{H}_{33}]18:1-18:0\text{PC}$ (■) and $c18:1-[]^2\text{H}_{35}]18:0\text{PC}$ (□). $M_1$ is plotted logarithmically for clarity. The values given for the transition temperature $T_m$ in Table 1 are the midpoint of the sharp drop in moment that accompanies chain melting. ....	138
5.4 FFT depaked spectra derived from the powder pattern spectra at $45\text{ }^\circ\text{C}$ b) $t[{}^2\text{H}_{33}]18:1-18:0\text{PC}$ and b) $c[{}^2\text{H}_{33}]18:1-18:0\text{PC}$ . ....	139
5.5 $^2\text{H}$ NMR spectra at $45\text{ }^\circ\text{C}$ for a) $t[{}^2\text{H}_{33}]18:1-18:0\text{PC}$ and b) $c[{}^2\text{H}_{33}]18:1-18:0\text{PC}$ . ....	140

## LIST OF ABBREVIATIONS

TFA	<i>trans</i> fatty acid(s)
CFA	<i>cis</i> fatty acid(s)
EA	elaidic acid
OA	oleic acid
SA	stearic acid
PC	phosphatidylcholine(s)
PE	phosphatidylethanolamine(s)
DHA	docosahexaenoic acid
PUFA	polyunsaturated fatty acid(s)
DPH	1, 6-diphenyl hexatriene
AS	anthroyloxy stearic acid
MD	molecular dynamics
CHOL	Cholesterol
Tris	Tris(2-aminoethyl)amine
<i>t</i> 18:1-18:0PC	1-elaidoyl-2-stearoyl- <i>sn</i> -glycero-3-phosphatidylcholine
<i>c</i> 18:1-18:0PC	1-oleoyl-2-stearoyl- <i>sn</i> -glycero-3-phosphatidylcholine
18:0-18:0PC	1, 2-distearoyl- <i>sn</i> -glycero-3-phosphatidylcholine

[ <sup>2</sup> H <sub>31</sub> ]16:0SM	[ <sup>2</sup> H <sub>31</sub> ]-N-palmitoylsphingomyelin
16:0-18:1PE	1-palmitoyl-2-oleoyl- <i>sn</i> -glycero-3-phosphoethanolamine
16:0-22:6PE	1-palmitoyl-2-docosahexaenoyl- <i>sn</i> -glycero-3- phosphoethanolamine
16:0-16:0PC	1, 2-dipalmitoyl- <i>sn</i> -glycero-3-phosphatidylcholine

## ABSTRACT

Soni Smita Pravin, Ph.D., Purdue University, May 2010. The Effect of Acyl Chain Unsaturation on Phospholipid Bilayer. Major Professor: Stephen R. Wassall.

Each biological cell is surrounded by a membrane that consists of many different kinds of lipids. The lipids are mainly composed of phospholipids, which form a fluid bilayer that serves as the platform for the function of membrane bound proteins regulating cellular activity. In the research described in this thesis we employed solid state  $^2\text{H}$  NMR, complemented by DSC (differential scanning calorimetry) and MD (molecular dynamics) simulations, to study the effect of PUFA (polyunsaturated fatty acids) and TFA (*trans* fatty acids) on molecular organization in protein-free model membranes of controlled composition. These two classes of unsaturated fatty acid incorporate into membrane lipids and have, respectively, a beneficial and harmful impact on health. The aim is to gain insight into the molecular origin of this behavior. DHA (docosahexaenoic acid), which with 6 “natural” *cis* double bonds is the most highly unsaturated PUFA found in fish oils, and EA (elaidic acid), which with only a single “unnatural” *trans* double bond is the simplest manmade TFA often found in commercially produced food, were the focus.

$^2\text{H}$  NMR spectra for [ $^2\text{H}_{31}$ ]-N-palmitoylsphingomyelin ( $[^2\text{H}_{31}]16:0\text{SM}$ ) in  $\text{SM}/16:0-22:6\text{PE}$  (1-palmitoyl-2-docosahexaenoylphosphatidylethanolamine)/cholesterol

(1:1:1 mol) mixed membranes were recorded. This system served as our PUFA-containing model. The spectra are consistent with lateral separation into nano-sized (< 20 nm) domains that are SM-rich/cholesterol-rich (raft), characterized by higher chain order, and DHA-rich/cholesterol-poor (non-raft), characterized by lower chain order. The aversion cholesterol has for DHA, as opposed to the affinity cholesterol has for predominantly saturated SM, excludes the sterol from DHA-containing PE-rich domains and DHA from SM-rich/cholesterol-rich domains. It is the formation of highly disordered membrane domains that we hypothesize is responsible, in part, for the diverse health benefits associated with dietary consumption of DHA.

$^2\text{H}$  NMR spectra for 1-elaidoyl-2- $^{[2}\text{H}_{35}]$ stearoylphosphatidylcholine (*t*18:1- $^{[2}\text{H}_{35}]$ 18:0PC) and 1-oleoyl-2- $^{[2}\text{H}_{35}]$ stearoylphosphatidylcholine (*c*18:1- $^{[2}\text{H}_{35}]$ 18:0PC) were recorded to compare membranes with respect to a *trans* vs. *cis* (“natural”) double bond. The spectra indicate that while a *trans* double bond produces a smaller deviation from linear conformation than a *cis* double bond, membrane order is decreased by a comparable amount because the energy barrier to rotation about the C-C single bonds either side of a *trans* or *cis* double bond is reduced. Although EA adopts a conformation somewhat resembling a saturated fatty acid, the TFA is almost as disordered as its *cis* counterpart oleic acid (OA). We speculate that EA could be mistaken for a saturated fatty acid and infiltrate lipid rafts to disrupt the high order therein that is necessary for the function of signaling proteins.

## CHAPTER 1: LIPID MEMBRANES

Membranes enclose each cell and the organelles within a cell (1). They are comprised of a lipid bilayer that is  $<50 \text{ \AA}$  thick in which are embedded and to which are bound a wide variety of proteins. Not only do membranes separate the inside and outside of a cell or organelle but also, via interactions of the constituent molecules, they regulate cellular activity. The complexity of this thin layer is enormous. The relative amounts of lipid and protein vary from membrane to membrane, and there are a vast number of different lipids and proteins that also vary from membrane to membrane. To study membranes we employ protein-free model membranes of controlled lipid content. How specific changes in the molecular structure of a lipid affect membrane organization may then be identified, with the aim of developing a relationship between structural and biological function.

In this thesis we focus on the effects of two kinds of fatty acid – polyunsaturated fatty acids (PUFA) and *trans* fatty acids (TFA) – that incorporate into membrane lipids when consumed. We study the effects of docosahexaenoic acid (DHA), the most highly unsaturated PUFA commonly found in nature containing 6 *cis* double bonds, and elaidic acid (EA), the simplest TFA containing a single *trans* double bond, on molecular organization in model membranes. The motivation is to gain an understanding at the

molecular level and so shed light on the origin of the beneficial and deleterious impact on health of dietary consumption of PUFA (2) and TFA (3), respectively. Chapter 1 will introduce the topic of membranes.

### Membrane structure

Since its conception more than 30 years ago, “the fluid mosaic model” has been the most widely accepted model for the structure of the plasma membrane (4). In this model, the phospholipid bilayer is the basic structural unit (Figure 1.1a). It is formed when phospholipids mix with water due to the amphiphilic nature of these molecules that possess a hydrophilic head group and a pair of hydrophobic fatty acyl chains. Other lipids such as cholesterol are dispersed in the bilayer, while membrane proteins are embedded or bound at the surface. Protein and lipids move laterally throughout a fluid membrane.

The fluid mosaic model has been recently revised. Instead of consisting of a homogenous mixture of lipid and protein, it is now generally accepted that these membrane components are arranged in patches, called domains, of differing and rapidly varying composition (5-8). The purpose of these domains is to provide the local environment necessary for the function of a resident protein. They are formed as a consequence of unequal affinities between different lipid species or between lipids and membrane proteins. The lipid raft is the domain that has received considerable attention. Rafts are liquid ordered ( $l_o$ ) regions enriched in cholesterol and saturated sphingolipid that are 10-200 nm in size floating in a sea of liquid disordered ( $l_d$ ) phospholipids (9-13). When clustered together they serve as a site for the function of essential cell signaling

proteins such as GPI-linked proteins in the outer leaflet of the plasma membrane (14). Non-raft domains that must exist within the surrounding matrix of  $l_d$  phospholipids have received very little attention (15). Domains rich in PUFA-containing phospholipids, in particular, are an example of a non-raft domain in which the highly disordered environment is organizationally the antithesis of rafts (16). A schematic depiction of a membrane where a lipid raft and a PUFA-rich domain exist within a host membrane of bulk (monounsaturated) phospholipids is shown in Figure 1.1b.

### Lipids

Phospholipids are a major lipid component of the membrane (1). They consist of a glycerol backbone to which two hydrophobic fatty acids are attached at the *sn*-1 and *sn*-2 positions and a hydrophilic polar head group containing a phosphate group attached at the *sn*-3 position. Phospholipids differ in the polar (phosphate-containing) groups present and in terms of fatty acid chain length and degree of unsaturation (number of double bonds). Examples of phospholipids are included in Figure 1.2, while Figure 1.3 shows examples of head groups and fatty acids. Phosphatidylcholine (PC) with a phosphorylcholine head group, followed by phosphatidylethanolamine (PE) with a phosphorylethanolamine head group, is the most abundant phospholipid (1). A saturated fatty acid is predominantly esterified at the *sn*-1 position as opposed to the *sn*-2 position where there is usually an unsaturated chain. The fatty acid chains usually contain an even number of carbon atoms, typically between 14 and 24, and up to 6 double bonds. Stearic (SA, 18:0) is a common saturated fatty acid, while oleic (OA, 18:1) acid with a single double bond is the most



often found unsaturated fatty acid. The number of carbon atoms followed by a colon and the number of double bonds is the nomenclature used here, e.g. 18:0 (Figure 1.3a) represents SA containing 18 carbons and no double bond, while 18:1 indicates there are 18 carbons with one double bond in OA.

Sphingolipids derived from the aliphatic amino alcohol sphingosine are another important group of membrane lipids. One of the main types is sphingomyelin (SM) in which the sphingosine backbone is O-linked to a phosphorylcholine head group and amide-linked to a fatty acid. The *sn-1*-like chain of the sphingolipid is non-hydrolyzable and contains a *trans* double bond with the adjacent OH as opposed to the hydrolyzable *sn-1* fatty acid chain of a phospholipid. The *sn-2*-like chain of the sphingolipid that is amide-linked is almost always saturated unlike the unsaturated ester-linked fatty acid at the *sn-2* position of a phospholipid. These structural differences are responsible for cholesterol's preference for association with sphingolipids vs. phospholipids that leads to the formation and stability of lipid rafts. The linear conformation adopted by the predominantly saturated chains in sphingolipids is compatible with close proximity to the rigid steroid moiety of cholesterol and the sphingosine backbone amide hydrogen bonds to both the hydroxyl group of an adjacent sphingolipid and to the hydroxyl group of the sterol (17).

In addition to phospholipids and sphingolipids, cholesterol is a major lipid-constituent that comprises as much as 50 mol% of the total lipid in animal plasma membranes (Figure 1.2c) (18). The long molecular axis of the sterol generally aligns almost perpendicular to the plane of a membrane, with the hydroxyl group on the steroid moiety near the membrane surface and the short side chain at the opposite end of the molecule extending towards the middle of the membrane (19, 20). A primary role of

cholesterol is to modulate molecular organization within membranes and to drive the sorting of lipids into domains on the basis of its differential affinity for different lipids (21).

### Molecular organization in model membrane

Molecular organization in membranes is determined by the molecular structure of the constituent molecules. How PUFA and TFA affect the phase behavior of model membranes and acyl chain order within the interior of the membrane is the focus of the research in this thesis. A general description of the effect of molecular structure on these two properties in model membranes will now be presented. 1,2-dipalmitoylphosphatidylcholine (16:0-16:0PC) with a saturated 16:0 acid chain at both *sn*-1 and -2 positions, which is the most thoroughly characterized model membrane system (22), will serve as point of reference.

### Membrane phase behavior

At low temperature disaturated PC bilayers such as 16:0-16:0PC with identical *sn*-1 and *sn*-2 chains exist in a gel, a.k.a. solid ordered ( $s_o$ ), state. The tightly packed lipid chains are rigid in a linear all-*trans* conformation and the bilayer is solid-like. At high temperature the bilayers adopt a liquid crystalline ( $L_\alpha$ ), a.k.a.  $l_d$ , phase. There are rapid rotations around C-C bonds in the chains and the bilayer is liquid-like. The transition from gel to liquid crystalline phase at which the chains melt occurs at a temperature is designated  $T_m$ . The value of  $T_m$  is largely determined by the strength of inter- and intra-

molecular van der Waals interactions between adjacent lipid molecules in the gel state. PCs with longer acyl chains have greater van der Waals attractive forces, resulting in a more stable bilayer that melts at higher temperature (23). Due to a smaller headgroup and concomitant closer packing within the bilayer, stronger van der Waals forces similarly elevate  $T_m$  in PE relative to PC (24). Graphs illustrating the dependence of  $T_m$  on chain length (Figure 1.4a) and head group (Figure 1.4b) are plotted in Figure 4.

Introducing a double bond into the *sn*-2 chain of PCs substantially lowers the temperature of the chain melting transition (Figure 1.4c) (24). Conformational constraints associated with the rigid double bond create a kink, causing the chain to deviate from a linear conformation. The distortion to chain packing weakens the van der Waals forces and is responsible for a reduction in stability of the gel phase. Adding a second double bond further perturbs chain packing and reduces  $T_m$ , albeit to a smaller extent than the first (25). After two double bonds  $T_m$  is little affected and, as shown in Figure 1.3c, can even rise slightly (25). When cholesterol is inserted into a bilayer,  $T_m$  is reduced and the transition becomes broader because the bulky steroid moiety disrupts chain packing in the gel  $s_o$  state and restricts the reorientation of chains in the liquid crystalline  $l_d$  state (26). The differential between phases is smeared out as the amount of sterol is increased until the transition becomes undetectable and a  $l_o$  phase, characterized by rapid reorientation but high conformational order, is formed. Phase diagrams constructed for homo-acid disaturated and hetero-acid saturated-monounsaturated PCs identify ~25 mol% cholesterol as the concentration at which the  $s_o$  and  $l_d$  states disappear and only the  $l_o$  state is present (26, 27).

## Acyl chain order

In the liquid crystalline phase, which is the physiologically relevant phase, there is a significant degree of molecular motion within the membrane. Rotation about the C-C bonds in the lipid chains and, at a somewhat slower rate, about the long molecular axis that wobbles relative to the bilayer normal produces a fluid membrane. The degree of anisotropy of motion or order of a chain segment within the membrane interior is described by an order parameter  $S_{CD}$  (defined in Chapter 2). Unless geometric issues complicate the situation, order parameters measured for  $C^2H_2$  segments fall in the range  $0 \leq S_{CD} \leq 1/2$  (28). The upper limit represents an all-*trans* chain that is lined up with the bilayer normal undergoing fast axial rotation (most order), while the lower limit represents a chain segment undergoing isotropic motion (most disorder).

A profile of order along the perdeuterated  $[^2H_{31}]$  acid *sn*-1 chain in  $[^2H_{31}]16:0-16:0PC$  bilayers (■) is shown in Figure 1.5a. It consists of a plateau region of slowly decreasing order in the upper portion of the chain (C2-C9) where there is a high probability for *trans* rotational isomeric states that align the chain parallel to the bilayer normal. Order then falls off more rapidly in the lower portion of the chain due to an increase in the probability for *gauche* segments. This shape for the profile is a characteristic of phospholipid membranes (28). It is retained in the profile plotted for  $[^2H_{31}]16:0-18:1PC$  (□) that reveals a double bond in the *sn*-2 chain increases disorder throughout the *sn*-1 chain (Figure 1.5a). A reduced energy barrier to rotation about the single C-C bonds next to the double bond is the origin of the disordering (29). The trend at higher levels of unsaturation is towards greater disorder (Figure 1.5b). The form of

profile, with a slight shortening of the plateau region, is unchanged (30). In the presence of cholesterol, which raises order because the steroid moiety inhibits chain motion, the shape still remains the same (31). Order is uniformly elevated in the plateau region in the upper part of the chain and is progressively less increased in the lower part towards the end of the chain.

## References

1. Gennis, R. B. 1989. Biomembranes. Molecular Structure and Functions, Springer-Verlag, New York.
2. Stillwell, W., and S. R. Wassall. 2003. Docosahexaenoic acid: membrane properties of a unique fatty acid. *Chem Phys Lipids* 126:1-27.
3. Willett, W. C. 2006. Trans fatty acids and cardiovascular disease-epidemiological data. *Atheroscler Suppl* 7:5-8.
4. Singer, S. J., and G. L. Nicolson. 1972. The fluid mosaic model of the structure of cell membranes. *Science* 175:720-731.
5. Edidin, M. 1993. Patches and fences: probing for plasma membrane domains. *J Cell Sci Suppl* 17:165-169.
6. Edidin, M. 2001. Shrinking patches and slippery rafts: scales of domains in the plasma membrane. *Trends Cell Biol* 11:492-496.
7. Edidin, M. 2003. The state of lipid rafts: from model membranes to cells. *Annu Rev Biophys Biomol Struct* 32:257-283.
8. Glaser, M. 1993. Lipid domains in biological membranes. *Curr Opin Struct Bio.* 3:475-481.
9. Simons, K., and E. Ikonen. 1997. Functional rafts in cell membranes. *Nature* 387:569-572.
10. Brown, D., and E. London. 1998. Structure and origin of ordered lipid domains in biological membranes. *J. Membrane Biology* 164:103-114.

11. Brown, D., and E. London. 1997. Structure of detergent-resistant membrane domains: Does phase separation occur in biological membranes? *Biochem Biophys Res Commun* 240:1-7.
12. Ahmed, S. N., D. A. Brown, and E. London. 1997. On the origin of sphingolipid/cholesterol-rich detergent-insoluble cell membranes: physiological concentrations of cholesterol and sphingolipid induce formation of a detergent-insoluble, liquid-ordered lipid phase in model membranes. *Biochemistry* 36:10944-10953.
13. Pike, L. J. 2006. Rafts defined: a report on the Keystone symposium on lipid rafts and cell function. *J. Lipid Res.* 17:1597-1598.
14. Simons, K., and R. Ehehalt. 2002. Cholesterol, lipid rafts, and disease. *J Clin Invest* 110:597-603.
15. Shaikh, S. R., and M. A. Edidin. 2006. Membranes are not just rafts. *Chem Phys Lipids* 144:1-3.
16. Wassall, S. R., and W. Stillwell. 2008. Docosahexaenoic acid domains: the ultimate non-raft membrane domain. *Chem Phys Lipids*.
17. Brown, R. E. 1998. Sphingolipid organization in biomembranes: what physical studies of model membranes reveal. *J Cell Sci* 111 ( Pt 1):1-9.
18. Yeagle, P. L. 1987. *The Membranes of Cells*. Academic Press, Orlando, FL.
19. Léonard, A., C. Escriv, M. Laguerre, E. Pebay-Peyroula, W. Néri, T. Pott, J. Katsaras, and E. J. Dufourc. 2001. Location of cholesterol in DMPC membranes. A comparative study by neutron diffraction and molecular mechanics simulation. *Langmuir* 17:2019-2030.

20. Silvius, J. R. 2003. Role of cholesterol in lipid raft formation: lessons from lipid model systems. *Biochim Biophys Acta* 1610.
21. Marsan, M. P., L. Muller, C. Ramos, F. Rodriguez, F. J. Dufourc, J. Czaplicki, and A. Milon. 1999. Cholesterol orientation and dynamics in dimyristoylphosphatidylcholine bilayers: A solid state deuterium NMR analysis. *Biophys J* 76:351-359.
22. Mills, T. T, Juyang Huang, G. W. Feigenson, and J. F. Nagle. 2009. Effects of cholesterol and unsaturated DOPC lipid on chain packing of saturated gel-phase DPPC bilayers. *Gen. Physiol. Biophys* 28:126-139
23. Koynova, R, and M. Caffrey. 1998. Phases and phase transitions of the phosphatidylcholines *Biochim Biophys Acta* 1376:91-145.
24. Huang, C., and S. Li. 1999. Calorimetric and molecular mechanics studies of the thermotropic phase behavior of membrane phospholipids. *Biochim Biophys Acta* 1422:273-307.
25. Niebylski, C. D., and N. Salem, Jr. 1994. A calorimetric investigation of a series of mixed-chain polyunsaturated phosphatidylcholines: effect of sn-2 chain length and degree of unsaturation. *Biophys J* 67:2387-2393.
26. Vist, M. R., and J. H. Davis. 1990. Phase equilibria of cholesterol/dipalmitoylphosphatidylcholine mixtures: <sup>2</sup>H nuclear magnetic resonance and differential scanning calorimetry. *Biochemistry* 29:451-464.
27. Thewalt, J. L., and M. Bloom. 1992. Phosphatidylcholine: cholesterol phase diagrams. *Biophys J* 63:1176-1181.



28. Seelig, J. 1977. Deuterium magnetic resonance: theory and application to lipid membranes. *Q Rev Biophys* 10:353-418.
29. Soni, S. P., J. A. Ward, S. E. Sen, S. E. Feller, and S. R. Wassall. 2009. Effect of trans unsaturation on molecular organization in a phospholipid membrane. *Biochemistry* 48:11097-11107.
30. Holte, L. L., S. A. Peter, T. M. Sinnwell, and K. Gawrisch. 1995. <sup>2</sup>H nuclear magnetic resonance order parameter profiles suggest a change of molecular shape for phosphatidylcholines containing a polyunsaturated acyl chain. *Biophys J* 68:2396-2403.
31. Shaikh, S. R., V. Cherezov, M. Caffrey, W. Stillwell, and S. R. Wassall. 2003. Interaction of cholesterol with a docosahexaenoic acid-containing phosphatidylethanolamine: trigger for microdomain/raft formation? *Biochemistry* 42:12028-12037.

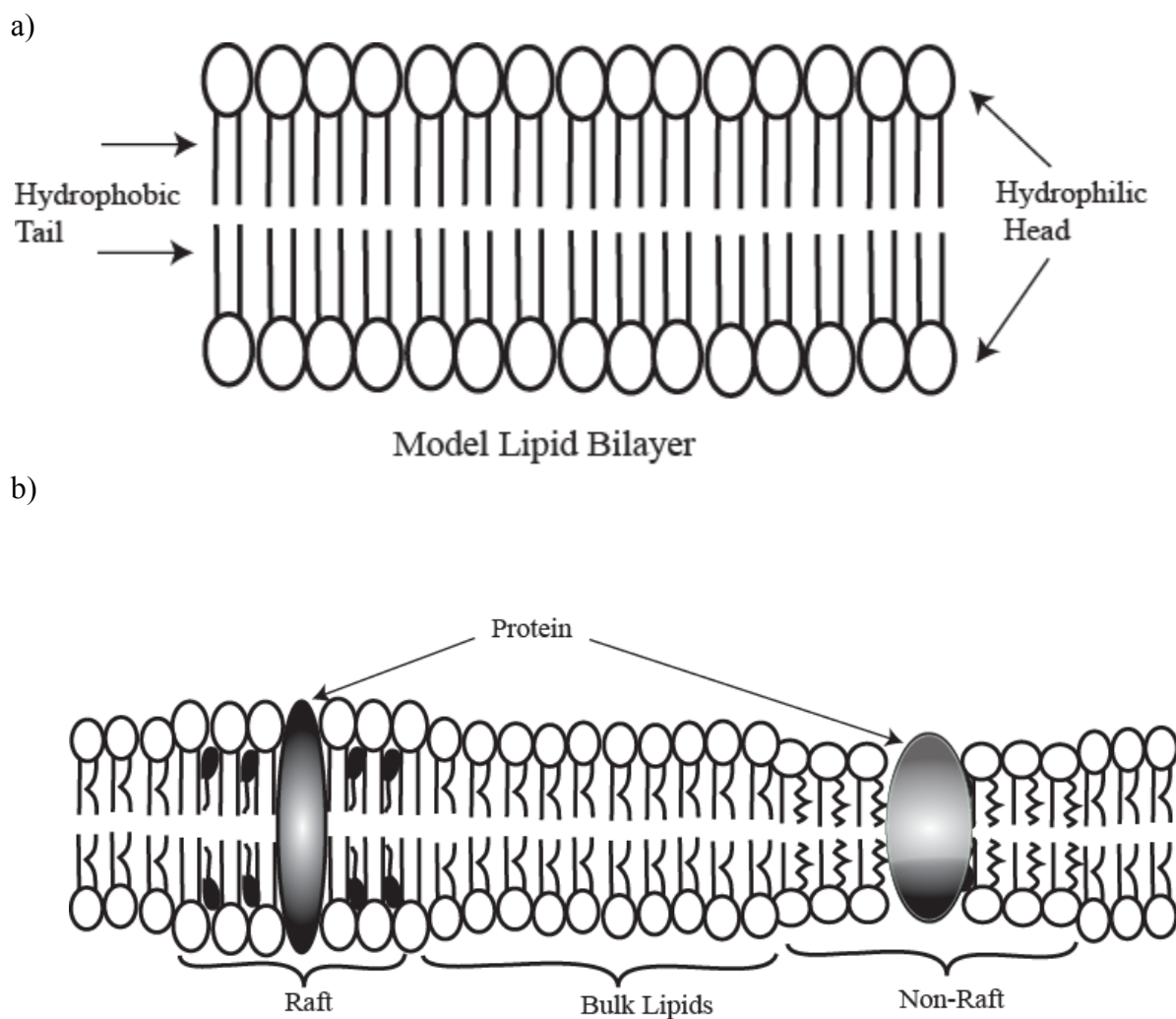


Figure 1.1: Lateral view of a biological membrane schematically depicting lipids, cholesterol and protein arranged in domains

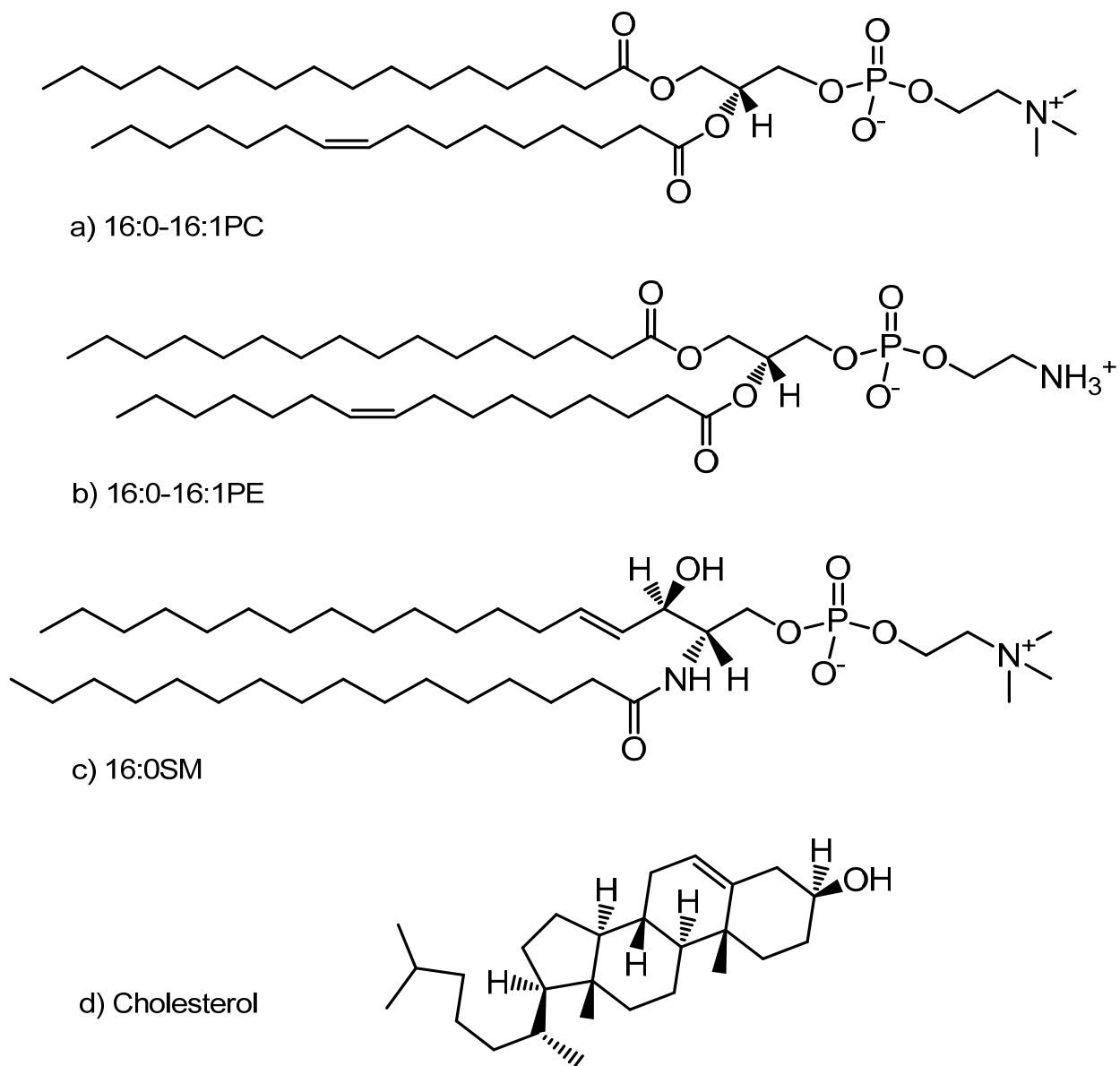


Figure 1.2: Examples of different types of lipids found in membranes. a) Phosphatidylcholine (16:0-16:1PC), b) Phosphatidylethanolamine (16:0-16:1PE), c) Sphingomyelin (16:0SM), d) Cholesterol

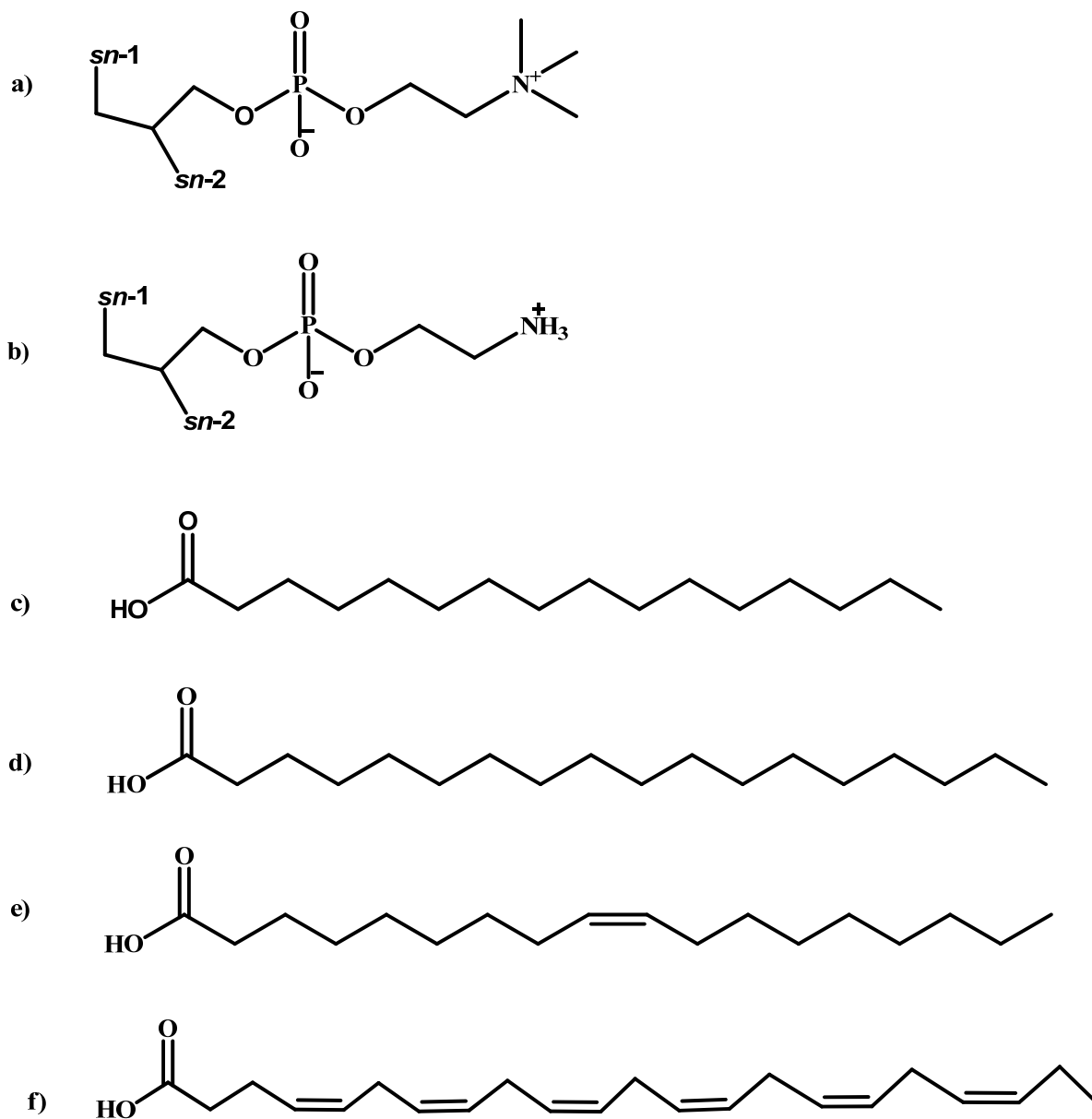


Figure 1.3: Examples of common headgroups and fatty acid types, stick intersections represent a carbon atom and hydrogen atoms are implicit. a) Glycero-Phosphocholine, b) Glycero-Phosphoethanolamine, c) Palmitic acid (16:0), d) Stearic acid (18:0), e) Oleic acid (18:1), f) Docosahexaenoic acid (22:6)

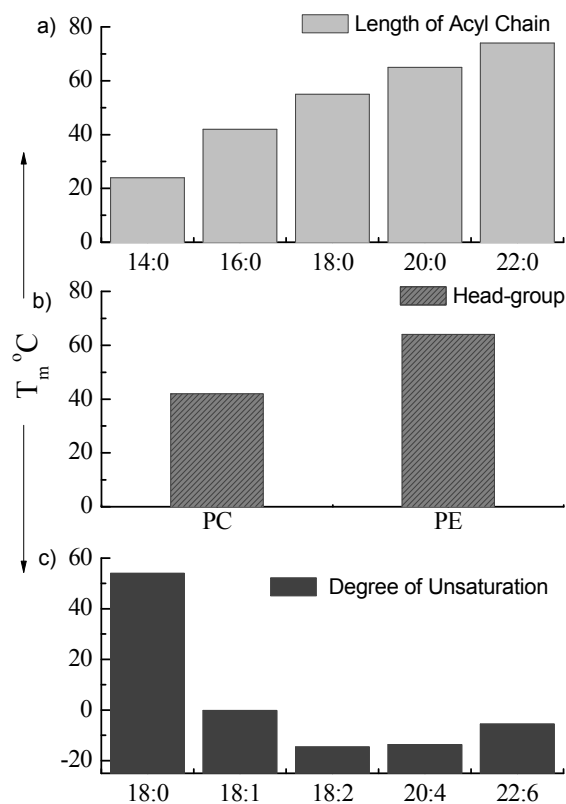


Figure 1.4: a) The graph showing the chain melting temperature dependence on the acyl chains of the diacylphospholipids<sup>1</sup>, b) Chain melting dependence on the headgroup for 16:0-16:0 PC and PE<sup>2</sup>, c) Degree of unsaturation present in the *sn*-2 acyl chain's affect on the phase transition temperature<sup>3</sup>

<sup>1</sup>Caffrey, M. and Koynova, R., 1998, *Biochim. Biophys. Acta* 1376:91-145.

<sup>2</sup>Petrov, A. G., K. Gawrisch, G. Brezesinski, G. Klose, and A. Möps. 1982. *BBA Biomembr.* 690:1-7 for PE and Janiak, M. J., D. M. Small, and G. G. Shipley. 1976. *Biochemistry.* 15:4575-4580 for PC.

<sup>3</sup>Niebylski, C. and Salem, N. 1994. *Biophys J.* 67:2387-2393.

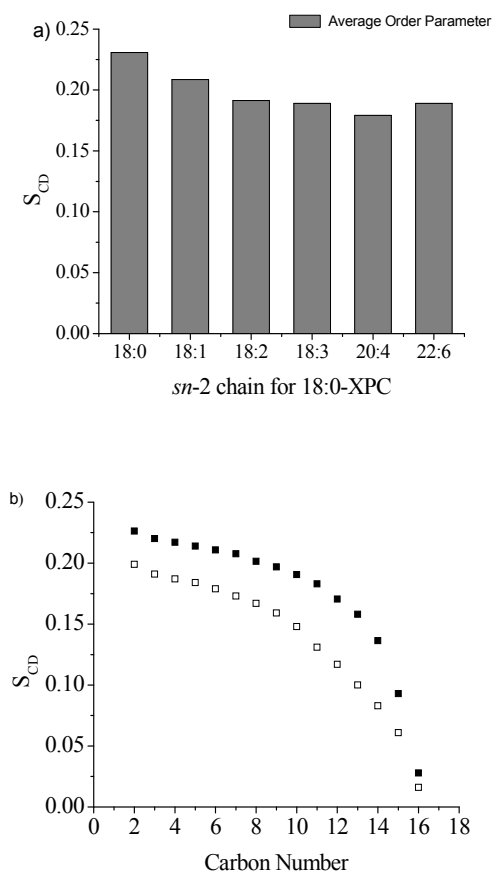


Figure 1.5: a) Average order parameter reduced due to increase in degree of unsaturation for 18:0-XPC lipid<sup>1</sup>, b) Order parameter profile for  $[^2\text{H}_{31}]16:0-16:0\text{PC}$  (■) at 43 °C and  $[^2\text{H}_{31}]16:0-18:1\text{PC}$  (□) at 42 °C

<sup>4</sup>Separovic, F. and Gawrisch, K. 1996. Biophys. J. 71:274-282.

## CHAPTER 2: SOLID STATE $^2\text{H}$ NMR OF MEMBRANES

Solid state deuterium nuclear magnetic resonance ( $^2\text{H}$  NMR) provides an essentially non-invasive approach for investigating molecular organization and dynamics in membranes (1-3). Isotopic substitution of deuterium ( $^2\text{H}$ ) for hydrogen ( $^1\text{H}$ ) in a lipid molecule has minimal effect on a membrane, offering a substantial advantage over techniques that rely on bulky probe moieties such as electron spin resonance (ESR) spin labels and fluorescent labels. Also with selective deuteration, only the specific part of interest in a molecule is observed and problems of assignment associated with nuclei of high natural abundance are avoided. Because molecular motions within a membrane are restricted, the quadrupolar interaction responsible for the spectral lineshape is incompletely motionally averaged and the techniques of solid state NMR are required to collect the resultant broad spectra. In this chapter we will describe in brief the basic theory of  $^2\text{H}$  NMR and then the methods of lineshape analysis we employ to investigate phase behavior and acyl chain order in model membranes containing lipids perdeuterated throughout an acyl chain.

### Basic Theory

Nuclei, dependent upon their structure (number of neutrons and protons), may possess spin angular momentum  $I\hbar$  and an associated magnetic (dipole) moment  $\boldsymbol{\mu}$  that are related to each other according to

$$\boldsymbol{\mu} = \gamma\hbar\mathbf{I}, \quad (1)$$

where  $\gamma$  is the gyromagnetic ratio (4). When placed in an external magnetic field  $\mathbf{B} = B_o\mathbf{k}$  applied in the  $z$  direction, a magnetic dipole will interact with the magnetic field and the interaction potential energy is given by

$$\mathbf{E} = -\boldsymbol{\mu} \cdot \mathbf{B} = -\mu_z B. \quad (2)$$

Here  $\mu_z$  represents the  $z$  component of the dipole moment that is quantized into  $2I + 1$  possible values

$$\mu_z = \gamma\hbar m, \quad (3)$$

defined by  $m = -I, -I + 1, \dots, I - 1, I$ . The previously degenerate energy states of the nucleus are, thus, split (Zeeman effect) into  $2I + 1$  equally spaced energy levels

$$E_m = -\gamma\hbar B_o m \quad (4)$$

separated by

$$\Delta E = \gamma\hbar B_o \quad (5)$$

Transitions between these energy levels ( $\Delta m = \pm 1$ ) are induced when an oscillating magnetic field  $\mathbf{B}_1$  with angular frequency  $\omega_o$  satisfying the resonance (Larmor) condition

$$\omega_o = \gamma B_o \quad (6)$$

is applied perpendicular to the static field  $\mathbf{B}_o$ .



The deuterium nucleus has a spin of  $I = 1$ . The 3 Zeeman energy levels produced by interaction with a static magnetic field are perturbed because the nucleus has a quadrupole moment due to its non-spherical charge distribution that interacts with an electric field environment having less than cubic symmetry (Figure 2.1) (4). When bonded to a carbon, a deuterium is situated in an electric field gradient that is axially symmetric about the bond and the spectrum observed in the static case consists of a doublet separated by the quadrupolar splitting

$$\Delta\nu_Q(\theta') = \frac{3}{4} \left( \frac{e^2qQ}{h} \right) (3\cos^2\theta' - 1) \quad (7)$$

where  $\theta'$  is the angle between the C-<sup>2</sup>H bond (principal axis of the electric field gradient) and  $\mathbf{B}_0$ , and  $\left( \frac{e^2qQ}{h} \right) = 167 \text{ kHz}$  is  $\left( \frac{e^2qQ}{h} \right)$  the static quadrupolar coupling constant (1). For deuterons undergoing rapid reorientation, the angular dependent term  $(3\cos^2\theta' - 1)$  in eq. 7 is averaged over the angular fluctuations appropriate to the motion involved and the quadrupolar splitting is reduced. Thus, while random isotropic motion averages the splitting to zero in a liquid, the averaging is incomplete in lipid bilayers where molecular motion is restricted and a residual splitting characteristic of the anisotropy of the motion remains.

### Lipid Bilayers

The motion of lipid chains in a liquid crystalline membrane is axially symmetric about the normal to the bilayer surface and eq. 7 may be rewritten

$$\Delta\nu_Q(\theta) = \frac{3}{2} \left( \frac{e^2qQ}{h} \right) \frac{1}{2} (3\cos^2\beta - 1) \frac{1}{2} (3\cos^2\theta - 1) \quad (8)$$

for a deuterated chain segment (1). Here  $\theta$  is the angle the bilayer normal makes with the magnetic field,  $\beta$  is the time dependent angle between the C-<sup>2</sup>H bond and the bilayer normal, and the angular brackets represent a time average (Figure 2.2). The time averaged part represents the angular fluctuation undergone by the C-<sup>2</sup>H bond vector with respect to the bilayer normal and corresponds to the order parameter

$$S_{CD} = \frac{1}{2} \langle 3\cos^2\beta - 1 \rangle \quad (9)$$

that is employed to characterize molecular organization within membranes (1-3). For C-<sup>2</sup>H bonds in a saturated lipid chain,  $S_{CD}$  typically takes values in the range

$$0 \leq |S_{CD}| \leq 0.5 \quad (10)$$

The lower limit represents random isotropic motion where, due to rotations about C-C bonds in the chain, a C-<sup>2</sup>H bond vector samples all orientations on the <sup>2</sup>H NMR timescale ( $10^{-5}$  s). The upper limit represents the opposite extreme in which the chain is rigid and undergoes axial rotation in an all-*trans* configuration, as result of which the orientation of a C-<sup>2</sup>H bond vector relative to the bilayer normal is fixed at  $\beta = 90^\circ$ .

Unless aligned in some manner such as between glass plates, lipid bilayer samples consist of randomly oriented bilayers. The spectrum is a superposition of doublets from bilayers at all orientations, each of which is scaled in intensity in accordance with its probability ( $p(\theta)d\theta = \sin\theta d\theta$ ) (1). Two peaks separated by

$$\Delta\nu_r = \frac{3}{4} \left( \frac{e^2 q Q}{h} \right) |S_{CD}| \quad (11)$$

that correspond to the most probable orientation ( $\theta = 90^\circ$ ) dominate the resultant powder pattern (Figure 2.3).

## Lineshape Analysis

In our experiments, the samples were prepared from phosphatidylcholine (PC) and sphingomyelin (SM) perdeuterated throughout, respectively, the *sn*-1 or *sn*-2 chain and amide-linked (*sn*-2-like) chain. The resultant spectra are a superposition of powder patterns from all deuterated positions along the chain (Figure 2.4). Although more complex in shape than for a selectively deuterated lipid, they may be analyzed to investigate phase behavior and chain order. That details of order for the entire chain can be obtained from a single spectrum is a clear advantage over the large number of experiments necessary using selectivity deuterated lipids.

### Moments

Figure 2.4 shows spectra for a sample prepared from a PC with a perdeuterated chain. They are representative of spectra observed in the gel (lower temperature, Figure 2.4a) and liquid crystalline (higher temperature, Figure 2.4b) phase. The gel-state spectrum is relatively featureless with edges at  $\pm 63$  kHz and a central pair of peaks split by  $\sim 12$  kHz. Slow axial rotation of chains that are rigid in a largely all-trans configuration is responsible. In contrast, the liquid crystalline-state spectrum is much narrower and individual pairs of peaks appear within the spectrum because the chains are melted and there is rapid rotation about the C-C bonds. It is a superposition of powder patterns of the form shown in Figure 2.3. Methylenes with similar order in the upper portion of the chain produce sharp edges at  $\sim \pm 15$  kHz, while less ordered methylenes in the lower part of the

chain give rise to individual peaks within the spectrum and the highly mobile terminal methyl is responsible for the central pair of peaks.

The sensitivity to membrane phase illustrated by the spectra in Figure 2.4 can be used to map membrane phase behavior. Our approach is to use spectral moments to characterize the lineshape (2). The  $n$ th moment  $M_n$  is defined by

$$M_n = \frac{\int_{-\infty}^{+\infty} |\omega^n| f(\omega) d\omega}{\int_{-\infty}^{+\infty} f(\omega) d\omega} \quad (12)$$

Here  $f(\omega)$  is the lineshape as function of frequency  $\omega$  with respect to the central Larmor frequency. In Figure 2.5, the first moment  $M_1$  measured from spectra for  $[^2\text{H}_{31}]16:0-16:0\text{PC}$  is plotted vs. temperature. The gel to liquid crystalline phase transition at which the chains melt is identified by the mid-point in an abrupt drop in the value of  $M_1$  at 39.5 °C. Moments that slowly decrease with increasing temperature characterize the gel ( $M_1 \geq 11 \times 10^4 \text{ s}^{-1}$ ) and liquid crystalline ( $M_1 \leq 5 \times 10^4 \text{ s}^{-1}$ ) phases. The small discontinuity that is apparent at ~34 °C reflects the pretransition between  $L_{\beta'}$  (lamellar) and  $P_{\beta}$  (ripple) states that precedes the main chain melting transition (5, 6).

In the liquid crystalline phase where powder pattern spectra of the form shown in Figure 2.3 superpose from each position in the perdeuterated chain to yield the resultant spectrum (Figure 2.4b), an average order parameter  $\bar{S}_{CD}$  for the entire chain may also be derived from the first moment (2). The moment, which represents the magnitude of the average quadrupolar splitting, equates to  $\bar{S}_{CD}$  with

$$M_1 = \frac{\pi}{\sqrt{3}} \left( \frac{e^2 q Q}{h} \right) \bar{S}_{CD} \quad (13)$$

## Depaking

On yet another level of sophistication of lineshape analysis, depaking enables details of the gradient of order within a bilayer to be obtained from  $^2\text{H}$  NMR data for lipids with a perdeuterated chain (7-12). This numerical procedure calculates a spectrum characteristic of single alignment from powder pattern data, conferring enhanced resolution that greatly simplifies interpretation. It is applicable to spectra governed by axially symmetric second rank tensor interactions that possess a  $P_2(\cos\theta)$  dependence upon orientation, where  $\theta$  is the angle between the symmetry axis and the magnetic field. Such is the case for  $^2\text{H}$  NMR spectra of lipid chains undergoing fast axial rotation about the bilayer normal in the liquid crystalline state, as reflected in eq. 8. Different depaking algorithms have been developed (7-12). FFT depaking that may be implemented with modest modification to standard computer software code is the one employed here (11, 12).

In Figure 2.6 the improvement in resolution achieved by FFT depaking is demonstrated for 1- $[\text{}^2\text{H}_{31}]$ palmitoyl-2-palmitoylphosphatidylcholine ( $[\text{}^2\text{H}_{31}]16:0-16:0\text{PC}$ ). The depaked spectrum (Figure 2.6b) corresponds to the spectrum for a planar membrane with the bilayer normal aligned parallel ( $\theta = 90^\circ$ ) to the magnetic field. Unlike the equivalent powder pattern derived from the same NMR data where the central signal due to the mobile terminal methyl is the only clearly resolved feature in a superposition of powder patterns from the entire perdeuterated chain (Figure 2.6a), an outermost composite doublet and 7 distinct doublets with smaller splitting comprise the depaked spectrum (Figure 2.6b). The outermost composite doublet is attributed to similarly

ordered chain segments in upper part of the chain while the well resolved doublets are attributed to individual chain segments in the lower portion of the chain that have progressively less order. On the assumption that order decreases monotonically along the chain toward the terminal methyl, it is then possible to construct a smoothed profile of order parameter (13) by assigning equal intensity to each methylene segment and rewriting eq. 8 to equate doublet splitting to order parameter via

$$\Delta\nu(\theta) = \frac{3}{2} \left( \frac{e^2 q Q}{h} \right) |S_{CD}| P_2(\cos \theta) \quad (14)$$

The order parameter profile obtained in this manner for the [ $^2\text{H}_{31}$ ]palmitic (16:0) acid *sn*-1 chain in [ $^2\text{H}_{31}$ ]16:0-16:0PC from the depaked spectrum as in Figure 2.6b is plotted in Figure 2.7. With a plateau region of slowly decreasing order in the upper part (C2-C9) of the chain followed by more rapidly decreasing order in the lower part (C10-C16), from one spectrum it reproduces the profile determined with specifically deuterated 16:0-16:0PC in the pioneering work by Seelig that entailed the preparation and observation of multiple samples (1). This signature shape is seen in model membranes and biological membranes (2).

## References

1. Seelig, J. 1977. Deuterium magnetic resonance: theory and application to lipid membranes. *Q Rev Biophys* 10:353-418.
2. Davis, J. H. 1983. The description of membrane lipid conformation, order and dynamics by  $^2\text{H}$ -NMR. *Biochim Biophys Acta* 737:117-171.
3. Brown, M. F. 1996. Membrane structure and dynamics studied with NMR spectroscopy. In *Biological Membranes: A Molecular Perspective from Computation and Experiment*. (Merz, K. M, and Roux, B., Eds) Birkhauser, Boston. 175-252.
4. Andrew, E. R. 1955. *Nuclear Magnetic resonance*. Cambridge University Press, UK.
5. Janiak, M. J., D. M. Small, and G. G. Shipley. 1979. Nature of the thermal pretransition of synthetic phospholipids: dimyristoyl- and dipalmitoyllecithin. *Biochemistry* 15:4575-4580.
6. Wassall, S. R., J. L. Thewalt, L. Wong, H. Gorrissen, and R. J. Cushley. 1986. Deuterium NMR study of the interaction of alpha-tocopherol with a phospholipid model membrane. *Biochemistry* 25:319-326.
7. Bloom, M., J. H. Davis, and A. L. Mackay. 1981. Direct determination of the oriented sample nmr spectrum from the powder spectrum for systems with local axial symmetry. *Chem. Phys. Lett.* 80:198-202.
8. Sternin, E., M. Bloom, and A. L. Mackay. 1983. De-pake-ing of NMR spectra. *J Magn. Reson.* (1969) 55:274-282.

9. Whittall, K., E. Sternin, M. Bloom, and A. MacKay. 1989. Time- and frequency-domain “dePakeing” using inverse theory. *J Magn. Reson* 84:64-71.
10. Schafer, H., B. Madler, and F. Volke. 1995. De-Pake-ing of NMR powder spectra by nonnegative least-squares analysis with Tikhonov regularization. *J Magn. Reson. A* 116:145-149.
11. McCabe, M. A., and S. R. Wassall. 1995. Fast-Fourier-transform dePaking. *J Magn. Reson. B* 106:80-82.
12. McCabe, M. A., and S. R. Wassall. 1997. Rapid deconvolution of NMR powder spectra by weighted fast Fourier transformation. *Solid State Nucl Magn Reson* 10:53-61.
13. Lafleur, M., B. Fine, E. Sternin, P. R. Cullis, and M. Bloom. 1989. Smoothed orientational order profile of lipid bilayers by  $^2\text{H}$ -nuclear magnetic resonance. *Biophys J* 56:1037-1041.



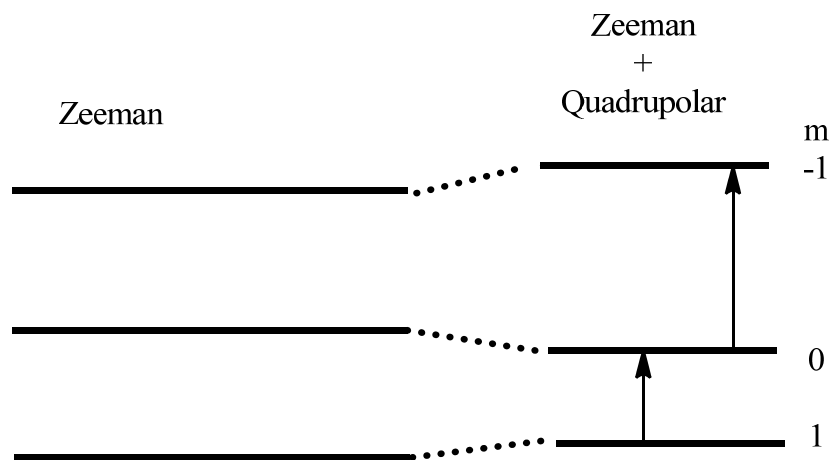


Figure 2.1: Energy levels for a deuterium nucleus showing the perturbation of the Zeeman energy levels by the quadrupolar interaction with the electric field gradient due to a C-<sup>2</sup>H bond

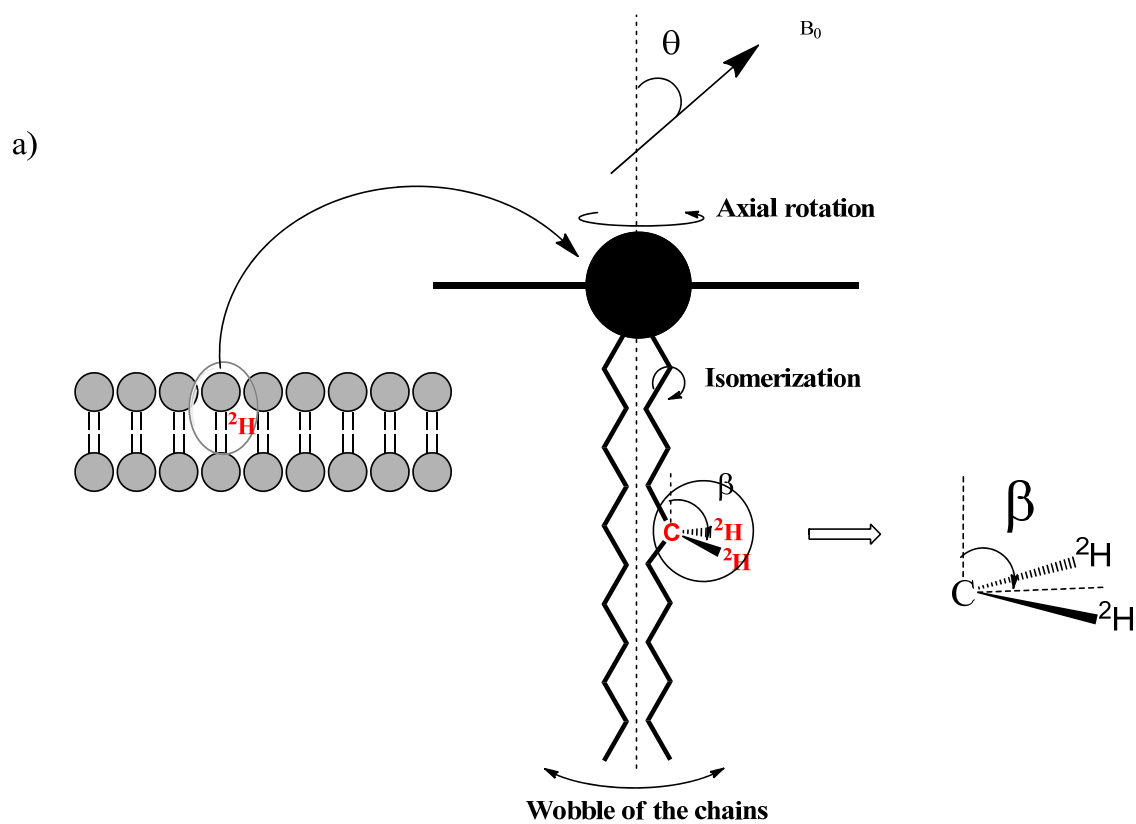


Figure 2.2a: Schematic view of a lipid bilayer illustrating the orientation of a C- $^2H$  bond

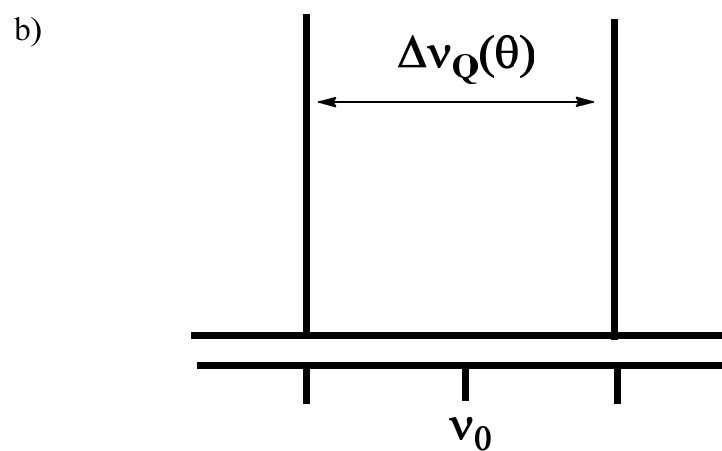


Figure 2.2b: Doublet and quadrupolar splitting observed for a planar membrane

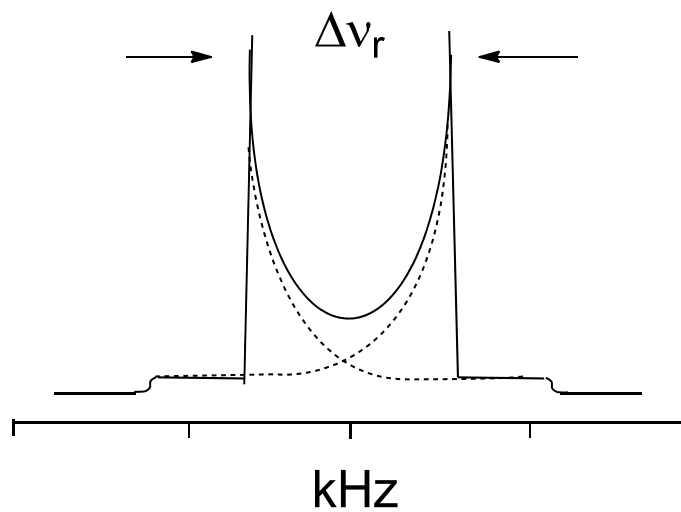


Figure 2.3:  $^2\text{H}$  NMR powder pattern. The dashed lines indicate the transitions between  $m = -1$  to  $0$  and  $m = 0$  to  $1$  states while the solid line is the sum of the two components

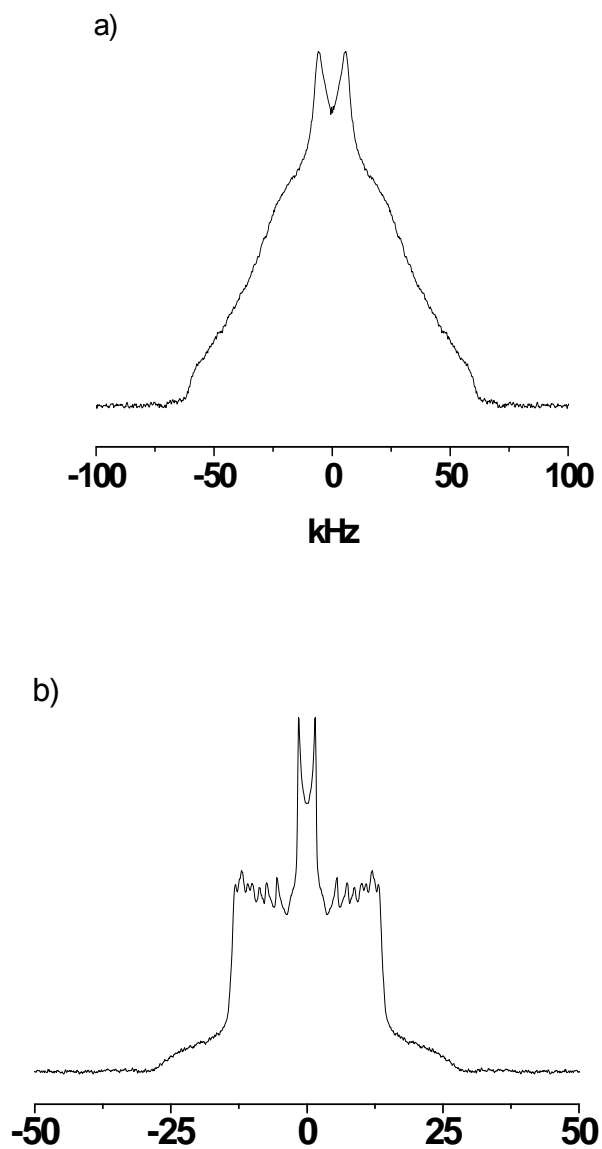


Figure 2.4:  $^2\text{H}$  NMR spectra for  $[^2\text{H}_{31}]16:0-16:0\text{PC}$  in the a) gel ( $20^\circ\text{C}$ ) and b) liquid crystalline ( $45^\circ\text{C}$ ) state

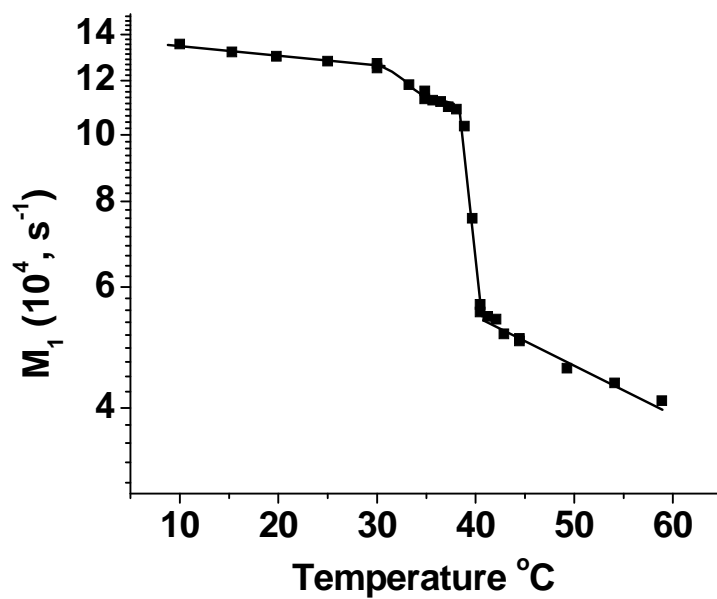


Figure 2.5: A plot of first moment  $M_1$  vs. temperature for  $[^2H_{31}]16:0-16:0PC$  showing the marked distinction in the value of the moment for gel and liquid crystalline states. The mid-point of the discontinuity identifies the chain melting temperature ( $T_m$ )

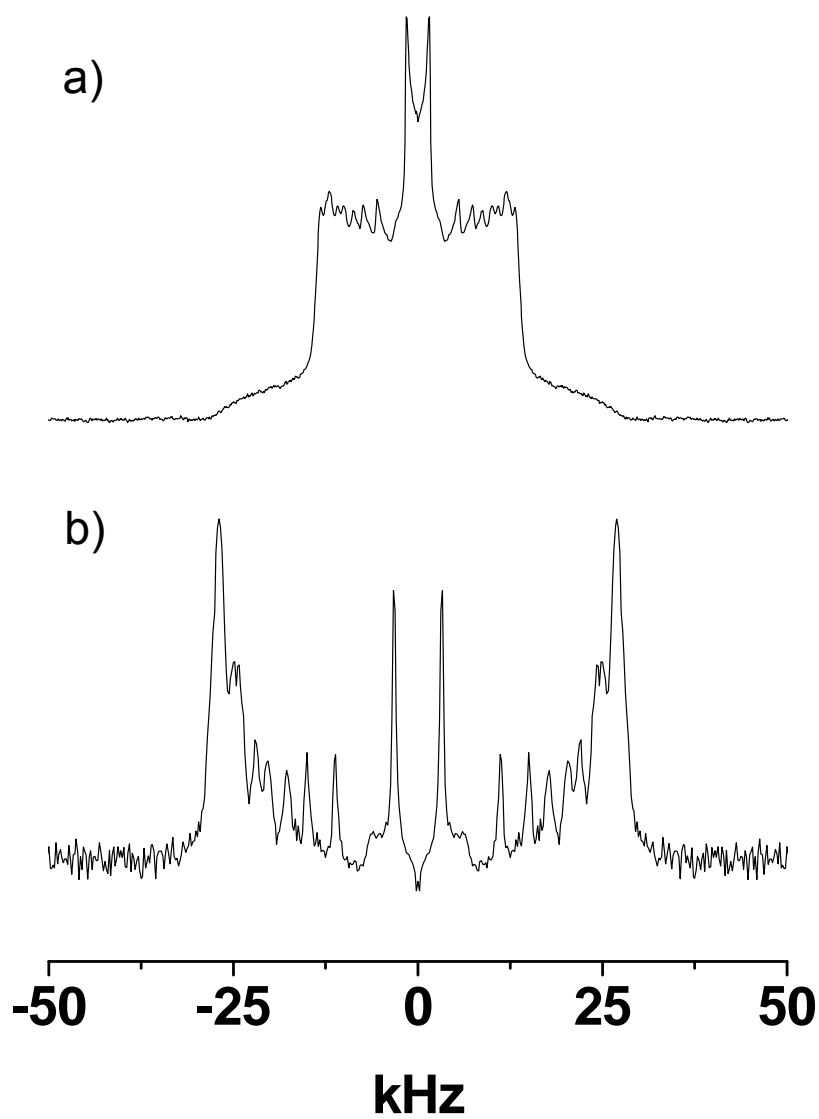


Figure 2.6: Depaking. A comparison of a) powder pattern vs., b) FFT depaked spectra for  $[^2\text{H}_{31}]16:0-16\text{PC}$  at  $45\text{ }^\circ\text{C}$  illustrating the enhancement in resolution accomplished by depaking

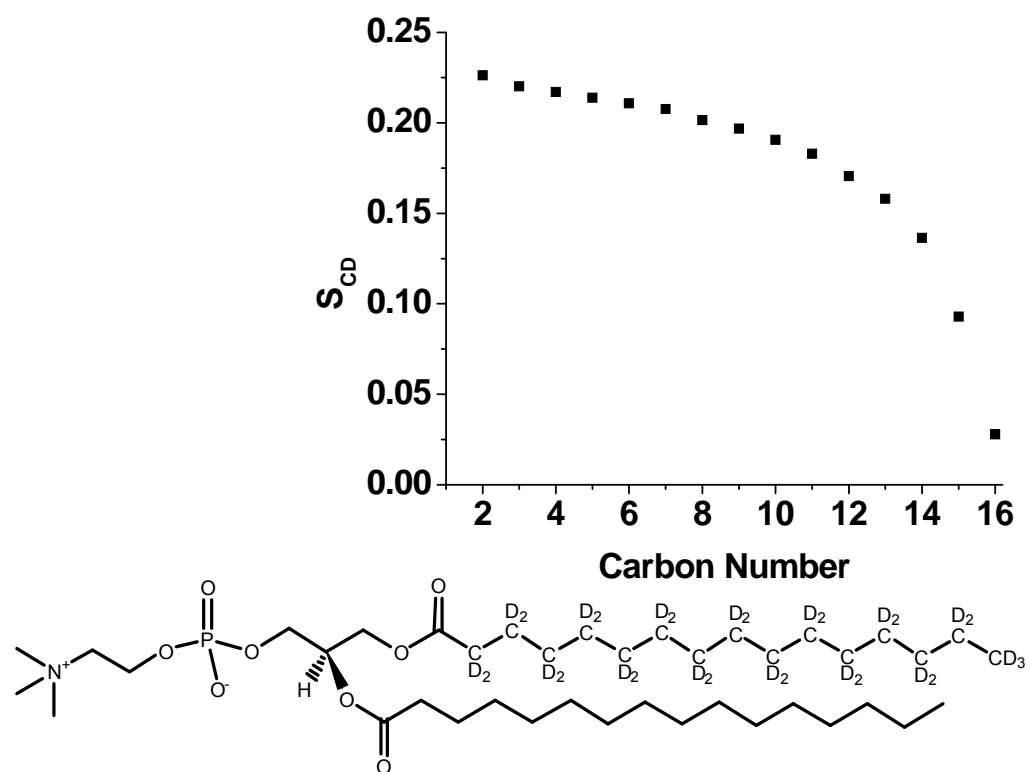


Figure 2.7: Order parameter profile. A plot of order parameter  $S_{CD}$  vs. carbon number for the  $[^2\text{H}_{31}]16:0$  *sn*-1 chain in  $[^2\text{H}_{31}]16:0$ - $16:0\text{PC}$  at  $45^\circ\text{C}$  constructed from depaked data (Figure 2.6b). The carbon positions in the molecule line up with the abscissa of the plot.

### CHAPTER 3: THE EFFECT OF *TRANS* UNSATURATION ON MOLECULAR ORGANIZATION IN A PHOSPHOLIPID MEMBRANE

*Trans* fatty acids (TFA) produced during the partial hydrogenation of vegetable oils are a class of unsaturated fatty acid currently attracting a great deal of attention (1, 2). These “manmade” fatty acids that have become an insidious component in contemporary nutrition (3, 4) adversely affect health such as increasing the risk for coronary heart disease (4, 5), developing diabetes (6), and colorectal and other cancers (7, 8) by a mechanism that remains to be established. They possess one or more *trans* double bonds that place the two hydrogen atoms on the opposite side of the double bond, instead of on the same side as occurs in physiologically prevalent *cis* double bonds (Figure 3.1). This apparently subtle modification in molecular structure causes a reduction in protein function (9) and induces abnormal morphology (10) in membranes when TFA-containing lipids replace their *cis* counterpart. The implication is that changes in the architecture of plasma membranes following incorporation into phospholipids may contribute to the detrimental impact upon health of dietary TFA (11-13).

Because of the distinction in the geometric disposition of the hydrogen atoms, the torsional states preferred by the single bonds next to a *trans* or *cis* double bond differ markedly (14). The energy minimized structure obtained by gas phase *ab initio*



calculations for elaidic acid (EA, *t*18:1), the simplest TFA with a single *trans* double bond between carbons 9 and 10, deviates much less than oleic acid (OA, *c*18:1), its *cis* counterpart, from the linear configuration adopted by stearic acid (SA, 18:0) that is the corresponding saturated chain (15). Although modeling a free fatty acid oversimplifies the situation in a bilayer, the inference is that a *trans* double bond will pack more favorably than a *cis* double bond resulting in greater stability for the gel-state and a smaller reduction in the temperature  $T_m$  for the chain melting transition. The  $T_m$  values measured for EA-, OA- and SA-containing phosphatidylcholines (PC) support this view (16). To predict the effect of *trans* unsaturation on acyl chain organization in the biologically relevant liquid crystalline phase is less straightforward. There are two contrary schools of thought advocating similarity to saturated and *cis*-unsaturated chains, respectively. On the one hand a *trans* double bond produces a minor discontinuity in the linear conformation adopted by a saturated chain (15). On the other hand, and as for a *cis* double bond (albeit subject to different torsional constraints), rotation about a *trans* double bond is prohibited while the energy barrier to rotation about the immediately adjacent single bonds is reduced relative to a saturated chain (14). Two computer simulations of 1-palmitoyl-2-elaidoylphosphatidylcholine (16:0-*t*18:1PC) that provide the only order profiles reported to date within *trans* unsaturated bilayers do not resolve the issue. Close resemblance to 1,2-dipalmitoylphosphatidylcholine (16:0-16:0PC) was revealed by Langevin dynamics in the one case (17) and to 1-palmitoyl-2-oleoylphosphatidylcholine (16:0-*c*18:1PC) in the other by molecular dynamics (MD) simulation (18). The findings from a sparse collection of experimental studies are equally inconclusive. Steady state fluorescence polarization of DPH (1,6-diphenyl hexatriene)

and AS (anthroyloxy stearic acid) probes indicated that 18:0-*t*18:1PC bilayers are less fluid than 18:0-*c*18:1PC bilayers (16). There is, in contrast, negligible difference between average order parameters  $\bar{S}_{CD}$  derived for the *sn*-1 chain from  $^2\text{H}$  NMR spectra for  $[^2\text{H}_{35}]18:0\text{-}t18:1\text{PC}$  (19) and  $[^2\text{H}_{35}]18:0\text{-}c18:1\text{PC}$  (20).

A study by solid state  $^2\text{H}$  NMR spectroscopy, complemented by atomistic MD calculations, of molecular organization in 1-elaidoyl-2- $[^2\text{H}_{35}]$ stearoylphosphatidylcholine (*t*18:1- $[^2\text{H}_{35}]18:0\text{PC}$ ) bilayers is presented here. This molecule was chosen because EA is highly abundant in partially hydrogenated vegetable oils (PHVO) (4, 21) and, unlike *cis* fatty acids (CFA) that usually incorporate as the *sn*-2 chain (22), preferentially substitutes at the *sn*-1 position normally occupied by a saturated chain (4, 23-25). Perdeuterated  $[^2\text{H}_{35}]18:0$  acid was esterified at the *sn*-2 position to allow essentially non-invasive observation. Comparison was made with 1-oleoyl-2- $[^2\text{H}_{35}]$ stearoylphosphatidylcholine (*c*18:1- $[^2\text{H}_{35}]18:0\text{PC}$ ). Figure 3.1 shows the molecular structure of both *t*18:1-18:0PC and *c*18:1-18:0PC. The experiments represent the first direct comparison of TFA- vs. CFA-containing phospholipids, which are otherwise identical, that does not rely on a perturbing extrinsic probe.

## Experimental Procedures

### Materials

*l*18:1-[<sup>2</sup>H<sub>35</sub>]18:0PC, as a custom synthesis, and 1-acyl-2-hydroxyphosphatidcholines (18:0lysoPC and *c*18:1lysoPC) were purchased from Avanti Polar Lipids (Alabaster, AL). Cambridge Isotope Laboratories (Andover, MA) and Sigma Chemical Co. (St. Louis, MO) were the source of [<sup>2</sup>H<sub>35</sub>]18:0 acid and deuterium depleted water, respectively.

### Synthesis of deuterated PCs

18:0-[<sup>2</sup>H<sub>35</sub>]18:0PC and *c*18:1-[<sup>2</sup>H<sub>35</sub>]18:0PC were synthesized using the method described by Sun et al. (26), with a few minor changes. The synthesis was accomplished via dicyclohexylcarbodiimide (DCC, 0.8 mmol) coupling of [<sup>2</sup>H<sub>35</sub>]18:0 acid (0.4 mmol) with the appropriate lysoPC (0.2 mmol) in the presence of N,N-dimethylaminopyridine (DMAP, 0.8 mmol) dissolved in dry, distilled chloroform (4 mL). The mixture was stirred for 72 h under argon atmosphere and, following concentration, the residue was purified by flash chromatography on silica gel in a chloroform/methanol/water (58/35/4, vol/vol/vol) solvent system to give the desired product (80% yield). <sup>1</sup>H NMR in C<sup>2</sup>HCl<sub>3</sub> at 500 MHz was performed to confirm the product, which was further purified by HPLC with a reverse-phase silica C18 column (methanol solvent).

Molecular mass (825.36 for 18:0-[<sup>2</sup>H<sub>35</sub>]18:0PC and 823.34 for *c*18:1-[<sup>2</sup>H<sub>35</sub>]18:0PC) was confirmed by LC-mass spectrometry.

### NMR Sample Preparation

*t*18:1-[<sup>2</sup>H<sub>35</sub>]18:0PC, *c*18:1-[<sup>2</sup>H<sub>35</sub>]18:0PC or 18:0-[<sup>2</sup>H<sub>35</sub>]18:0PC (60-90 mg) was thoroughly vortex mixed by with an equal weight (60-90 μL) of 50 mM Tris buffer (pH 7.5) at a temperature above the gel to liquid crystalline phase transition for each phospholipid. Deuterium depleted water (~ 2 mL) was added to the mixture to allow measurement of pH which was adjusted to 7.5. Three lyophilizations in the presence of excess deuterium depleted water were then performed to remove naturally abundant <sup>2</sup>HHO. After a final hydration to 50 wt%, the resultant sample was transferred to a 5 mm NMR tube that was sealed with a Teflon coated plug. It was stored at -80 °C and equilibrated at room temperature before the experiments.

### <sup>2</sup>H NMR Spectroscopy

Solid State <sup>2</sup>H NMR experiments were performed on a home-built spectrometer operating at 27.6 MHz with a 4.2 T Nalorac superconducting magnet (27). A desktop computer controlled the spectrometer. Pulse programming was accomplished using an in-house assembled programmable pulse generator with a design based upon an Am2910 processor (Advanced Micro Devices, Sunnyvale, CA) (28), while signals were acquired in quadrature using a Rapid Systems R1200 M dual channel digital oscilloscope (Seattle, WA). Sample temperature was regulated to ±0.5 °C by a Love Controls 1600 Series

temperature controller (Michigan City, IN). A phase alternated quadrupolar echo sequence  $(90^\circ_x-\tau-90^\circ_y\text{-acquire-delay})_n$  that eliminates spectral distortion due to receiver recovery time was implemented to collect spectra (29). Unless otherwise stated, spectral parameters were:  $90^\circ$  pulse width  $\approx 4 \mu\text{s}$ ; separation between pulses  $\tau = 50 \mu\text{s}$ ; delay between pulse sequences = 1.0 s (gel phase) or 1.5 s (liquid crystalline phase); sweep width =  $\pm 250$  kHz (gel phase) or  $\pm 100$  kHz (liquid crystalline phase); dataset = 2K; and number of transients = 1024.

### Analysis of $^2\text{H}$ NMR Spectra

First moments  $M_1$  (30) were calculated from the powder pattern spectra with

$$M_n = \frac{\int_{-\infty}^{+\infty} |\omega^n| f(\omega) d\omega}{\int_{-\infty}^{+\infty} f(\omega) d\omega} \quad (1)$$

Where  $f(\omega)$  represents the lineshape as a function of frequency  $\omega$  relative to the central Larmor frequency  $\omega_o$ . In practice the integration was a summation over the digitized data. The value of  $M_1$  is a sensitive indicator of membrane phase, and equates via the static quadrupolar coupling constant  $\left(\frac{e^2qQ}{h}\right) = 167$  kHz to an average order parameter  $\bar{S}_{CD}$  for the perdeuterated  $[^2\text{H}_{35}]18:0$  *sn*-2 chain in the liquid crystalline state according to

$$M_1 = \frac{\pi}{\sqrt{3}} \left(\frac{e^2qQ}{h}\right) \bar{S}_{CD} \quad (2)$$

The FFT depaking algorithm was applied to deconvolute the powder pattern signal to an aligned spectrum representative of a planar bilayer to further elaborate order within the liquid crystalline bilayer (27). The depaked spectrum consists of doublets with quadrupole splittings  $\Delta\nu(\theta)$  that relate to order parameters  $S_{CD}$  by

$$\Delta v(\theta) = \frac{3}{2} \left( \frac{e^2 q Q}{h} \right) |S_{CD}| P_2(\cos \theta) \quad (3)$$

where  $\theta = 0^\circ$  is the angle the normal to the membrane surface makes with the magnetic field and  $P_2(\cos \theta)$  is the second-order Legendre polynomial. A smoothed profile of order parameter was generated then on the basis of integrated intensity assuming monotonic variation towards the terminal methyl in the disordered center of the membrane (31).

### MD Simulations

MD simulations for *t*18:1-18:0PC and *c*18:1-18:0PC bilayers at 45 °C of 5 ns duration were carried out using eight processors on a Beowulf-type parallel computer. Each simulation cell contained 72 lipids (36 per monolayer) and 1930 waters, corresponding to full hydration. The Chemistry at HARvard Molecular Mechanics (CHARMM) program (32) was employed with the PARAM22b4b all-atom parameter set (33) and its extension to *cis* unsaturated lipids (34), while a new set was developed for the EA chain by previously described methods (34). Initial conformations were taken from the end of previously equilibrated simulations by applying restraints to the double bond torsions to produce the desired conformers during energy minimization. Electrostatic interactions were introduced via the particle mesh Ewald summation (35). All bonds involving hydrogen were fixed at their equilibrium distances with the SHAKE algorithm (36). The time step was 2 fs implemented with a leapfrog Verlet integration scheme. A flexible simulation cell was used with the z dimension (bilayer normal) adjusted to maintain  $P_{zz} = 1$  atm, and the x and y dimensions were adjusted to maintain a

surface area of  $65.9 \text{ \AA}^2/\text{molecule}$ . The fixed area ensemble was chosen to insure that the molecular areas were consistent with experiment. The number of lipids in the simulation cell, while smaller than some studies, has been used in a number of published reports from our laboratory that were successfully used to aid in the interpretation of NMR experiments and has been shown to be more than adequate for the computation of equilibrium structural properties (37). Coordinates were saved every ps for subsequent analysis that included the calculation of order parameters.

## Results

### $^2\text{H}$ NMR

Solid state  $^2\text{H}$  NMR spectra for 50 wt% aqueous dispersions of *t*18:1-18:0[ $^2\text{H}_{35}$ ]PC, *c*18:1-18:0[ $^2\text{H}_{35}$ ]PC and, as the saturated control, 18:0-18:0[ $^2\text{H}_{35}$ ]PC in 50 mM Tris (pH 7.5) were collected as a function of temperature to investigate the changes EA vs. OA cause to phase behavior and membrane organization.

### Phase Behavior

Representative examples of spectra at selected temperatures for 18:0-18:0[ $^2\text{H}_{35}$ ]PC, *t*18:0-18:0[ $^2\text{H}_{35}$ ]PC and *c*18:1-18:0[ $^2\text{H}_{35}$ ]PC are shown in Figure 3.2. The dramatic narrowing of spectral shape that accompanies the melting of acyl chains at the transition between gel and liquid crystalline states is apparent for each phospholipid, and inspection reveals differences in the effect of EA and OA on membrane phase behavior.

All three phospholipids exhibit spectra characteristic of the lamellar gel phase at  $-5\text{ }^{\circ}\text{C}$  (Figure 3.2a, e and i), the lowest temperature, and of the lamellar liquid crystalline phase at  $60\text{ }^{\circ}\text{C}$  (Figure 3.2d, h and l), the highest temperature (30, 38). In the gel phase, the  $[^2\text{H}_{35}]\text{18:0}$  *sn*-2 chains are rigid and their slow rotational diffusion confers non axial symmetry on a featureless broad spectrum with shoulders at  $\pm 63\text{ kHz}$  (Figure 3.2a, e and i). Rapid isomerization about C-C bonds in the  $[^2\text{H}_{35}]\text{18:0}$  *sn*-2 chain is responsible in the liquid crystalline phase for a much narrower spectrum with well-defined edges at approximately  $\pm 15\text{ kHz}$  that correspond to the plateau region of relatively constant order in the upper part of the chain (Figure 3.2d, h and l). The individual peaks within the spectrum arise from less ordered methylenes in the lower part of the acyl chain, and the highly mobile terminal methyl is represented by a central pair of peaks. It is in between the two extreme temperatures where differences in phase behavior become evident in the spectra. The spectra for  $18:0\text{-}18:0[^2\text{H}_{35}]\text{PC}$  (Figure 3.2b) and  $t18:0\text{-}18:0[^2\text{H}_{35}]\text{PC}$  (Figure 3.2f) remain gel-like at  $20\text{ }^{\circ}\text{C}$ , while that for  $c18:1\text{-}18:0[^2\text{H}_{35}]\text{PC}$  (Figure 3.2j) indicates that the CFA-containing membrane has become liquid crystalline. Upon a further  $25\text{ }^{\circ}\text{C}$  rise in temperature to  $45\text{ }^{\circ}\text{C}$ , TFA-containing  $t18:0\text{-}18:0[^2\text{H}_{35}]\text{PC}$  (Figure 3.2g) as well as  $c18:0\text{-}18:0[^2\text{H}_{35}]\text{PC}$  (Figure 3.2k) exhibits a spectrum typical of the liquid crystalline state and only for disaturated  $18:0\text{-}18:0[^2\text{H}_{35}]\text{PC}$  (Figure 3.2c) does the spectrum imply the gel phase.

The spectra presented in Figure 3.2 are examples of spectra that were acquired over a span in temperature from  $-10$  to  $65\text{ }^{\circ}\text{C}$ . They illustrate the sensitivity of spectral lineshape to membrane phase. The first moment,  $M_1$ , defined by eq.1, offers a method of quantifying the shape and monitoring phase behavior when plotted against temperature



(30). Figure 3.3 presents  $M_1$  as a function of temperature for  $t18:1-[^2\text{H}_{35}]18:0\text{PC}$ ,  $c18:1-[^2\text{H}_{35}]18:0\text{PC}$  and  $18:0-[^2\text{H}_{35}]18:0\text{PC}$ . There are two ranges of temperature for each PC where  $M_1$  values vary slowly separated by an abrupt discontinuity. In the case of  $t18:1-[^2\text{H}_{35}]18:0\text{PC}$  ( $\bullet$ ), gel phase is signified by  $M_1 > 11.1 \times 10^4 \text{ s}^{-1}$  below  $30.5 \text{ }^\circ\text{C}$  while liquid crystalline state characterized by  $M_1 < 4.8 \times 10^4 \text{ s}^{-1}$  applies above  $32.5 \text{ }^\circ\text{C}$ . A similar discontinuity is seen at lower temperature for  $c18:1-[^2\text{H}_{35}]18:0\text{PC}$  ( $\diamond$ ) where  $M_1 > 10.9 \times 10^4 \text{ s}^{-1}$  and  $M_1 < 5.7 \times 10^4 \text{ s}^{-1}$ , respectively, signify the gel phase below  $6 \text{ }^\circ\text{C}$  and liquid crystalline state above  $9 \text{ }^\circ\text{C}$ . In the saturated lipid,  $18:0-[^2\text{H}_{35}]18:0\text{PC}$  ( $\square$ ), the moments  $M_1 > 11.0 \times 10^4 \text{ s}^{-1}$  remain symptomatic of the gel state until  $50 \text{ }^\circ\text{C}$  and then the liquid crystalline is indicated by  $M_1 < 5.1 \times 10^4 \text{ s}^{-1}$  for temperatures in excess of  $56 \text{ }^\circ\text{C}$ .

The dramatic drop in the value of  $M_1$  corresponds to the tremendous change in lineshape that accompanies acyl chain melting when the lipid undergoes the transition from gel to liquid crystalline state. It is clear from the plots in Figure 3.3 that the temperature at which  $t18:1-[^2\text{H}_{35}]18:0\text{PC}$  melts lies approximately midway between those for  $18:0-[^2\text{H}_{35}]18:0\text{PC}$  and  $c18:1-[^2\text{H}_{35}]18:0\text{PC}$ . The values for the temperature of the phase transition  $T_m$  derived from the center of the discontinuity in each plot are given in Table 1. For the lipid with a SA *sn*-1 chain  $T_m$  occurs at  $53.0 \text{ }^\circ\text{C}$ , which is much higher than the  $T_m$  of  $7.0 \text{ }^\circ\text{C}$  for the lipid with an OA *sn*-1 chain. In between at  $31.5 \text{ }^\circ\text{C}$  is the  $T_m$  for the lipid with an EA *sn*-1 chain.

### Acyl Chain Order

In the liquid crystalline phase where rapid molecular reorientation results in spectra symptomatic of axially symmetry, the first moment  $M_1$  is related to the average order parameter  $\bar{S}_{CD}$  for the entire  $[^2\text{H}_{35}]18:0$  *sn*-2 chain via eq. 2. The values obtained for  $\bar{S}_{CD}$  in *t*18:1- $[^2\text{H}_{35}]18:0$ PC and *c*18:1- $[^2\text{H}_{35}]18:0$ PC bilayers at 45 °C, together with 18:0- $[^2\text{H}_{35}]18:0$ PC at 60 °C, are listed in Table 2. They reveal that order is only slightly greater in the EA-containing,  $\bar{S}_{CD} = 0.135$ , than OA-containing,  $\bar{S}_{CD} = 0.128$ , membrane. In both cases, order is lower than in the saturated membrane where  $\bar{S}_{CD} = 0.156$  at 60 °C. The calculation was performed at a higher temperature for 18:0- $[^2\text{H}_{35}]18:0$ PC because the saturated lipid, unlike *t*18:1- $[^2\text{H}_{35}]18:0$ PC and *c*18:1- $[^2\text{H}_{35}]18:0$ PC, is gel state at 45 °C. Thus, the data in Table 2 underestimate the differential in order between unsaturated and saturated systems.

To elaborate upon the distribution of order along the chain the NMR signal was FFT depaked (27). Application of this procedure results in a spectrum equivalent to that obtained for a planar membrane with the bilayer normal aligned parallel to the magnetic field, consisting of a superposition of doublets as illustrated in Figure 3.4 for *t*18:1- $[^2\text{H}_{35}]18:0$ PC and *c*18:1- $[^2\text{H}_{35}]18:0$ PC. For each lipid an outermost composite doublet, representing ordered methylenes in the upper part of the  $[^2\text{H}_{35}]18:0$  *sn*-2 chain, and a series of well resolved doublets with smaller splittings, predominantly corresponding to the methylenes and terminal methyl that display progressively less order in the lower portion of the chain, are clearly discernible in the depaked spectrum.

The vast enhancement in resolution achieved facilitates the generation of a profile of order parameter.

The smoothed order parameter profile shown in Figure 3.5 for  $t18:1-[^2\text{H}_{35}]18:0\text{PC}$  and  $c18:1-[^2\text{H}_{35}]18:0\text{PC}$  membranes (Figure 3.5a) were created from the depaked spectra (Figure 3.4) by assigning equal intensity to each methylene group and assuming a continuous decrease of order towards the terminal methyl (31). It should be noted that constraints imposed upon the initial orientation of the *sn*-2 chain render the C2 position an exception to the assumption that order varies monotonically (39). The inequivalent  $S_{CD}$  values plotted for the two deuterons at this position were calculated from the splittings of doublets that were assigned on the basis of intensity and comparison with work on selectively deuterated PCs (34). Inspection of the profiles reveals that they are quite similar for the TFA- and CFA-containing membranes. Apart from the C2 position, there is a characteristic plateau region of slowly decreasing order in each of the lipids in the upper portion of the perdeuterated acyl chain followed in the lower portion by a progressively greater reduction in order towards the bottom of the chain. Slightly higher order in the lower half (C9 onwards) of the  $[^2\text{H}_{35}]18:0$  *sn*-2 chain for the EA- (●) than the OA- (◇) containing membrane is the only difference. Consistent with the values for average order parameter presented in Table 2, higher order is exhibited throughout the profile for  $18:0-[^2\text{H}_{35}]18:0\text{PC}$  at 60 °C (Figure 3.5a, solid line) that is also included in Figure 3.5.

## MD Simulations

### Acyl chain order

MD simulations of *t*18:1-18:0PC and *c*18:1-18:0PC bilayers were performed to aid interpretation of the NMR data. The advantage of the computer modeling technique is its ability to provide an atomic level picture of molecular conformations and temporal dynamics that can only come indirectly from interpretation of experimental data (40, 41). However, validation with experimental results is crucial because simulations require the input of initial conditions and empirically derived expression for force fields. Testing against the  $S_{CD}$  values measured by  $^2\text{H}$  NMR for the  $[^2\text{H}_{35}]18:0$  *sn*-2 chain in *t*18:1- $[^2\text{H}_{35}]18:0\text{PC}$  and *c*18:1- $[^2\text{H}_{35}]18:0\text{PC}$  fulfils that purpose here.

The order parameter profiles generated from MD simulations on *t*18:1-18:0PC and *c*18:1-18:0PC are displayed in Figure 3.5. Table 2 includes the associated values for the value of the average order parameter  $\overline{S}_{CD}$ . The simulated values of  $S_{CD}$  were calculated as a time and ensemble average over trajectories according to

$$S_{CD} = \frac{1}{2} \langle 3\cos^2\beta - 1 \rangle \quad (4)$$

In this equation, which serves as the definition of the deuterium order parameter (42),  $\beta$  is the instantaneous angle that a C- $^2\text{H}$  bond vector makes with respect to the bilayer normal and the angular brackets designate a time average. The C2 position was omitted from the calculations in view of the recognized failure of simulations to reproduce experimental order parameters at this location in either the *sn*-1 or *sn*-2 chain (43). It can

be seen that the overall shape of the computationally derived profile for the SA *sn*-2 chain (Figure 3.5b) possesses good agreement with experiment (Figure 3.5a). The “signature” plateau region of virtually constant order in the upper part of the chain followed by gradually decreasing order in the lower part is clearly exhibited by the simulated data that, like the experimental data, furthermore reveal slightly less disorder in *t*18:1-18:0PC (●) than *c*18:1-18:0PC (◇) bilayers. There is a trend of somewhat higher order in the simulation for both TFA- and CFA-containing lipids ( $\bar{S}_{CD} = 0.148$  and  $0.146$ , respectively) relative to the  $^2\text{H}$  NMR data ( $\bar{S}_{CD} = 0.135$  and  $0.128$ , respectively), which we ascribe to a choice for the area/molecule that may be a few percent too low or potentially from incomplete sampling in the finite length simulation. Another factor is the contribution from the C2 position, where  $S_{CD}$  is small, to the NMR derived data that the simulation does not include.

Order parameters extracted for the EA and OA *sn*-1 chains from the MD simulations for *t*18:1-18:0PC and *c*18:1-18:0PC are also plotted vs. carbon number in Figure 3.5 (Figure 3.5c). Major differences exist in comparison to the gradient of order along the 18:0 *sn*-1 chain. The  $S_{CD}$  values for the *trans* and *cis* unsaturated chains are lower and are not characterized by a region of uniform order in the upper portion. In the case of the *t*18:1 *sn*-1 chain (●) they gradually decrease throughout the chain towards the terminal methyl end. The small deviations from monotonic variation that are apparent would be expected to disappear in simulations of longer duration. As expected from the geometry of a *trans* double bond that aligns the C-H bonds parallel to each other, and confirmed by the single quadrupolar splitting measured for 16:0-[9,10- $^2\text{H}_2$ ]18:1PC with selectively deuterated EA in the *sn*-2 chain (44), the order parameters at positions 9 and

10 are the same. There is no dramatic dip in  $S_{CD}$  value near the *trans* double bond of the kind seen by simulation in the vicinity of the *cis* double bond in the OA sn-1 chain for *c*18:1-18:0PC (Figure 3.5c,  $\diamond$ ). This dip is consistent with the greatly diminished  $S_{CD}$  values at the C9, C10 and surrounding positions measured experimentally and computer modeled for OA esterified to the *sn*-2 position in 16:0-*c*18:1PC and *sn*-1 and *sn*-2 positions in 1,2-dioleoylphosphatidylcholine (*c*18:1-*c*18:1PC) (44-46). Extremely high disorder within the *cis* unsaturated chain is not the reason. Taking into account geometrical factors, prior analysis of  $^2\text{H}$  NMR splittings measured for 16:0-[9,10- $^2\text{H}_2$ ]*c*18:1PC established that an average orientation close to the bilayer normal for the *cis* double bond is responsible (44).

### Discussion

The aim of this work is to elucidate molecular organization within a model membrane comprised of PC molecules in which EA, the simplest and most common TFA, replaces the saturated fatty acid normally found at the *sn*-1 position. Solid state  $^2\text{H}$  NMR and MD simulations were employed to compare phase behavior and acyl chain order in *t*18:1-18:0PC and, the CFA-containing counterpart, *c*18:1-18:0PC.

#### EA Packs Better than OA in the Gel Phase

$^2\text{H}$  NMR spectra for *t*18:1-[ $^2\text{H}_{35}$ ]18:0PC, *c*18:1-[ $^2\text{H}_{35}$ ]18:0PC and 18:0-[ $^2\text{H}_{35}$ ]18:0PC at representative temperatures from a range that spans -5 to 65 °C are presented in Figure 3.2. In each case they reveal upon heating a change in spectral shape

from entirely characteristic of the gel phase to entirely characteristic of the liquid crystalline phase. The introduction of unsaturation clearly depresses the temperature at which the phase transition occurs, the depression associated with OA exceeding that with EA. Whereas only the spectrum at 60 °C for 18:0-[<sup>2</sup>H<sub>35</sub>]18:0PC (Figure 3.2d) signifies the membrane has become liquid crystalline, the spectra at 45 and 60 °C for *t*18:0-[<sup>2</sup>H<sub>35</sub>]18:0PC (Figure 3.2g and h) and at 20, 45 and 60 °C for *c*18:1-18:0PC (Figure 3.2j, k and l) demonstrate that these membranes entered the liquid crystalline state at lower temperature.

The phase behavior of the three membranes is elaborated in Figure 3.3 by a plot against temperature of first moment  $M_1$  calculated from all spectra collected. A sharp drop in the value of  $M_1$  that accompanies the melting of the [<sup>2</sup>H<sub>35</sub>]18:0 *sn*-2 chain is well defined for *t*18:1-[<sup>2</sup>H<sub>35</sub>]18:0PC, *c*18:1-[<sup>2</sup>H<sub>35</sub>]18:0PC and 18:0-[<sup>2</sup>H<sub>35</sub>]18:0PC. The midpoint is identified as the transition temperature  $T_m$  and Table 1 lists the values measured. As was surmised by visual inspection of the spectra,  $T_m$  is reduced less by a *trans* than *cis* double bond. The transition temperature for *t*18:1-[<sup>2</sup>H<sub>35</sub>]18:0PC (31.5 °C) lies midway between those for 18:0-[<sup>2</sup>H<sub>35</sub>]18:0PC (53.0 °C) and *c*18:1-[<sup>2</sup>H<sub>35</sub>]18:0PC (7.0 °C). To the best of our knowledge, a transition temperature has not previously been reported for *t*18:1-18:0PC. Values for  $T_m$  have been measured by differential scanning calorimetry (DSC) for 18:0-*t*18:1PC (31.1 °C) and 18:0-*c*18:1PC (5.5 °C) where the *sn*-1 and -2 chains are interchanged relative to the current work (16). They show the same behavior. Adding a single *trans* double bond to the *sn*-2 chain, like to the *sn*-1 chain, lowers the transition temperature about half as much as a *cis* double bond. The phase transition temperatures published for homoacid PC with two identical monounsaturated

chains are predictably much lower than for heteroacid PC with a combination of saturated and monounsaturated chains at the *sn*-1 and *sn*-2 positions or vice-versa. In common with the corresponding heteroacid species, the transition for EA-containing 1,2-dielaidoylphosphatidylcholine (*t*18:1-*t*18:1PC,  $T_m = 11.1$  °C) is depressed substantially less than OA-containing 1,2-dioleoylphosphatidylcholine (*c*18:1-*c*18:1PC,  $T_m = -18.1$  °C) (12). Under physiological conditions where EA replaces a saturated fatty acid such as SA in the *sn*-1 position of phospholipids and is typically paired with an unsaturated CFA in the *sn*-2 position (25), a lowering of the transition temperature would result due to a higher degree of unsaturation.

The lowering of the transition temperature for *t*18:1-18:0PC and *c*18:1-18:0PC is attributable to the deviation from a linear conformation that results when a *trans* and, to a greater degree, *cis* double bond is introduced into a saturated fatty acid chain. Looser packing and a consequent reduction in intra- and inter-molecular van der Waals' interactions within the ordered interior of the bilayer in the gel state decrease stability, manifest as a depression of the temperature at which the chains melt. Energy-minimized structures are presented in Figure 3.6 to illustrate the point. The saturated SA chain at the *sn*-2 position in *t*18:1-18:0PC (Figure 3.6a) or *c*18:1-18:0PC (Figure 3.6b) is straight. All of the single C-C bonds are in *trans* (*t*) conformation. The monounsaturated EA (Figure 3.6a) or OA (Figure 3.6b) chain at the *sn*-1 position, on the contrary, is kinked. A  $t s^- \Delta s^- t$  or  $t s^- \Delta s^- g^-$  sequence of rotational states ( $s^\pm$  and  $g^\pm$  specify, correspondingly, *skew* ( $\pm$ ) and *gauche* ( $\pm$ ) conformation) is preferred in the vicinity of the rigid *trans* or *cis* double ( $\Delta$ ) bond, respectively. The structure modeled for SA and EA



attached to a phospholipid matches the conformation modeled as a free fatty acid. The structure modeled for OA esterified to PC, as discussed by Huang and Li (47), includes a *trans*  $\rightarrow$  *gauche* isomerization next to the  $s^- \Delta s^-$  sequence to create a crankshaft-like motif as opposed to the twisted boomerang shape modeled as a free fatty acid. That the EA chain in *t*18:1-18:0PC (Figure 3.6a) has a less accentuated kink and deviates from linearity to a smaller extent than the OA chain in *c*18:1-18:0PC (Figure 3.6b), and would pack more favorably in the gel state, is evident in the lowest energy conformers obtained here with individual molecules in the gas phase. Consistent with greater stability, moreover, stronger van der Waals' interaction between *sn*-1 and -2 chains is computed using the interaction energy facility in CHARMM for the lowest energy conformers modeled for the EA- than OA-containing PC. The interaction energy is, accordingly, -1.8 vs. -0.7 kcal/mol (between carbons 10-18 and their associated hydrogens) in the bottom of the chain where EA, unlike OA, lines up close to the SA chain. In the top of the chain where EA and OA adopt a similar conformation, the interaction energy is -2.2 kcal/mol (between carbons 1-9) and the same.

#### EA Disorders Almost as Much as OA in the Liquid Crystalline Phase

The plot of first moment  $M_1$  vs. temperature in Figure 3.3 shows that the  $M_1$  values for *t*18:1- $[\text{}^2\text{H}_{35}]$ 18:0PC consistently lie just above ( $\sim 7\%$ ) those for *c*18:1- $[\text{}^2\text{H}_{35}]$ 18:0PC, and well below ( $\sim 25\%$ ) those for 18:0- $[\text{}^2\text{H}_{35}]$ 18:0PC, when the membranes are examined in the physiologically relevant liquid crystalline state. Invoking the relationship between  $M_1$  and average order parameter  $\bar{S}_{CD}$  (eq. 2), thus, establishes that

introducing a *trans* or *cis* double bond increases disorder. Furthermore, order within the EA-containing membrane is much closer to the OA-containing than the disaturated membrane.

Table 2 lists the average order parameters determined from the  $^2\text{H}$  NMR spectra recorded for *t*18:1- $^{[2}\text{H}_{35}$ ]18:0PC and *c*18:1- $^{[2}\text{H}_{35}$ ]18:0PC at 45 °C, which were analyzed in detail to elucidate and compare acyl chain organization within the membranes. They confirm the trend gleaned from the moments. While *t*18:1- $^{[2}\text{H}_{35}$ ]18:0PC ( $\bar{S}_{CD} = 0.135$ ) is a little more ordered than *c*18:1- $^{[2}\text{H}_{35}$ ]18:0PC ( $\bar{S}_{CD} = 0.128$ ), both membranes possess substantially greater disorder than 18:0- $^{[2}\text{H}_{35}$ ]18:0PC ( $\bar{S}_{CD} = 0.153$ ). It should be noted that the  $\bar{S}_{CD}$  value for 18:0- $^{[2}\text{H}_{35}$ ]18:0PC was measured at 60 °C because the disaturated membrane is in the gel phase at 45 °C and, as a point of reference, underestimates the reduction in order produced at the lower temperature when a double bond is introduced. That a *trans* and *cis* double bond exert a comparable effect on membrane order is consistent with earlier published  $^2\text{H}$  NMR work on  $^{[2}\text{H}_{31}$ ]16:0-*t*18:1PC (19) and  $^{[2}\text{H}_{31}$ ]16:0-*c*18:1PC (20) with EA and OA attached at the *sn*-2 position, respectively. A reservation about this comparison is that it is based upon data collected in two independent studies under experimental conditions that were not necessarily equivalent.

Profiles of order along the saturated  $^{[2}\text{H}_{35}$ ]18:0 *sn*-2 chain in *t*18:1- $^{[2}\text{H}_{35}$ ]18:0PC and *c*18:1- $^{[2}\text{H}_{35}$ ]18:0PC membranes that were generated from depaked spectra (Figure 3.4) to investigate the small differential in average order between the membranes are presented in Figure 3.5. The general shape for the two membranes is similar (Figure 3.5a) and matches that universally seen with saturated chains in liquid crystalline phospholipid bilayers (41). Except for the C2 position that is constrained in orientation by the glycerol

backbone (38), order varies monotonically. A plateau region of slowly decreasing order parameter in the upper portion is followed by a progressively more rapid decrease towards the terminal methyl in the lower portion. The plateau region of almost constant order is due to a predominance of *trans* rotational isomeric states aligning segments parallel to the bilayer normal, together with approximately constant probability for conformations with other orientations, in the upper portion of the chain (48). In the lower portion a decrease in number of *trans* segments oriented parallel to the bilayer normal is responsible for the loss in order. Figure 3.5 reveals that slightly higher order below the C9 position in the EA-containing membrane, which extends the plateau region in *t*18:1-[<sup>2</sup>H<sub>35</sub>]18:0PC (C3-C11) relative to *c*18:1-[<sup>2</sup>H<sub>35</sub>]18:0PC (C3-C9), is the origin of the difference in the value of  $\bar{S}_{CD}$  determined with the two types of monounsaturated membrane (Table 2). Above the C9 position, the profiles are almost identical. Comparison with the plateau region (C3-C11) in the profile for 18:0-[<sup>2</sup>H<sub>35</sub>]18:0PC (Figure 3.5a, solid line) indicates that the disordering caused by a *trans* double bond does not entail the shortening of the plateau region associated with a *cis* double bond.

We attribute the disordering associated with EA and OA to the reduced energy barrier to rotation for the C-C single bond on each side of a *trans* (~2.25 kcal/mol) or *cis* (~1.1 kcal/mol) C=C double bond (vs. ~3.5 kcal/mol in a saturated chain) that more than compensates for the rigidity of a double bond. MD simulations that were performed in conjunction with the <sup>2</sup>H NMR experiments provide insight. In particular, they reveal details on the motions of the *trans* and *cis* double bond in the *sn*-1 chain of *t*18:1-18:0PC and *c*18:1-18:0PC bilayers, respectively, for which we do not have <sup>2</sup>H NMR data. Before focusing on the EA and OA *sn*-1 chain, our first step was to establish confidence in the

simulated data by confirming that the profile of order parameter along the SA *sn*-2 chain generated by simulation (Figure 3.5b) reproduces the trend seen by NMR (Figure 3.5a). The quality of agreement is good. The shape of the simulation-obtained profile is characteristic of the saturated chains of phospholipids in the lamellar liquid crystalline phase (42). There is a plateau region of slowly varying order in the upper half of the chain that falls-off in the lower half of the chain towards the middle of the bilayer. As in the NMR-obtained data, the EA-containing bilayer is slightly more ordered than the OA-containing one and the difference exists in the lower portion of the chain.

The profiles of order along the EA and OA *sn*-1 chain in the two monounsaturated membranes calculated from the MD simulations differ markedly from the saturated SA *sn*-2 chain and from each other (Figure 3.5c). A largely continuous decrease in  $S_{CD}$  values along the whole EA chain towards the terminal methyl group is displayed in the profile for *t*18:1-18:0PC. Either absent or truncated is a plateau region of slowly varying order in the upper portion that characterizes the neighboring SA *sn*-2 chain and the value of  $S_{CD}$  is less at each position. Like in earlier computer simulations of 16:0-*t*18:1PC (17, 18), there is no major deviation from monotonic variation at the *trans* double bond and is in stark contrast to the dip in  $\bar{S}_{CD}$  values close to the *cis* double bond observed in the profile for the OA *sn*-1 chain of *c*18:1-18:0PC. The distinction is predominantly attributed to a different orientation for the *trans* and *cis* double bonds rather than a major difference in the extent of the angular fluctuations they undergo. This issue can be understood with the aid of histograms that represent a normalized population distribution for the orientation of C-H bonds relative to the bilayer normal that were calculated from the simulated data generated in the current study.

In Figure 3.7, the distribution of orientation for the C-H bonds at the C9 and C10 positions in the EA and OA *sn*-1 chain of *t*18:1-18:0PC and *c*18:1-18:0PC, respectively, are plotted. A schematic depiction of the most probable orientation is presented alongside each plot. The equivalent information for the C-H bonds on the C9 carbon in the SA *sn*-2 chain that is included in the figure serves as a point of reference (Figure 3.7c). In the case of the saturated chain, the distribution of orientation is approximately symmetric in shape about a most probable angle of  $\beta \sim 90^\circ$ . The width at half height of the distribution is  $\sim 70^\circ$ , reflecting the angular range through which the C-H bonds move due to isomerization about C-C bonds along the chain and wobbling of the long molecular axis. Similarly, a distribution of orientation that is approximately symmetric about  $\beta \sim 90^\circ$  characterizes the C-H bond on the C9 and C10 carbons in the EA *sn*-1 chain (Figure 3.7a). The curves are essentially identical at the two positions because the C-H bonds are parallel. Their width at half height,  $\sim 80^\circ$ , is greater than in the SA *sn*-1 chain. We ascribe the additional motion in the unsaturated chain to the reduced energy barrier for rotation about the C-C bonds next to a *trans* double bond. Unlike either EA or SA, the curves that describe the distribution of orientation for the C-H bond at the C9 and C10 positions in the OA *sn*-1 chain are shifted and asymmetric (Figure 3.7b). They do not coincide and  $\sim 70^\circ$  and  $\sim 120^\circ$ , respectively, constitute the most probable orientation. It is the enhanced proportion of orientations near the “magic angle”  $\beta = 54^\circ 44'$ , or its supplemental angle ( $180^\circ - \beta$ ), for which  $S_{CD} = 0$  (eq. 4) that results in a low order parameter here. As indicated by the width at half height of the distribution,  $\sim 85^\circ$ , the amplitude of angular fluctuation is not much bigger than in the EA chain.

This modest increase in the amount of angular motion arises from a further reduction in the energy barrier for rotation around the C-C bonds adjacent to a *cis* double bond.

Only one direct comparison of molecular organization in EA- and OA-containing membranes has previously been published (16). The study by Roach *et al.* employed a battery of biophysical techniques to compare PC having TFA and CFA with 1 or 2 double bonds. Most closely related to the current discussion were measurements on 18:0-*t*18:1PC vs. 18:0-*c*18:1PC of membrane “fluidity” as probed by steady state fluorescence polarization of DPH and AS, and of area/molecule from pressure-area isotherms for lipid monolayers. Lower fluidity and a smaller area/molecule were found in the *trans*-unsaturated system, qualitatively agreeing with the higher order seen here for *t*18:1-18:0PC relative to *c*18:1-18:0PC. The modest differential in order between the two unsaturated membranes and the much greater order for saturated 18:0-18:0PC that we detected by  $^2\text{H}$  NMR (Table 2), however, belies the sweeping assessment made in the earlier study that TFA produce membranes properties more similar to those of saturated chains than CFA. A more nuanced appraisal is necessary recognizing that on the one hand the conformation of EA somewhat resembles saturated SA while on the other hand EA is dynamically more similar to *cis*-unsaturated OA.

Over the last decade it has become generally accepted that lipids are not homogeneously distributed in biological membranes but instead are organized in patches of specific composition to provide the environment that supports the activity of a resident protein (49-51). Formation of lipid domains is the consequence of unequal affinities between different lipid species or between the lipids and membrane proteins. Lipid rafts are the domain that has attracted considerable attention (50-52). They are  $l_o$  (liquid

ordered) domains enriched in predominantly saturated sphingolipids and cholesterol that are thought to serve as the platform for cell signaling proteins such as GPI-anchored proteins in the outer leaflet of the plasma membrane. At the opposite extreme of rafts are domains formed by polyunsaturated fatty acid (PUFA)-containing phospholipids from which cholesterol is excluded (53-56). The highly disordered environment in these domains is necessary for the function of certain proteins, notably rhodopsin in the disk membrane of the rod outer segment (57), and has been hypothesized to play a central role in the alleviation of a multiplicity of health problems by dietary PUFA (58). We, as have others (9-13, 16), speculate TFA are a rogue class of fatty acid that substitute into membrane lipids and locally affect molecular organization to produce a change in protein activity adversely influencing biological function. The possibility that EA may be mistakenly identified as a saturated fatty acid on the basis of its conformation yet disrupts membrane order almost as much as OA is suggested by our results.

### Conclusion

The picture of the relative effect of *trans* vs. *cis* unsaturation on molecular organization in a membrane that emerges from our  $^2\text{H}$  NMR experiments and computer simulations is one in which a *trans* double produces a smaller kink in the linear conformation adopted by a saturated chain than a *cis* double bond. Thus, there is better chain packing in the gel state and the temperature of the gel to liquid crystalline transition is depressed less for *t*18:1-18:0PC than *c*18:1-18:0PC. Acyl chain order in the physiologically relevant liquid crystalline phase is reduced almost as much by a *trans* as

*cis* double bond. Average order parameters measured for *t*18:1-18:0PC and *c*18:1-18:0PC coincide within ~7%, but are >25% lower than for 18:0-18:0PC. The reduction in order relative to the saturated membrane is ascribed to the additional flexibility conferred upon an monounsaturated chain by the lower energy barrier to rotation about the single C-C bonds either side of a double C=C bond. We are in the process of synthesizing analogs of *t*18:1-18:0PC deuterated in the EA chain to experimentally examine conformational organization in the region of the *trans* double bond. In future work, we also plan to investigate how the incorporation of TFA into a membrane affects the interaction of cholesterol.



### Acknowledgements

We wish to thank Bruce D. Ray, Daniel S. LoCascio and Jennifer Runyon for their assistance during synthesis of the deuterated phospholipids.

This chapter was published in *Biochemistry* 48(46), 11097-107 (2009) as a paper entitled “ Effect of trans unsaturation on molecular organization in a phospholipid membrane.” by Smita P. Soni, Jesse A. Ward, Stephanie Sen, Scott E. Feller and Stephen R. Wassall.

This work was supported by a grant from the American Chemical Society Petroleum Research Fund (43281-AC7) and under an award from the National Sciences Foundation (MCB-0543124)

## References

1. Sébédio, J. L., and W. W. Christie, editors. 1998. *Trans Fatty Acids in Human Nutrition*. The Oily Press, Dundee, Scotland.
2. Stender, S., J. Dyerberg, and H. S. Hansen. 2006. First international symposium on trans fatty acids and health. *Atherosclerosis* 7: 1-72.
3. Albers, M. J., L. J. Harnak, L. M. Steffen, and D. R. Jacobs, Jr. 2008. 2006 market survey of trans-fatty acid content of margarines and butters, cookies and snack cakes, and savory snacks. *J. Am. Diet. Assoc* 108:367-370.
4. Allison, D. B., M. A. Denke, J. M. Dietschy, E. A. Emken, P. Kris-Etherton, and R. J. Nicolosi. 1995. Trans fatty acids and coronary heart disease risk. Report of the expert panel on trans fatty acids and coronary heart disease. *Am. J. Clin. Nutr.* 62:655S-708S.
5. Dariush, M. Martijn, B. K., Ascherio A, S. M J, and Willett, W. C. 2006. Trans fatty acids and cardiovascular disease. *N Engl J Med* 354:1601-1613.
6. Salmeron, J., F. B. Hu, J. E. Manson, M. J. Stampfer, G. A. Colditz, E. B. Rimm, and W. C. Willett. 2001. Dietary fat intake and risk of type 2 diabetes in women. *Am. J. Clin. Nutr.* 73,:1019-1026.
7. Vinikoor, L. C., J. C. Schroeder, R. C. Millikan, J. A. Satia, C. F. Martin, J. Ibrahim, J. A. Galanko, and R. S. Sandler. 2008. Consumption of trans-fatty acid and its association with colorectal adenomas. *Am. J. Epidemiol* 168:289-297.
8. Thompson, A. K., D. I. Shaw, A. M. Minihane, and C. M. Williams. 2008. Trans-fatty acids and cancer: the evidence reviewed. *Nutr. Res. Rev.* 21:174-188.

9. Nui, S. L., D. C. Mitchell, and B. J. Litman. 2005. Trans fatty acid derived phospholipids show increased membrane cholesterol and reduced receptor activation as compared to their cis analogs. *Biochemistry* 44:4458-4465.
10. Gudheti, M. V., M. Mlodzianoski, and S. T. Hess. 2007. Imaging and shape analysis of giant unilamellar vesicles (GUVs) as model plasma membranes: Effect of trans-DOPC (dielaidoyl phosphatidylcholine) on membrane properties. *Biophys J*.
11. Zaloga, G. P., K. A. Harvey, W. Stillwell, and R. Siddiqui. 2006. Trans Fatty Acids and coronary Heart disease. *Nutr. Clin. Pract.* 21:505-512.
12. Bjorkbom, A., B. Ramstedt, and J. P. Slotte. 2007. Phosphatidylcholine and sphingomyelin containing an elaidoyl fatty acid can form cholesterol-rich lateral domains in bilayer membranes. *Biochim Biophys Acta* 1768:1839-1847.
13. Siddiqui, A., K. Harvey, S. J. Miller, and G. P. Zaloga. 2008. Impact of *omega*-3 and *trans* fatty acids on vascular remodeling: opposing roles in cardiovascular health. *Curr. Enzym. Inhib.* 4:60-72.
14. Rey, A., A. Kolinski, J. Skolnick, and Y. K. Levine. 1992. Effect of double bonds on the dynamics of hydrocarbon chains. *J Chem Phys* 97:1240-1249.
15. Emken, E. A. 1991. Do *trans* acids have adverse health consequences? G.J. Nelson, Ed, AOCS Press, Champaign, IL: 245-263.
16. Roach, C., S. E. Feller, J. A. Ward, S. R. Shaikh, M. Zerouga, and W. Stillwell. 2004. Comparison of cis and trans fatty acid containing phosphatidylcholines on membrane properties. *Biochemistry* 43:6344-6351.

17. Pearce, L. L., and S. C. Harvey. 1993. Langevin dynamics studies of unsaturated phospholipids in a membrane environment. *Biophys J* 65:1084-1092.
18. Rog, T., K. Murzyn, R. Gurbiel, Y. Takaoka, A. Kusumi, and M. Pasenkiewicz-Gierula. 2004. Effects of phospholipid unsaturation on the bilayer nonpolar region: a molecular simulation study. *J Lipid Res.* 45:326-336.
19. Linseisen, F., J. L. Thewalt, M. Bloom, and T. M. Bayerl. 1993. <sup>2</sup>H-NMR and DSC study of SEPC-cholesterol mixtures. *Chem. Phys Lipids* 65:141-149.
20. Holte, L. L., S. A. Peter, T. M. Sinnwell, and K. Gawrisch. 1995. <sup>2</sup>H nuclear magnetic resonance order parameter profiles suggest a change of molecular shape for phosphatidylcholines containing a polyunsaturated acyl chain. *Biophys J* 68:2396-2403.
21. Wolf, R. L., D. Precht, and J. Molkenin. 1998. Occurrence and distribution profiles of trans 18:1 acids in edible fats of natural origin. In *Trans Fatty Acids in Human Nutrition* (Edited by Jean Louis Sébédio and William W. Christie). The Oily Press, Dundee Scotland:1-33.
22. Gennis, R. B., editor. 1989. *Biomembranes*. Springer-Verlag, New York.
23. Holmer, G. 1998. Biochemistry of trans-monoenoic fatty acids. In *Trans Fatty Acids in Human Nutrition* (Sebedio, J.L. and Christie, W.W., Eds.). The Oily Press, Dundee Scotland:163-189.
24. Wolff, R. L., and B. Entressangles. 1994. Steady-state fluorescence polarization study of structurally defined phospholipids from liver mitochondria of rats fed elaidic acid. *Biochim Biophys Acta* 1211:198-206.

25. Woldseth, B., K. Retterstol, and B. O. Christophersen. 1998. Monounsaturated trans fatty acids, elaidic acid and trans-vaccenic acid, metabolism and incorporation in phospholipid molecular species in hepatocytes. *Scand J Clin Lab Invest* 58:635-645.
26. Sun, M., Y. Deng, E. Batyreva, W. Sha, and R. G. Salomon. 2002. Novel Bioactive Phospholipids: Practical Total Syntheses of Products from the Oxidation of Arachidonic and Linoleic Esters of 2-Lysophosphatidylcholine. *J Org Chem* 67:3575-3584.
27. McCabe, M. A., and S. R. Wassall. 1997. Rapid deconvolution of NMR powder spectra by weighted fast Fourier transformation. *Solid State Nuc Mag Res* 10:53-61.
28. Sternin, E. 1985. Data acquisition and processing: a systems approach. *Rev. Sci. Instrum* 56:2043-2049.
29. Davis, J. H., K. R. Jeffery, E. T. Bloom, M. I. Valic, and T. P. Higgs. 1976. Quadrupolar echo deuteron magnetic resonance spectroscopy in ordered hydrocarbon chains. *Chem. Phys. Lett.* 42:390-394.
30. Davis, J. H. 1983. The description of membrane lipid conformation, order and dynamics by  $^2\text{H}$ -NMR. *Biochim Biophys Acta* 737:117-171.
31. Lafleur, M., B. Fine, E. Sternin, P. R. Cullis, and M. Bloom. 1989. Smoothed orientational order profile of lipid bilayers by  $^2\text{H}$ -nuclear magnetic resonance. *Biophys J* 56:1037-1041.

32. Brooks, B. R., R. E. Bruccoleri, B. D. Olafson, D. J. States, S. Swaminathan, and M. Karplus. 1983. CHARMM: a program for macromolecular energy, minimization and dynamics calculation. *J. Comp. Chem.* 4:187-217.
33. Schlenkrich, M., J. Brickmann, A. D. J. Mackerell, and M. Karplus. 1997. An empirical potential energy function for phospholipids: criteria for parameter optimization and applications. In *Biological Membranes: A Molecular Perspective from Computational and Experiment*, (Merz, K.M. Jr and Roux, B., Eds.) Birkhauser, Boston, MA:31-81.
34. Feller, S. E., D. Yin, R. W. Pastor, and A. D. MacKerell, Jr. 1997. Molecular dynamics simulation of unsaturated lipid bilayers at low hydration: parameterization and comparison with diffraction studies. *Biophys. J.* 73:2269-2279.
35. Essmann, W., L. Perera, M. L. Berkowitz, T. Darden, H. Lee, and L. G. Pedersen. 1995. A Smooth particle mesh Ewald method. *J. Chem. Phys.* 103:8577-8593.
36. Ryckaert, J. P., G. Ciccotti, and H. J. C. Berendsen. 1977. Numerical integration of the cartesian equations of motion of a system with constraint: molecular dynamics of n-alkanes. *J. Comp. Phys.* 103:8577-8593.
37. Roark, M., and S. E. Feller. 2009. Molecular dynamics simulation study of correlated motions in phospholipid bilayer membranes. *J. Phys. Chem. B* 113:13229-13234.
38. Wassall, S. R., J. L. Thewalt, L. Wong, H. Gorrissen, and R. J. Cushley. 1986. Deuterium NMR study of the interaction of alpha-tocopherol with a phospholipid model membrane. *Biochemistry* 25:319-326.

39. Engel, A. K., and D. Cowburn. 1981. The origin of multiple quadrupole couplings in the deuterium NMR spectra of the 2 chain of 1,2 dipalmitoyl-sn-glycero-3-phosphorylcholine. *FEBS letters* 126:169-171.
40. Scott, H. L. 2002. Modeling the lipid component of membranes. *Curr. Opin. Struct. Bio.* 12:495-502.
41. Feller, S. E. 2007. Molecular dynamics simulations as a complement to nuclear magnetic resonance and X-ray diffraction measurements. *Methods in molecular biology* Clifton, N.J 40:89-102.
42. Seelig, J. 1977. Deuterium magnetic resonance: theory and application to lipid membranes. *Q Rev Biophys* 10:353-418.
43. Scott, E. F., and A. D. J. Mackerrell. 2000. An improved empirical potential energy function for molecular simulations of phospholipids. *J Phys. Chem B* 104:7510-7515.
44. Seelig, J., and N. Waespe-Sarcevic. 1978. Molecular order in cis and trans unsaturated phospholipid bilayers. *Biochemistry* 17:3310-3315.
45. Seelig, J., L. Tamm, L. Hymel, and S. Fleischer. 1981. Deuterium and phosphorus nuclear magnetic resonance and fluorescence depolarization studies of functional reconstituted sarcoplasmic reticulum membrane vesicles. *Biochemistry* 20:3922-3932.
46. Chiu, S. W., E. Jakobsson, S. Subramaniam, and H. L. Scott. 1999. Combined monte carlo and molecular dynamics simulation of fully hydrated dioleoyl and palmitoyl-oleoyl phosphatidylcholine lipid bilayers. *Biophys. J.* 77:2462-2469.

47. Huang, C., and S. Li. 1999. Calorimetric and molecular mechanics studies of the thermotropic phase behavior of membrane phospholipids. *Biochim. Biophys Acta* 1422:273-307.
48. Schindler, H., and J. Seelig. 1975. Deuterium order parameters in relation to thermodynamic properties of a phospholipid bilayer. A statistical mechanical interpretation. *Biochemistry* 14:2283-2287.
49. Jacobson, K., E. D. Sheets, and R. Simson. 1995. Revisiting the fluid mosaic model of membranes. *Science* 268:1441-1442.
50. Simons, K., and E. Ikonen. 1997. Functional rafts in cell membranes. *Nature* 387:569-572.
51. Edidin, M. 2003. The state of lipid rafts: from model membranes to cells. *Ann Rev. Biophys. Biomol. Struct.* 32:257-283.
52. Brown, D. A., and E. London. 2000. Structure and function of sphingolipid- and cholesterol-rich membrane rafts. *J. Bio. Chem.* 275:17221-17224.
53. Huster, D., K. Arnold, and K. Gawrisch. 1998. Influence of docosahexaenoic acid and cholesterol on lateral lipid organization in phospholipid mixtures. *Biochemistry* 37:17299-17308.
54. Mitchell, D. C., and B. J. Litman. 1998. Molecular order and dynamics in bilayers consisting of highly polyunsaturated phospholipids. *Biophys. J.* 74:879-891.
55. Shaikh, S. R., and M. A. Edidin. 2006. Membranes are not just rafts. *Chem. Phys. Lipids* 144:1-3.
56. Wassall, S. R., and W. Stillwell. 2008. Docosahexaenoic acid domains: the ultimate non-raft membrane domain. *Chem. Phys. Lipids*.



57. Polozova, A., and B. J. Litman. 2000. Cholesterol dependent recruitment of di22:6-PC by a G protein-coupled receptor into lateral domains. *Biophys. J.* 79:2632-2643.
58. Wassall, S. R., and W. Stillwell. 2009. Polyunsaturated fatty acid-cholesterol interactions: domain formation in membranes. *Biochim. Biophys. Acta* 1788:24-32.

Table 3.1: Temperature  $T_m$  for the gel to liquid crystalline phase transition determined by moment analysis of  $^2\text{H}$  NMR spectra

<b>Lipid Composition</b>	$T_m$ °C
18:0- $^{[2}\text{H}_{35}]$ 18:0PC	53.0
<i>t</i> 18:1- $^{[2}\text{H}_{35}]$ 18:0PC	31.5
<i>c</i> 18:1- $^{[2}\text{H}_{35}]$ 18:0PC	7.0

Table 3.2: Average order parameter  $\bar{S}_{CD}$  calculated from the first moment  $M_1$  for the  $[^2\text{H}_{35}]18:0$  *sn*-2 chain in *t*18:1- $[^2\text{H}_{35}]18:0\text{PC}$  and *c*18:1- $[^2\text{H}_{35}]18:0\text{PC}$  at 45 °C, and the corresponding value calculated from MD simulations. A temperature of 60 °C applies to the value of  $\bar{S}_{CD}$  stated for 18:0- $[^2\text{H}_{35}]18:0\text{PC}$

Lipid Composition	$\bar{S}_{CD}$	
	$^2\text{H}$ NMR	MD
<i>t</i> 18:1- $[^2\text{H}_{35}]18:0\text{PC}$	0.135	0.148
<i>c</i> 18:1- $[^2\text{H}_{35}]18:0\text{PC}$	0.128	0.146
18:0- $[^2\text{H}_{35}]18:0\text{PC}$	0.156	- <sup>a</sup>

<sup>a</sup> MD simulations were not performed on 18:0-18:0PC

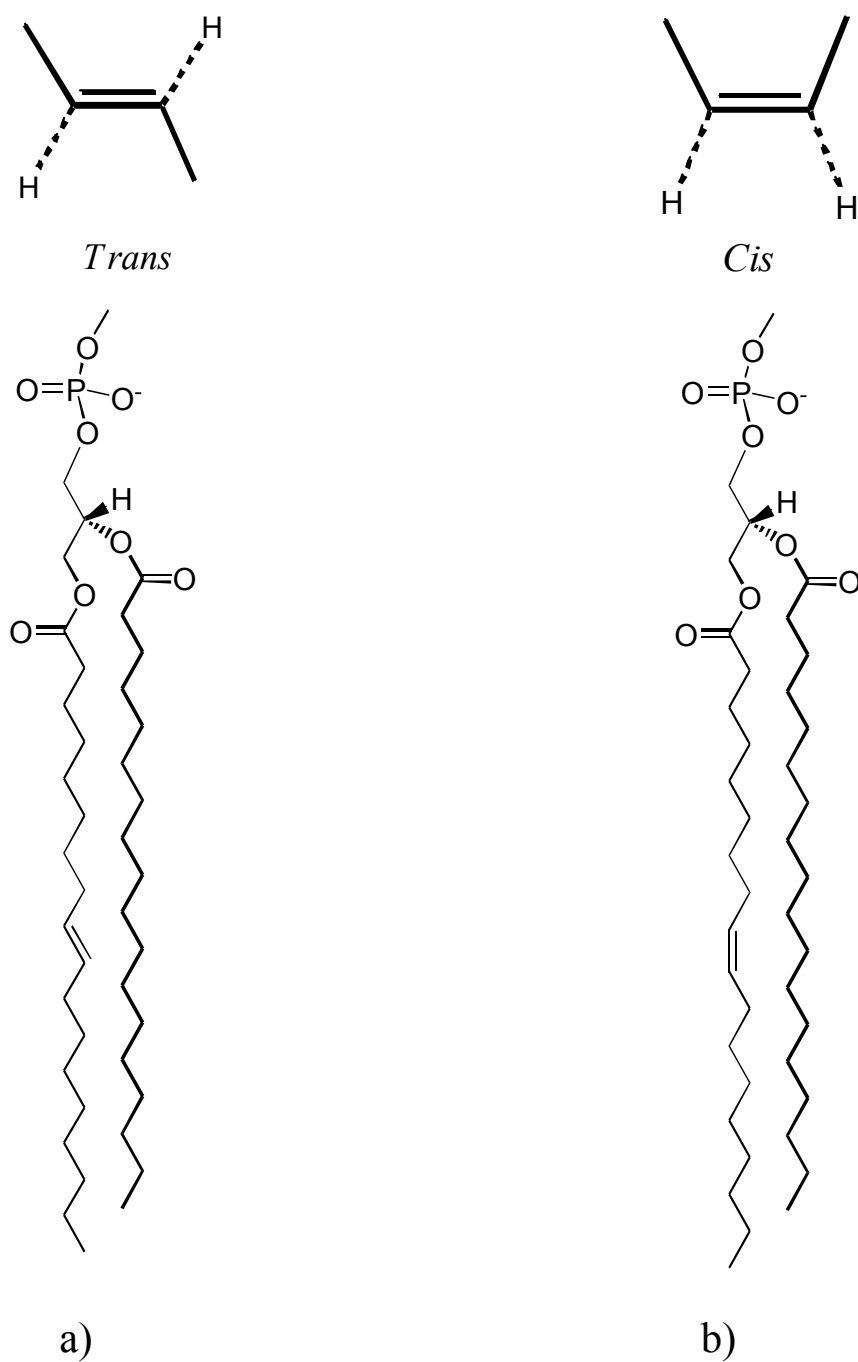


Figure 3.1: Molecular structure of a) *t*18:1-18:0PC and, b) *c*18:1-18:0PC. The dashed lines used in the figure are to emphasize the distinction in configuration between *trans* and *cis* double bonds

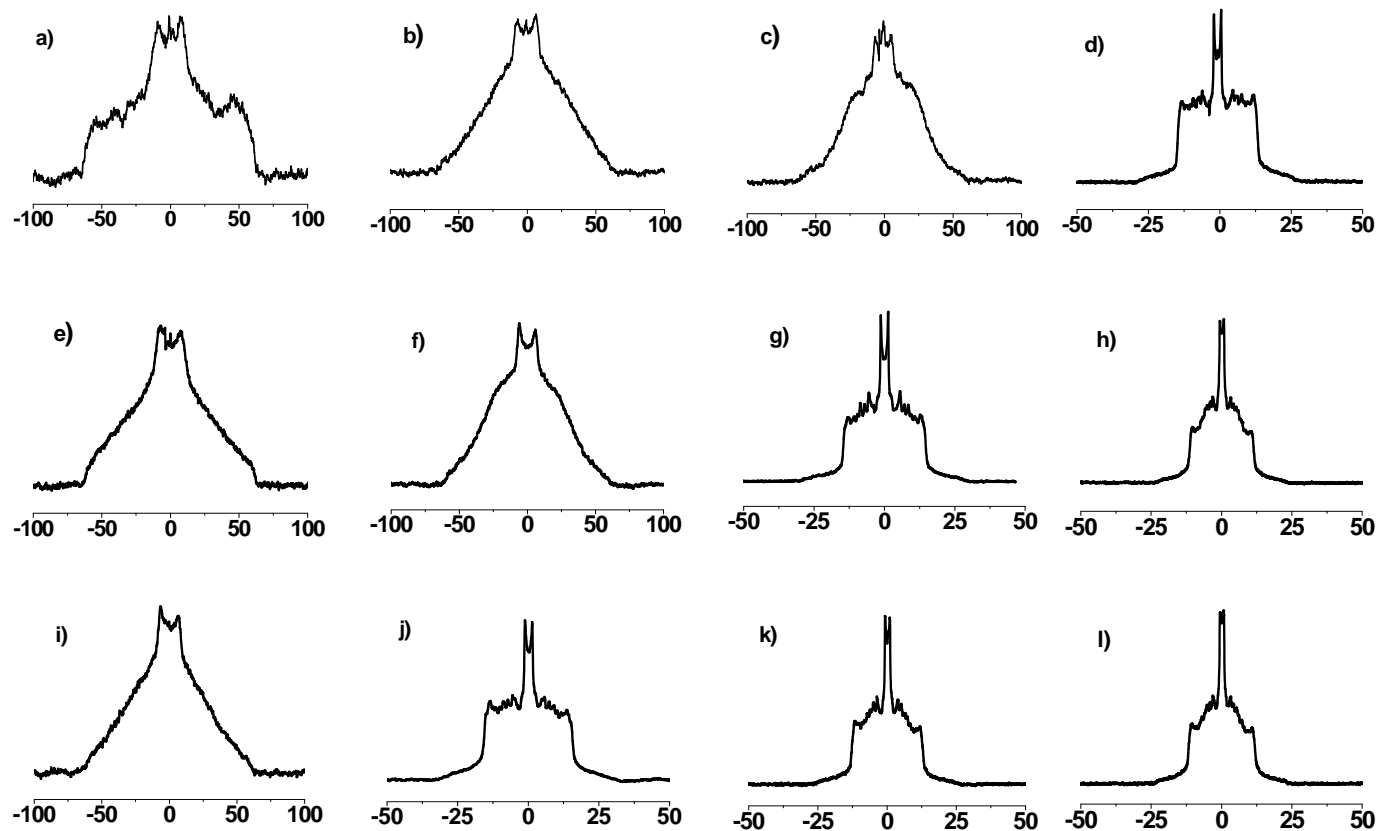


Figure 3.2:  $^2\text{H}$  NMR spectra for 50 wt% aqueous dispersions in 50 mM Tris (pH 7.5) of (a-d) 18:0- $[\text{}^2\text{H}_{35}]18:0\text{PC}$ , (e-h) *t*18:0- $[\text{}^2\text{H}_{35}]18:0\text{PC}$  and (i-l) *c*18:1- $[\text{}^2\text{H}_{35}]18:0\text{PC}$ . The spectra were recorded at (a, e and i)  $-5\text{ }^\circ\text{C}$ , (b, f and j)  $20\text{ }^\circ\text{C}$ , (c, g and k)  $45\text{ }^\circ\text{C}$  and (d, h and l)  $60\text{ }^\circ\text{C}$

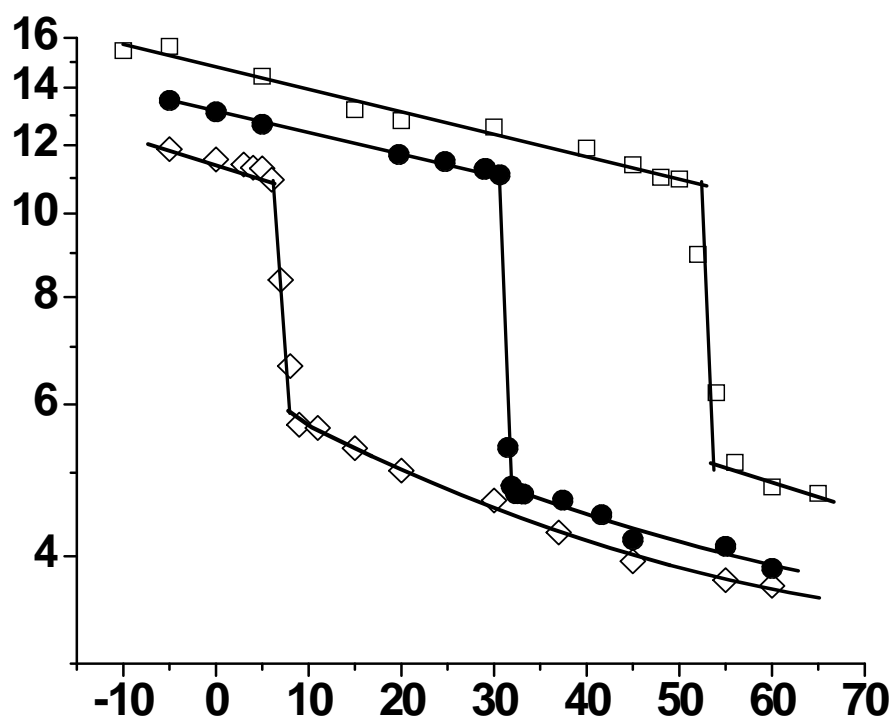


Figure 3.3: Variation of the first moment ( $M_1$ ) as a function of temperature for 18:0- $^{2}\text{H}_{35}$ 18:0PC (□), *t*18:0- $^{2}\text{H}_{35}$ 18:0PC (●) and *c*18:1- $^{2}\text{H}_{35}$ 18:0PC (◇).  $M_1$  is plotted logarithmically for clarity. The values given for the transition temperature  $T_m$  in Table 1 are the midpoint of the sharp drop in moment that accompanies chain melting

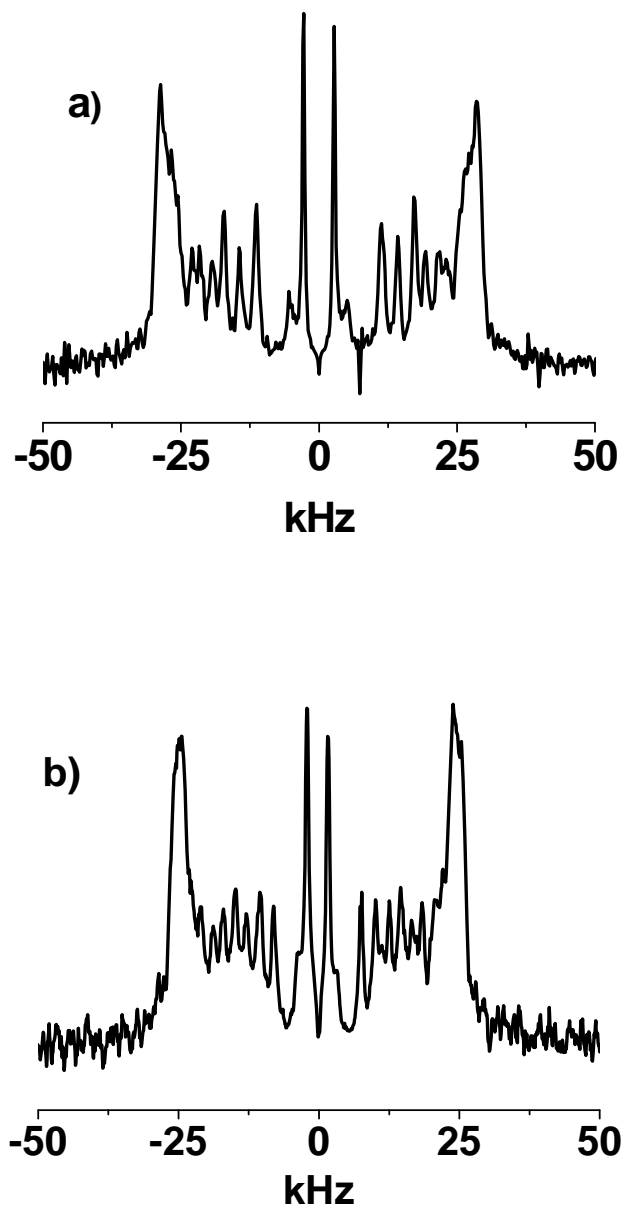


Figure 3.4: FFT depaked spectra for (a) *t*18:1- $^{2}\text{H}_{35}$ 18:0PC and (b) *c*18:1- $^{2}\text{H}_{35}$ 18:0PC at 45 °C

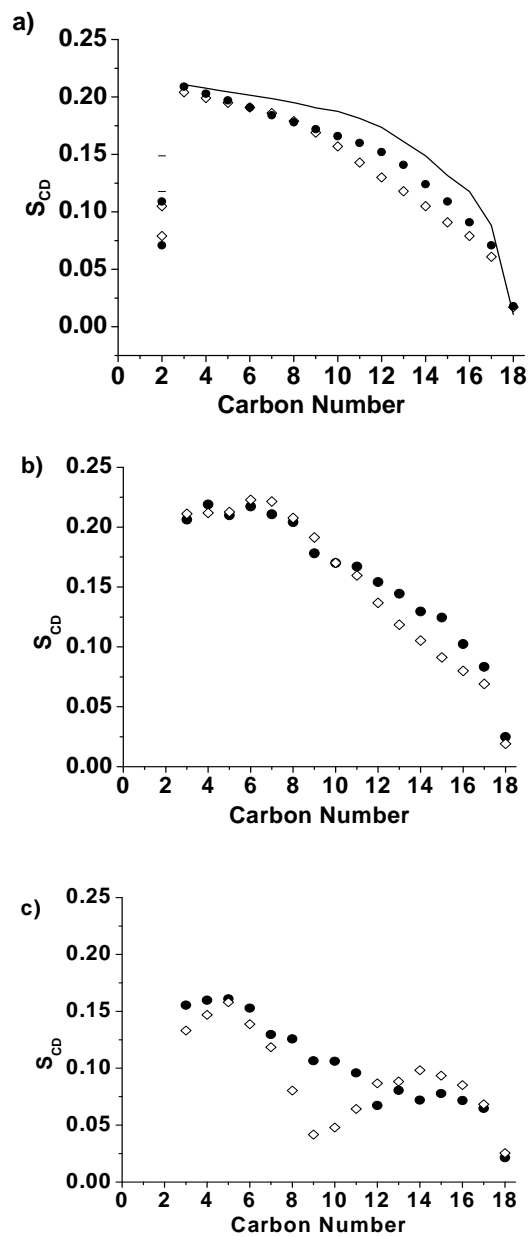


Figure 3.5: Order parameter profiles for  $t18:1-18:0PC$  (●) and  $c18:1-18:0PC$  (◇) at 45 °C generated from FFT depaked spectra for, a) the  $sn-2$  chain and from MD simulations for, b) the  $sn-2$  chain and, c) the  $sn-1$  chain. The continuous line included in (a) is the order parameter profile generated from depaked spectra for the  $sn-2$  chain of  $18:0-18:0PC$  at 60 °C



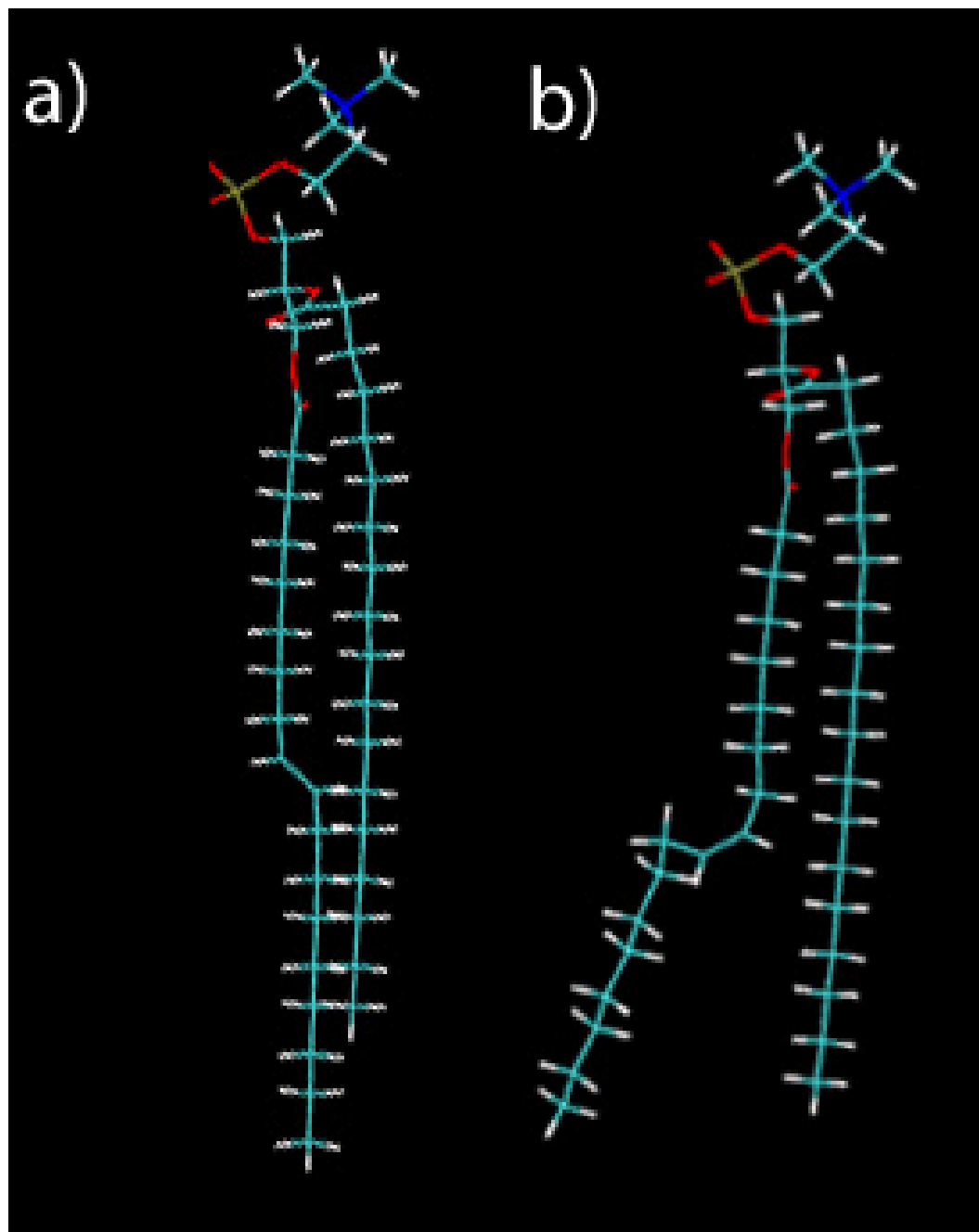


Figure 3.6: Energy minimized structure for, a) *t*18:1-18:0PC and, b) *c*18:1-18:0PC

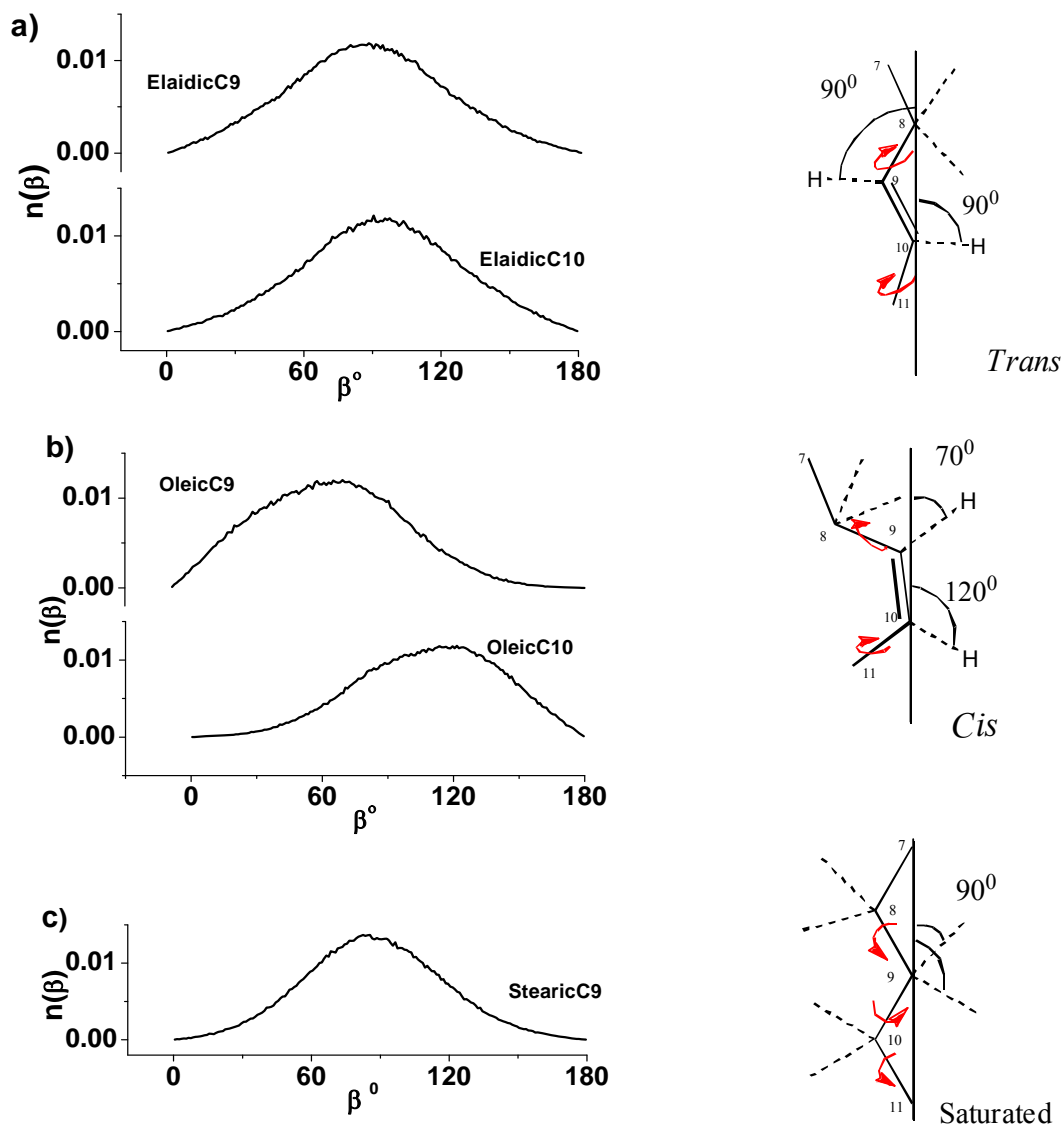


Figure 3.7: Normalized population distribution for the orientation of C-H bonds relative to the bilayer normal calculated from MD simulations for, a) the C9 and 10 positions in the *sn*-1 chain of *t*18:1-18:0PC, b) the C9 and 10 positions in the *sn*-1 chain of *c*18:1-18:0PC and, c) the C9 position in the *sn*-2 chain. To the right is a schematic representation of the most probable orientation implied by the maximum in each plot. The arrows indicate where rotations occur between carbons C8 and C11 (H atoms are omitted except on C9 and 10 at the double bond)

#### CHAPTER 4: DOCOSAHEXAENOIC ACID ENHANCES SEGREGATION OF LIPIDS BETWEEN RAFT AND NON-RAFT DOMAINS: $^2\text{H}$ NMR STUDY

The disease-counteracting benefits and necessity for neurological function of the  $\omega$ -3 family of polyunsaturated fatty acids (PUFA) are well documented (1,2). Docosahexaenoic acid (DHA,  $22:6^{\Delta 4,7,10,13,16,19}$ ), which with 22 carbons and 6 double bonds is the longest and most unsaturated member of this family found naturally, is particularly influential (3). The numerous varieties of human affliction that it alleviates include heart disease, cancer, rheumatoid arthritis, asthma, lupus and schizophrenia (3-5). To participate in so many seemingly unrelated processes, DHA must function at a fundamental level, common to most cells. We (3-5), and others (6,7), have proposed that the plasma membrane is a major site of action. According to our model, low affinity of DHA for cholesterol accentuates the formation of liquid disordered ( $l_d$ ) regions enriched in DHA-containing phospholipids and liquid ordered ( $l_o$ ) lipid rafts enriched in sphingomyelin (SM) and cholesterol. Introduction of DHA from the diet enhances the lateral segregation of these two distinct types of domain and accompanying changes in location of signaling proteins, for which rafts serve as the platform, then modulate cellular events.

Biological membranes were initially envisaged in the fluid mosaic model as a phospholipid bilayer matrix within which lipids and proteins were homogeneously mixed (8). A refinement of this picture has evolved over the last decade, whereby they contain functional domains characterized by different composition and spatial arrangement of the membrane-constituting lipids (9-11). These domains are the result of unequal affinities between lipids species or between lipids and membrane proteins. A lipid domain that has received a lot of attention is the lipid raft,  $l_o$  regions 10-200 nm in size enriched in cholesterol and sphingolipids that float in a “sea” of  $l_d$  phospholipids (10-13). When clustered together they serve as a site for the function of essential cell signaling proteins such as glycosylinositol phospholipid (GPI) -linked proteins in the outer leaflet of the plasma membrane (14). Raft formation is attributed to the saturated nature of sphingolipid acyl chains (15). Their predominantly all-trans extended conformation packs well with the rigid steroid moiety of cholesterol, while raft stability is further conferred by hydrogen bonding of the sphingosine backbone amide to the hydroxyl group of an adjacent sphingolipid as well as to the hydroxyl group of the sterol (16). Phospholipids containing DHA, in contrast, represent the opposite extreme to sphingolipids in affinity for cholesterol. Because polyunsaturated chains are tremendously disordered, close proximity to the steroid moiety is deterred by the wide variety of rapidly varying conformers adopted and affinity for the sterol is low (4). We hypothesize that when DHA-containing phospholipids are introduced into mixed membranes that include the lipid raft molecules SM and cholesterol, they enhance the segregation of cholesterol into SM-rich/sterol-rich rafts and away from DHA-rich domains that exclude the sterol (3-5). Modulation of cellular events produced by movement of signaling proteins in and/or out

of rafts due to changes in the architecture of plasma membranes following the incorporation of DHA from the diet into phospholipids is, in part, the origin we attribute for the myriad of health benefits associated with consumption of the PUFA.

Evidence in support of our hypothesis has been garnered applying a range of biophysical methodologies to a membrane model that we have developed comprised of 1-palmitoyl-2-docosahexaenoyl-*sn*-glycero-3-phosphoethanolamine (16:0-22:6PE, PDPE) in mixtures with SM and cholesterol (17). PE, which after phosphatidylcholine (PC) is the second most abundant phospholipid in mammalian plasma membranes (18), was selected since it is preferred over PC for the uptake of DHA that occurs at the *sn*-2 position while a saturated chain occupies the *sn*-1 position (19,20). It possesses a reduced affinity for cholesterol relative to PC and SM that is exemplified by the smaller solubility measured for the sterol in DHA-containing PE vs. PC (21). Differential scanning calorimetry (DSC), detergent extraction and solid state  $^2\text{H}$  NMR spectroscopy are among the principal techniques that we have applied to PE/SM and PE/SM/cholesterol mixtures in a series of studies (17, 22). Detergent extraction of PDPE/egg SM/cholesterol (1:1:1 mol) membranes showed that egg SM and cholesterol phase separate almost exclusively (>90%) into a detergent resistant membrane (DRM) fraction, the biochemical hallmark of lipid rafts (11), whereas PDPE predominantly phase separates (70%) into a non-raft detergent soluble membrane (DSM) fraction (17). Much less phase separation (22%) into DSM, on the contrary, was seen for 1-palmitoyl-2-oleoyl-*sn*-glycero-3-phosphoethanolamine (16:0-18:1PE, POPE) in POPE/egg SM/cholesterol (1:1:1 mol) where polyunsaturated DHA was replaced by more “typical” monounsaturated oleic acid (OA) (18) at the *sn*-2 position of PE. As in the DHA-containing system, egg SM and

cholesterol were almost entirely (>90%) found in DRM in the control OA-containing system. Solid state  $^2\text{H}$  NMR spectra comparing the effect of cholesterol on  $[\text{}^2\text{H}_{31}]16:0-22:6\text{PE}$  (PDPE\*)/egg SM (1:1:1 mol) and  $[\text{}^2\text{H}_{31}]16:0-18:1\text{PE}$  (POPE\*)/egg SM (1:1:1 mol) demonstrated a diminished interaction between the sterol and DHA- relative to OA-containing PE (17). The increase in average order  $\bar{S}_{CD}$  of the perdeuterated  $[\text{}^2\text{H}_{31}]16:0$  *sn*-1 chain for the polyunsaturated component ( $\Delta\bar{S}_{CD} = 0.039$ ) in the mixed membrane was more than a factor of 2 less than for the monounsaturated component ( $\Delta\bar{S}_{CD} = 0.100$ ) following the addition of cholesterol at 40 °C.

Here we switch the focus from PE to SM in our model system. Solid state  $^2\text{H}$  NMR, complemented by DSC, is employed in the first report to compare  $[\text{}^2\text{H}_{31}]$ -N-palmitoylsphingomyelin ( $[\text{}^2\text{H}_{31}]16:0\text{SM}$ , PSM\*) in PDPE/PSM\* (1:1 mol) with POPE/PSM\* (1:1 mol) in the absence and presence of cholesterol (1:1:1 mol). PSM is the major constituent (~85%) of egg SM (23), so that the results obtained provide information about the impact of the sterol on the molecular organization of the SM component in mixed membranes that approximate very closely to those for which the PE component was previously observed. We examine whether our hypothesis that the aversion of cholesterol for DHA promotes the formation of PUFA-rich/sterol-poor domains, as implied by the spectra recorded for PDPE\* vs. POPE\* in PE/egg SM/cholesterol (1:1:1 mol) mixtures (17), is corroborated by the spectra observed for PSM\* in the corresponding PE/PSM/cholesterol (1:1:1 mol) mixtures.

## Materials and Methods

### Materials

POPE, PDPE and egg SM were purchased from Avanti Polar Lipids (Alabaster, AL). Cholesterol and deuterium depleted water were obtained from Sigma Chemical Co. (St. Louis, MO). Cambridge Isotope Laboratories (Andover, MA) was the source of [ $^2\text{H}_{31}$ ]palmitic acid. Lipid purity was confirmed by thin-layer chromatography.

### PSM\* synthesis

PSM\* was synthesized by *N*-acylation of *D*-erythro-sphingosylphosphocholine with the *p*-nitrophenyl ester of [ $^2\text{H}_{31}$ ]palmitic acid in dichloromethane/*N,N*-dimethylformamide (2:5 vol/vol.) at room temperature under nitrogen (24). The volatiles were removed under vacuum, and the product was purified by column chromatography (elution with chloroform/methanol/water 65:35:5 vol) followed by filtration through a Cameo filter to remove suspended silica gel and lyophilization.

### PSM isolation

PSM was isolated from egg SM by reverse-phase high-performance liquid chromatography (HPLC) (25). Briefly, egg SM was run through a dual-pump HPLC setup (Beckman Coulter, Inc., Fullerton, CA) utilizing an analytical reverse-phase Alltima C-18 RP column (5  $\mu\text{m}$  particle size, 250 mm x 10 mm)

(Alltech Associates, Inc., Deerfield, IL) and methanol with 6 vol% water as the eluent (4.2 mL/min at 40 °C). Purity of the PSM obtained was verified by  $^1\text{H}$  NMR spectroscopy and mass spectrometry.

### $^2\text{H}$ NMR sample preparation

Lipid mixtures (75-90 mg total lipid) comprised of POPE/PSM\* (1:1 mol), POPE/PSM\*/cholesterol (1:1:1 mol), PDPE/PSM\* (1:1 mol) and PDPE/PSM\*/cholesterol (1:1:1 mol) were co-dissolved in chloroform. The organic solvent was evaporated under a gentle stream of argon followed by vacuum pumping to ensure removal of traces of solvent. Each lipid mixture was hydrated to 50 wt % with 50 mM Tris buffer (pH 7.5) and vortexed vigorously. Deuterium depleted water (~2 mL) was added to allow measurement of pH which was adjusted to 7.5. Three lyophilizations in the presence of excess deuterium depleted water were then performed to remove naturally abundant  $^2\text{HHO}$ . After finally hydrating to 50 wt%, the resultant samples were transferred to a 5 mm NMR tube that was sealed with a Teflon coated plug. They were stored at -80 °C and equilibrated at room temperature before the experiments. Precautions to prevent oxidation were taken throughout sample preparation. All manipulations were carried out in an argon atmosphere within a homebuilt glovebox, buffer and deuterium depleted water were thoroughly degassed, and exposure to light was minimized (22).



## $^2\text{H}$ NMR Spectroscopy

Solid state  $^2\text{H}$  NMR experiments were performed on a home-built spectrometer operating at 27.6 MHz with a 4.2 T Nalorac super-conducting magnet (26). A PC controlled the spectrometer. Pulse programming was accomplished with a UBC programmable pulse generator (Vancouver, BC), while signals were acquired in quadrature using a Rapid Systems R1200 M dual channel digital oscilloscope (Seattle, WA). Sample temperature was regulated to  $\pm 0.5$  °C by a Love Controls 1600 Series temperature controller (Michigan City, IN). A phase alternated quadrupolar echo sequence ( $90^\circ_x - \tau - 90^\circ_y - \text{acquire} - \text{delay}$ )<sub>n</sub> that eliminates spectral distortion due to receiver recovery time was implemented to collect spectra (27). Unless otherwise stated, spectral parameters were:  $90^\circ$  pulse width  $\approx 6$   $\mu\text{s}$ ; separation between pulses  $\tau = 50$   $\mu\text{s}$ ; delay between pulse sequences = 1.0 s (gel phase) or 1.5 s (liquid crystalline phase); sweep width =  $\pm 250$  kHz (gel phase) or  $\pm 100$  kHz (liquid crystalline phase); dataset = 2K; and number of transients = 2048.

### Analysis of $^2\text{H}$ NMR spectra

First moments  $M_1$  were calculated from  $^2\text{H}$  NMR spectra for PSM\* in POPE/PSM\* (1:1 mol), POPE/PSM\*/cholesterol (1:1:1 mol), PDPE/PSM\* (1:1:1 mol) and PDPE/PSM\*/cholesterol (1:1:1 mol) mixtures with

$$M_n = \frac{\int_{-\infty}^{+\infty} |\omega|^n |f(\omega)| d\omega}{\int_{-\infty}^{+\infty} f(\omega) d\omega} \quad (1)$$

Where  $\omega$  is the frequency with respect to the central Larmor frequency  $\omega_o$  and  $f(\omega)$  is the lineshape (28). In practice the integral was a summation over the digitized data. The expression

$$M_1 = \frac{\pi}{\sqrt{3}} \left( \frac{e^2 q Q}{h} \right) \bar{S}_{CD} \quad (2)$$

relates the first moment  $M_1$  to the average order parameter  $\bar{S}_{CD}$  of the perdeuterated palmitoyl amide side chain via the static quadrupole coupling constant  $\left( \frac{e^2 q Q}{h} \right) = 167$  kHz in the lamellar liquid crystalline phase.

Spectra were also fast Fourier Transform (FFT) deconvoluted to enhance resolution in the lamellar liquid crystalline phase (26). This numerical procedure extracts from the powder pattern signal a spectrum that is representative of a planar membrane of single alignment. The deconvoluted spectra consist of doublets with quadrupolar splittings  $\Delta \nu(\theta)$  that equate to order parameters by

$$\Delta \nu(\theta) = \frac{3}{2} \left( \frac{e^2 q Q}{h} \right) |S_{CD}| P_2(\cos \theta) \quad (3)$$

where  $\theta = 0^\circ$  is the angle the membrane normal makes with the magnetic field and  $P_2(\cos \theta)$  is the second-order Legendre polynomial. Smoothed profiles of order along the perdeuterated palmitoyl amide side chain were then constructed on the basis of integrated intensity assuming monotonic variation towards the disordered center of the bilayer (29). Constraints imposed upon the initial orientation of the chain render the C2 position an exception to this assumption and  $S_{CD}$  values there were assigned on the basis of intensity and comparison with work on selectively deuterated analogs of PSM (30).

### Differential Scanning Calorimetry

DSC experiments were conducted as previously described (31). The preparation of aqueous dispersions of 0.5 wt% POPE/PSM (1:1 mol), POPE/PSM/cholesterol (1:1:1 mol), PDPE/PSM (1:1 mol) and PDPE/PSM/cholesterol (1:1:1 mol) in 10 mM phosphate

buffer (pH 7.4) was similar to that employed to prepare the NMR samples, except that lyophilization to remove natural abundance  $^2\text{H}$  was unnecessary. Degassing was particularly critical because dissolved gases not only have the potential to attack PUFA but also contribute noise to high sensitive calorimetry measurements. Heating and cooling scans for 500  $\mu\text{L}$  samples were run at 0.125  $^\circ\text{C}/\text{min}$  from -10 to 60  $^\circ\text{C}$  against a lipid-free control buffer on a Calorimetry Sciences MCDSC multi-cell differential scanning calorimeter (Calorimetry Sciences, Lindin, UT). Only the cooling scans are presented although data derived from both scans appeared nearly identical. Baseline subtraction was accomplished with CpCalc v2.1 (Applied Thermodynamics, Longwood, FL), while analysis of endotherms was carried out using Origin 7.0 graphing software (OriginLab, Northampton, MA).

## RESULTS

### Phase Behavior

#### $^2\text{H}$ NMR

Solid state  $^2\text{H}$  NMR spectra for 50 wt% aqueous dispersions of POPE/PSM\* (1:1 mol), PDPE/PSM\* (1:1 mol), POPE/PSM\*/cholesterol (1:1:1 mol) and PDPE/PSM\*/cholesterol (1:1:1 mol) in 50 mM Tris (pH 7.5) were obtained as a function of temperature to study the phase behavior of the perdeuterated sphingolipid in lipid mixtures with OA- and DHA-containing PE in the absence and presence of cholesterol. They were collected from -30 to 50  $^\circ\text{C}$ . This range of temperature encompasses the gel to liquid crystalline transition for single component membranes of PSM at 41  $^\circ\text{C}$  (32),

POPE at 25.5 °C (22) and for PDPE at 2.2 °C (22). Only one study of PSM\* has been published to date, employing membranes aligned between glass slides to improve spectral resolution (30). Here we employ multilamellar dispersions and apply lineshape analysis to the powder patterns observed that are comprised of a superposition of signals from the random orientational distribution of membranes that exists within a sample.

Representative examples of the spectra for POPE/PSM\* (1:1 mol) are shown in Figure 4.1 (left panel). They display changes in the spectral shape that accompany the transition between gel and liquid crystalline states as the suspension is heated. The wide, relatively featureless spectrum with edges at  $\pm 63$  kHz that was recorded at -23 °C is typical of a lamellar gel phase (Figure 4.1a). The [ $^2\text{H}_{31}$ ]16:0 chains of PSM\* are rigid and their slow rotational diffusion confers non-axial symmetry on the spectral shape (17). Upon raising the temperature, additional molecular motions are introduced that result in spectral narrowing. Inspection of the spectrum at 12 °C reveals that while still broad and gel-like, there is less intensity in the wings (Figure 4.1b). At higher temperature shoulders around  $\pm 20$  kHz appear superposed upon the broad gel component and grow at the expense of the broad component that by 27 °C has disappeared (Figure 4.1c). They indicate the initiation of fast axial rotation for PSM\* at the onset of its transition to the liquid crystalline phase within the mixture with POPE. As shown by the spectrum observed at 52 °C that characterizes the lamellar liquid crystalline state (27), a further increase in temperature leads to the resolution of peaks within the spectrum (Figure 4.1d). Rapid isomerization about C-C bonds in the [ $^2\text{H}_{31}$ ]16:0 chains of PSM\* is responsible. A superposition of doublets with similar splitting, corresponding to the plateau region of relatively constant order in the upper part of the chain, produces the well-defined edges at

$\pm 19$  kHz. Less ordered methylenes in the lower part of the acyl chain primarily give rise to doublets with dissimilar splitting that appear as the individual peaks within the spectrum, while the highly mobile terminal methyl is represented by the central pair of peaks.

Figure 4.1 (right panel) presents spectra for a 50 wt% aqueous dispersion of POPE/PSM\*/cholesterol (1:1:1 mol) in 50 mM Tris (pH 7.5) that illustrate the effect of cholesterol on the phase behavior of PSM\* in the OA-containing PE lipid mixture. Although gel-like in form, substantial narrowing due to the presence of cholesterol is apparent in the spectrum at  $-23$  °C (Figure 4.1e). This spectral narrowing reflects the sterol-induced disruption to the organized packing of acyl chains in the gel state. Even greater perturbation is apparent in the spectrum obtained at  $12$  °C (Figure 4.1f). Whereas the spectrum is entirely attributable to gel-phase lipid in the absence of cholesterol (Figure 4.1b), the spectrum for PSM\* in the mixture with POPE can be assigned completely to the lamellar liquid crystalline phase following the addition of sterol (Figure 4.1f). The spectra observed for POPE/PSM\*/cholesterol (1:1:1 mol) upon heating to  $27$  and  $52$  °C (Figure 4.1g and 4.1h) are similarly characteristic of the liquid crystalline state. There is spectral broadening associated with a reduction in gauche-trans isomerization along the fluid [ $^2\text{H}_{31}$ ]16:0 chain of the sphingolipid by the rigid steroid moiety that is exemplified by an increase from  $\pm 19$  to  $\pm 26$  kHz in the width of the sharp edges that the spectra without (Figure 4.1d) and with (Figure 4.1h) cholesterol possess at  $52$  °C.

The spectra in Figure 4.2 (left panel) were recorded for a 50 wt% aqueous dispersion of PDPE/PSM\* (1:1 mol) in 50mM Tris (pH 7.5) (1:1) under the same experimental conditions employed with the spectra shown for POPE/PSM\* (1:1 mol) in

Figure 4.1. Differences in the phase behavior of PSM\* when mixed with DHA- vs. OA-containing PE are revealed by comparing the spectra. The lineshape for PDPE/PSM\* (1:1 mol) (Figure 4.2a), as for POPE/PSM\* (1:1 mol) (Figure 4.1a), is gel-like at -23 °C. Greater restriction to chain motion is implied for PSM\* in the mixture with PDPE by enhanced intensity in the wings of the spectrum. At 12 °C the spectrum for PDPE/PSM\* (1:1 mol) (Figure 4.2b), unlike POPE/PSM\* (1:1 mol) (Figure 4.1b), no longer contains the shoulders at  $\pm 63$  kHz that designate gel phase. Instead, a component of width  $\pm 25$  kHz that represents methylene groups undergoing axial rotation together with a central methyl component comprise the entire spectrum. An additional rise in temperature introduces gauche-trans isomerization into the perdeuterated chain of PSM\* and leads to the appearance of individual peaks within the methylene component of the spectrum acquired at 27 °C (Figure 4.2c). These peaks become better resolved upon heating, resulting in the observation of the characteristic liquid crystalline powder pattern at 52 °C (Figure 4.2d). The spectra for PSM\* in the mixed membrane with polyunsaturated PDPE at these latter two temperatures resemble those seen with POPE at the equivalent temperatures (Figure 4.1c and 4.1d).

In Figure 4.2 (right panel),  $^2\text{H}$  NMR spectra that were acquired for an aqueous dispersion of PDPE/PSM\*/cholesterol (1:1:1 mol) in 50 mM Tris buffer (pH 7.5) examine how adding cholesterol affects the phase behavior of PSM\* in the DHA-containing PE mixed membrane. They are qualitatively similar to the spectra seen for POPE/PSM\*/cholesterol (1:1:1 mol) (Figure 4.1, right panel). Like in the OA-containing PE mixture, the response to sterol consists of a disordering and ordering of gel- and liquid crystalline-state PSM\*, respectively. Compared to the spectrum for PDPE/PSM\* at -23

°C (Figure 4.2a) that is typical of solely gel phase, a spectral component with shoulders at  $\pm 25$  kHz indicating the onset of fast axial rotation for the perdeuterated  $[^2\text{H}_{31}]16:0$  chain of PSM\* is apparent upon the broad gel-like background when cholesterol is present (Figure 4.2e). The spectrum becomes completely liquid crystalline-like upon heating to 12 °C (Figure 4.2f), displaying the peaks within the methylene envelope that signify rapid isomerization. Such peaks are not discernible at the corresponding temperature in the spectrum obtained in the absence of sterol (Figure 4.2b) and, as illustrated by the spectra at 27 (Figure 4.2c) and 52 °C (Figure 4.2d), do not appear and subsequently grow in resolution until higher temperature is reached. In contrast, the spectrum for PDPE/PSM\*/cholesterol (1:1:1 mol) changes little apart from modestly narrowing over the same temperature interval (Figure 4.2g and 4.2h). The differential in spectral width ( $\pm 25$  vs.  $\pm 18$  kHz) with (Figure 4.2h) and without (Figure 4.2d) cholesterol at 52 °C is symptomatic of the sterol-induced increase in order for liquid crystalline PSM\* in PDPE/PSM\* (1:1 mol).

The spectra shown in Figures 4.1 and 4.2 are representative of data obtained in each case over a temperature range that extends from -30 to 50 °C. They illustrate the sensitivity of spectral lineshape to membrane phase. To quantify the shape of all of the spectra and thereby monitor phase behavior, first moments  $M_1$  were calculated according to eq. 1 and are plotted against temperature in Figure 4.3 for POPE/PSM\* (1:1 mol) and for PDPE/PSM\* (1:1 mol) in the absence and presence of cholesterol (1:1:1 mol). Slowly varying moments of magnitude  $M_1 > 10 \times 10^4 \text{ s}^{-1}$ , signifying gel phase, and  $< 8 \times 10^4 \text{ s}^{-1}$ , signifying liquid crystalline phase, were measured for POPE/PSM\* (1:1 mol) at temperatures  $< 19$  and  $> 24$  °C, respectively (Figure 4.3a). The sharp drop in the value of

$M_1$  that accompanies the transition between states is  $\sim 5$  °C in width and centered at 22.5 °C. No discontinuity in the variation of first moment with temperature remains for PSM\* in the OA-containing PE mixture after the addition of cholesterol (Figure 4.3a). A broadening of the phase transition to near elimination is indicated by  $M_1$  values that gradually decrease from  $10.5 - 8.7 \times 10^4 \text{ s}^{-1}$  over the entire -30 to 50 °C span of temperature studied.

The variation with temperature of the first moments plotted for PDPE/PSM\* (1:1 mol) (Figure 4.3b) takes the same form as that seen for POPE/PSM\* (1:1 mol) (Figure 4.3a). There is an abrupt reduction in  $M_1$  value centered at 13.7 °C and  $\sim 4$  °C wide indicative of a precipitous increase in molecular motion. The moments otherwise vary slowly from  $13.4 \times 10^4 \text{ s}^{-1}$  at -32 °C to  $10.4 \times 10^4 \text{ s}^{-1}$  at 12 °C and from  $8.2 \times 10^4 \text{ s}^{-1}$  at 15 °C to  $6.2 \times 10^4 \text{ s}^{-1}$  at 52 °C. It should be noted that in the region where the dramatic change occurs, most markedly at 12 °C, the moments depend upon the delay time  $t$  between the two 90° pulses in the quadrupolar echo sequence. The values plotted there were obtained by extrapolation to zero delay of  $M_1$  measured as a function of  $t$ . We attribute this behavior to the presence of (intermediate) exchange of PSM\* between motionally distinct environments in the PDPE/PSM\* mixture on a timescale comparable to the delay between pulses. As with POPE/PSM\* (Figure 4.3a), the moments presented in Figure 4.3b for PSM\* in the DHA-containing mixed membrane no longer exhibit a discontinuity on the addition of 1:1:1 mol cholesterol. They slowly fall from  $10.3 \times 10^4 \text{ s}^{-1}$  at -32 °C to  $8.2 \times 10^4 \text{ s}^{-1}$  at 52 °C. The small range of the  $M_1$  values is consistent with a sterol-associated smearing out of changes in molecular organization with temperature.



## DSC

DSC cooling scans for 0.5 wt% aqueous dispersions of POPE/PSM (1:1 mol) (Figure 4.3c) and PDPE/PSM (1:1 mol) (Figure 4.3d) in 10 mM phosphate buffer (pH 7.4) are included in Figure 4.3 for purposes of comparison. The scan for POPE/PSM (1:1) consists of an endotherm that peaks at 25.8 °C and is 2.7 °C in width at half height (Figure 4.3c). It closely resembles the scan recorded employing egg SM instead of PSM in our earlier work (17), on the basis of which the broad endotherm is interpreted as a superposition of two transitions ascribed to POPE-rich/SM-poor and POPE-poor/SM-rich regions that possess very similar transition temperatures. Consistent with this interpretation, the mid-point in the discontinuity of the spectral moments measured here for the melting of PSM\* in POPE/PSM\* (1:1 mol) at 22.5 °C (Figure 4.3a) is close to that measured previously for POPE\* in POPE\*/egg SM (1:1 mol) at ~23 °C (17). The temperature for the peak of the composite endotherm lies slightly above the temperatures identified from NMR. A lowering by 3-4 °C of the transition temperature due to perdeuteration (30) is likely responsible for the difference. No endotherm is observed upon addition of cholesterol at 1:1:1 mol concentration (data not shown), in agreement with the behavior previously reported for POPE/egg SM/cholesterol (1:1:1 mol) (17).

The cooling scan for PDPE/PSM (1:1 mol) shown in Figure 4.3d, in contrast to POPE/PSM (1:1 mol) (Figure 4.3c), displays two separate endotherms as we previously saw with PDPE/egg SM (1:1 mol) (17). The peak temperature of the lower transition assigned to a PDPE-rich/PSM-poor phase is 11.6 °C, while that of the higher transition assigned to a PDPE-poor/PSM-rich phase is 26.8 °C. The temperature of the former

transition is near that of an abrupt drop in first moment recorded at  $\sim 7$  °C for PDPE\* in PDPE\*/egg SM (1:1 mol) in our earlier work (17), but the latter transition is much higher in temperature than the precipitous drop centered at 13.7 °C revealed in the current study by spectral moments for PSM\* in PDPE/PSM\* (1:1 mol) (Figure 4.3b). This divergence, which is too great to be explained by isotopic substitution, is due to the inherently different nature of the two types of measurement. Whereas the transition detected by DSC directly represents the excess specific heat absorbed when lipid acyl chains melt, other molecular motions can lead to the narrowing of NMR spectra reflected in a reduction in moment. This issue will be discussed later. Addition of cholesterol in 1:1:1 mol amount eliminates both endotherms (data not shown), as was similarly seen when the same concentration of cholesterol was added to PDPE/egg SM (1:1 mol) (17).

### Acyl Chain Order

The liquid crystalline phase is representative of the biological state of lipid molecules. In this phase where rapid reorientation of lipid molecules results in spectra symptomatic of axially symmetry, the first moment  $M_1$  calculated from  $^2\text{H}$  NMR spectra for perdeuterated lipid chains is related to the average order parameter  $\bar{S}_{CD}$  for the entire chain via equation 2. Table 1 lists the  $\bar{S}_{CD}$  values obtained at 35 °C for POPE/PSM\* (1:1 mol), POPE/PSM\*/cholesterol (1:1:1 mol), PDPE/PSM\* (1:1 mol) and PDPE/[ $^2\text{H}_{31}$ ]PSM\*/cholesterol (1:1:1 mol). Inspection reveals that, as expected, cholesterol restricts the molecular motion of PSM\* in both POPE/PSM\* and PDPE/PSM\*.

In the former mixture order increases by  $\Delta\bar{S}_{CD} = 0.059$  from  $\Delta\bar{S}_{CD} = 0.237$  to 0.296, while  $\Delta\bar{S}_{CD} = 0.064$  from  $\Delta\bar{S}_{CD} = 0.227$  to 0.291 is the increase in the latter mixture.

The relatively modest distinction between the response of the molecular organization of SM to the addition of sterol in the two systems contrasts with the markedly different increase in order revealed for the PE component by  $\bar{S}_{CD}$  values for POPE\*/egg SM (1:1 mol) and PDPE\*/egg SM (1:1 mol) (4) that are also included in Table 1. The data demonstrate that although the [ $^2\text{H}_{31}$ ]16:0 *sn*-1 chain of POPE\* ( $\bar{S}_{CD} = 0.167$ ) in POPE\*/egg SM (1:1 mol) and PDPE\* ( $\bar{S}_{CD} = 0.165$ ) in PDPE\*/egg SM (1:1 mol) possesses almost identical order, there is an appreciable differential in the effect of cholesterol (1:1:1 mol). Whereas  $\Delta\bar{S}_{CD} = 0.099$  characterizes the elevation in order of the OA-containing PE owing to the sterol, the corresponding change of  $\Delta\bar{S}_{CD} = 0.043$  for the DHA-containing PE is substantially less.

To elaborate upon the distribution of order along the perdeuterated [ $^2\text{H}_{31}$ ]16:0 amide chain of PSM\* in the mixed membranes, the NMR signals were FFT depaked (26). The result of the application of this algorithm to POPE/PSM\* (1:1 mol) (Figure 4.4a and 4.4b) and PDPE/PSM\* (1:1 mol) (Figure 4.4c and 4.4d) in the absence and presence of cholesterol (1:1:1 mol), respectively, at 44 °C is illustrated in Figure 4.4. The depaked spectra consist of an outermost composite doublet, representing comparably ordered methylene groups in the upper part of the chain, and a series of 4 doublets with smaller splittings, predominantly corresponding to increasingly less ordered methylene groups and terminal methyl group in the lower portion of the chain. The vast enhancement in resolution achieved relative to the powder pattern facilitates the generation of a profile of order parameter with the aid of equation 3. The procedure, apart from the C2 position,

consists of assigning equal intensity to each methylene group and assuming a continuous decrease of order towards the terminal methyl (29). Constraints imposed upon the initial orientation of the amide chain of SM (30), like with the *sn*-2 chain of phospholipids (33), render the C2 position an exception to the assumption that order varies monotonically. The two motionally inequivalent deuterons at this position possess different splittings that were assigned as indicated in Figure 4.4 on the basis of intensity and comparison with work on selectively deuterated PSM (30).

The order parameter profiles created from the depaked spectra in Figure 4.4 are shown in Figure 4.5. It is apparent that the same general form is observed in each case. There is a plateau region of approximately constant order in the upper portion of the chain (C3-C12) followed by progressively less order towards the bottom of the chain (C13-C16). This shape is characteristic of phospholipids (34) and sphingolipids (30) in the lamellar liquid crystalline phase. It is retained when cholesterol is added to POPE/PSM\* (1:1 mol) (Figure 4.5a) and PDPE/PSM\* (1:1 mol) (Figure 4.5b), with the increase in average order  $\bar{S}_{CD}$  calculated from the first moment  $M_1$  (Table 1) manifest as higher  $\bar{S}_{CD}$  values throughout the chain.

### Discussion

A diverse collection of health benefits accrues from the dietary consumption of PUFA, most notably DHA (35). We have hypothesized that changes in membrane architecture in response to elevated levels of DHA-containing phospholipids are, in part, responsible (3-5). Our hypothesis juxtaposes the tremendously high disorder of PUFA chains for which close proximity to cholesterol is incompatible, with the highly ordered

(l<sub>o</sub>) conformation adopted by the mostly saturated chains of sphingolipids in sterol-enriched lipid rafts. Due to the differential in affinity, cholesterol further segregates into lipid rafts away from PUFA-rich domains that form when polyunsaturated phospholipids substitute for bulk less unsaturated phospholipids in the plasma membrane. It is the concomitant movement of signaling proteins into and out of rafts and resultant modulation of cell signaling to which the relief of disease states by DHA is ascribed.

Mixtures of PDPE with SM and cholesterol are a model membrane system that we have developed to characterize the sorting of lipids into PUFA-rich/sterol poor (non raft) and SM-rich/sterol-rich (raft) domains. Early DSC work on ternary lipid/lipid/cholesterol mixtures indicated that cholesterol associates with PE less strongly than PC and SM (36). This finding, as well as diminished affinity for polyunsaturated phospholipids, was confirmed by an assay with cyclodextrin of partition coefficients for cholesterol in unilamellar vesicles (37). Unequivocal substantiation of aversion for the sterol is provided by the substantially lower solubility measured for cholesterol in PDPE (32 mol%) compared to the equivalent DHA-containing PC and PE or PC that does not possess a PUFA chain ( $\geq 50$  mol%) (21). A greater propensity for PDPE\* than monounsaturated POPE\* to separate into non-raft domains when mixed in 1:1:1 mol ratio with SM and cholesterol was inferred, in particular, on the basis of  $^2\text{H}$  NMR data in an earlier study (17). Here the same system is investigated from a different perspective. We compare  $^2\text{H}$  NMR spectra for PSM\* in 1:1:1 mol combination with PDPE or POPE and cholesterol, complemented by DSC, to elucidate molecular organization of the SM-component in the mixed model membrane system.

### Segregation into SM-rich and PE-rich nano-sized domains

The DSC results presented in Figure 4.3 reveal two separate endotherms in the scan for PDPE/PSM (1:1 mol) with peaks at 11.6 and 26.8 °C (Figure 4.3d), indicating that the two lipids mix inhomogeneously. Because the transition temperatures do not match those for single component PDPE and PSM membranes for which  $T_m = 2.2$  (22) and 41 (32) °C, respectively, the demixing is deemed incomplete. The lower temperature endotherm that is elevated 9 °C with respect to pure PDPE is assigned to a PE-rich/SM-poor phase, while the higher temperature one that is depressed 14 °C with respect to pure PSM is assigned to a PE-poor/SM-rich phase. This assignment corresponds to that in our earlier DSC work on PDPE/egg SM (1:1 mol) (17). Although, on the other hand, only one endotherm with a peak at 25.8 °C is seen for POPE/PSM (1:1 mol) (Figure 4.3c), inhomogeneous mixing into PE-rich/SM-poor and PE-poor/SM-rich domains is also concluded in mixtures with the monounsaturated PE. Thermograms recorded for different relative concentrations of lipid in the highly similar POPE/egg SM system exhibit two individual transitions that overlap at 1:1 mol ratio (17). We attribute this overlap to the higher transition temperature of pure POPE ( $T_m = 25.5$  °C) (22) compared to PDPE, which results in a smaller differential in temperature between the endotherms ascribed to PE-rich and SM-rich phases for mixtures of SM with OA- than DHA-containing PE.

Table 1 provides further insight into the segregation of PE and SM into domains. Average order parameters  $\bar{S}_{CD}$  derived from  $^2\text{H}$  NMR spectra at 35 °C are given there for PSM\* mixed at 1:1 mol with PDPE or POPE and for PDPE\* or POPE\* mixed at 1:1 mol with egg SM, both in the absence and presence of cholesterol at 1:1:1 mol concentration.

Higher  $\bar{S}_{CD}$  values for SM than PE are exhibited in each mixture, exemplified by  $\bar{S}_{CD}=0.291$  for PSM\* in PDPE/PSM\*/cholesterol vs.  $\bar{S}_{CD}=0.208$  for PDPE\* in PDPE\*/egg SM/cholesterol. The motional inequivalence that is implied is consistent with our interpretation of DSC data for PE/SM mixtures in terms of separation into domains. That a distinction in  $\bar{S}_{CD}$  value remains with PE/SM/cholesterol (1:1:1 mol) mixtures for which the addition of cholesterol broadens endotherms beyond detection by DSC, moreover, demonstrates that the separation of PE and SM into domains persists in the presence of the sterol.

Despite incomplete de-mixing of PE and SM, a superposition of individual spectral components from PSM\* in SM-rich/PE-poor and SM-poor/PE-rich domains is not discernible in the spectra for the various mixtures with PE and cholesterol (Figure. 1 and 2). The same assessment applies to our earlier published spectra for PDPE\* and POPE\* in the corresponding mixtures with egg SM and sterol (17). Fast exchange of lipids in and out of domains that occurs at a rate greater than the differential in quadrupolar splitting between the environments when the mixed membrane is entirely liquid crystalline is implied. The resultant spectrum is a time-average where the lipid contributes intensity weighted according to its population in each domain. Assuming that the spectra for deuterated SM and PE are approximately representative of SM- and PE-rich environments, respectively, an upper estimate to the size of domains may then be deduced with the aid of the average order parameters in Table 1. The calculation employs 0.08 for the difference in  $\bar{S}_{CD}$  value between domains, referring to PDPE/PSM\*/cholesterol vs. PDPE\*/egg SM/cholesterol for which the divergence is greatest and would yield the most generally applicable estimate for domain size. This

difference in  $\bar{S}_{CD}$  equates to a difference of  $\Delta\nu = 10$  kHz in average splitting, according to which the lifetime for the residency of lipid molecules in a domain must be less than  $\tau = (2\pi\Delta\nu)^{-1} = 2 \times 10^{-5}$  s. The exchange of lipids between domains is presumed to be mediated by lateral diffusion with  $D \sim 5 \times 10^{-12}$  m<sup>2</sup>s<sup>-1</sup> (38) so that an upper limit of <20 nm is placed upon radius of domains via the root mean displacement  $r = (4D\tau)^{1/2}$  associated with the lifetime. Such domains, if treated as circular, would contain <1800 lipid molecules of mean cross-sectional area  $70^\circ \text{\AA}^2$  (22) in each leaflet. They could certainly accommodate estimates of 52 and 75 for the number of PDPE and PSM molecules, respectively, undergoing a cooperative transition evaluated on the basis of the ratio of van't Hoff and calorimetric enthalpies (39) from the transitions ascribed to PE- and SM-rich domains in the DSC scan for PDPE/PSM (Figure 4.3d).

The size obtained here for domains falls at the low end of the 10-200 nm range reported for sphingolipid- and sterol-enriched membrane rafts (13) and is comparable with estimates for PUFA-rich patches in model membranes (6,40). 1-stearoyl-2-docosahexaenoylphosphatidylcholine (SDPC)/cholesterol clusters <25 nm in radius were identified in PC/PE/PS (4:4:1 mol) membranes on the basis of an appraisal of <sup>2</sup>H NMR data for perdeuterated analogs of each phospholipid (6). <sup>2</sup>H NMR powder pattern spectra recorded for 1,2-diarachidonylphosphatidylcholine (DAPC)/1-stearoyl-2-arachidonylphosphatidylcholine (SAPC)/[3 $\alpha$ -<sup>2</sup>H<sub>1</sub>]cholesterol (1:1:2 mol) were analyzed in terms of the partitioning of DAPC and SAPC into regions that extend for <16 nm, the sterol preferentially sequestering away from the dipolyunsaturated phospholipid (40).



An assumption of fast exchange of lipid back-and-forth between domains, as in the current work, is central to spectral interpretation in these earlier studies.

Exchange of SM among SM-rich/PE-poor and SM-poor/PE-rich domains offers a possible explanation for the apparent discrepancy in transition temperature identified by  $^2\text{H}$  NMR spectral moments (Figure 4.3b) and DSC (Figure 4.3d) for mixtures with DHA-containing PE. The abrupt drop in value of  $M_1$  for PSM\* in PDPE/PSM\* centers on 13.7 °C (Figure 4.3b), which is 13 °C lower than the temperature of the endotherm at 26.8 °C assigned to the SM-rich phase but only just above that of the endotherm at 11.6 °C assigned to the PE-rich phase in DSC scans for PDPE/PSM (Figure 4.3d). We attribute the reduction in first moment to the movement of PSM\* between gel-like SM-rich/PE-poor and liquid crystalline-like SM-poor/PE-rich regions. The dependence upon delay between pulses in the quadrupolar echo sequence employed to acquire data noted for  $M_1$  values in the vicinity of the discontinuity in their temperature variation implies an exchange rate that is intermediate in rate on a timescale comparable to the delay time. Slower lateral diffusion is presumably responsible. Only at higher temperatures above that ascribed to the transition for the SM-rich/PE-poor phase by DSC do the  $^2\text{H}$  NMR spectra for PSM\* in PDPE/PSM\* attain the resolution characteristic of the liquid crystalline state (Figure 4.2c and 4.2d). Exchange of PSM\* between gel- and liquid crystalline-like phases does not complicate spectral interpretation for POPE/PSM\* because, in contrast, the transitions due to PE-rich/SM-poor and PE-poor/SM-rich phases coincide in temperature for 1:1 mol mixtures with the OA-containing phospholipid (Figure 4.3c).

### PUFA-cholesterol aversion excludes sterol from DHA-containing PE-rich domains

The impact of cholesterol on the acyl chain order of each component in the mixtures of OA- and DHA-containing PE with SM (1:1:1 mol) is elaborated by the collation of average order parameters  $\bar{S}_{CD}$  given in Table 1. An increase in  $\bar{S}_{CD}$  value for all membrane constituents due to sterol is apparent, indicative of incorporation into SM-rich and PE-rich domains for both systems. It is an effect that the order parameter profiles shown for PSM\* with POPE or PDPE in Figure 4.5, and previously reported for POPE\* or PDPE\* with egg SM (17), demonstrate is manifest throughout the acyl chain. The plateau region of slowly varying order in the upper portion of the chain is elevated and overall shape of the profile is retained. A significant difference in the pattern of the cholesterol-induced change in average order  $\Delta\bar{S}_{CD}$  undergone, however, exists between the system containing the polyunsaturated phospholipid and the control containing the monounsaturated phospholipid. There is a slightly larger rise in order for PSM\* in PDPE/PSM\* ( $\Delta\bar{S}_{CD} = 0.064$ ) than in POPE/PSM\* ( $\Delta\bar{S}_{CD} = 0.059$ ), but the differential is comparable with the uncertainty ( $\pm 0.005$ ) that accompanies the reproducibility ( $\pm 1\%$ ) typically encountered with the measurement of first moments. In stark contrast, the  $\bar{S}_{CD}$  values included in Table 1 from our earlier work exhibit a substantially smaller increase due to the presence of sterol for PDPE\* in PDPE\*/egg SM ( $\Delta\bar{S}_{CD} = 0.043$ ) than for POPE\* in POPE\*/egg SM ( $\Delta\bar{S}_{CD} = 0.099$ ) (4).

To interpret the changes  $\Delta\bar{S}_{CD}$  in average order due to cholesterol listed in Table 1 in terms of the degree of localization of the sterol into a domain, it is necessary to have an appreciation of how each lipid individually responds to the presence of cholesterol. The

ordering effect of a given concentration of cholesterol on PDPE\* and POPE\* is comparable while SM, like PC, is more sensitive (41-43). In an earlier study we measured  $\bar{S}_{CD}$  rose by 0.04 when 50 mol% cholesterol was added to PDPE\* (41) that, recognizing the solubility of the sterol in PDPE is about 30 mol% (21), is similar to the increase of 0.05 in  $\bar{S}_{CD}$  seen for POPE\* with 30 mol% cholesterol (42). Increases of >0.1 in average order due to 30 mol% sterol were exerted on PSM\* (Beyer, unpublished) and, as detected with 5 mol% 1,2-dipalmitoylphosphatidylcholine (DPPC) perdeuterated in the *sn*-1 chain as a probe, bovine brain SM (43). That the increase  $\Delta\bar{S}_{CD}$  in average order for PDPE\* in PE/SM (1:1 mol) mixtures due to cholesterol (1:1:1 mol) is  $<1/2$  that for POPE\* (Table 1), thus, implies a greater tendency for PDPE\* than POPE\* to segregate into PE-rich domains depleted in sterol. The measurements made on PSM\* in this work, however, belie the simple expectation that the opposite trend might apply to the  $\Delta\bar{S}_{CD}$  values for PSM\* in the analogous PE/SM mixtures. Only a slightly greater increase in order (0.064 vs. 0.059) due to cholesterol is evident for PSM\* in the PDPE- than POPE-containing mixture and the resultant order for PSM\* in both systems is close (Table 1). We speculate that the effect of the sterol on the order of PSM\* is modulated by the presence of PE in the SM-rich domains. Remarkably, the SM-rich raft-like domains appear almost equally ordered in the PDPE/PSM\*/cholesterol and POPE/PSM\*/cholesterol membranes.

The net effect of DHA vs. OA in the presence of cholesterol is to accentuate the distinction in molecular organization between the environment within SM-rich (more ordered) and PE-rich (less ordered) domains. While the difference in average order  $\bar{S}_{CD}$  between the domains revealed by Table 1 in the POPE/SM/cholesterol mixture is 0.030 and modest, that in the PDPE/SM/cholesterol mixture is 0.083 and almost a factor of 3

bigger. These figures, which due to fast exchange of lipid molecules between domains underestimate the disparity, correspond to a differential of 11 and 33% (relative to the mean  $\bar{S}_{CD}$  for a mixture), respectively. Further physical insight into the molecular architecture of the domains is gleaned from  $\bar{S}_{CD}$  by invoking

$$\langle L \rangle = l(0.5 + |\bar{S}_{CD}|) \quad (4)$$

to obtain the average length  $\langle L \rangle$  of [ $^2\text{H}_{31}$ ]16:0 chains in a bilayer, where  $l=19.1 \text{ \AA}$  is the length of the chain projected onto the bilayer normal in the all-trans configuration (44,45). The thickness of the bilayer in SM-rich and PE-rich domains may then be estimated from the data in Table 1. There are two important assumptions involved. They are that the dominant contribution to the population-weighted average  $\bar{S}_{CD}$  values produced by fast exchange between domains comes from the environment in which a lipid is enriched, and that  $\langle L \rangle$  approximates to the thickness of a monolayer. The calculation yields estimates of 30.4  $\text{\AA}$  for PSM\* and 29.2  $\text{\AA}$  for POPE\* in their 1:1:1 mol mixtures with cholesterol, as opposed to 30.2  $\text{\AA}$  for PSM\* and 27.0  $\text{\AA}$  for PDPE\* in their 1:1:1 mol mixtures with cholesterol. Replacing OA with DHA, thus, increases the divergence in thickness between SM-rich and PE-rich domains from 1.2 to 3.2  $\text{\AA}$ .

We attribute the difference in response to cholesterol of the DHA- and OA-containing PE mixtures with SM to the mutual aversion that PUFA and sterol possess. A cartoon depicting our explanation is shown in Figure 4.6. In the absence of cholesterol, PDPE and SM segregate into nano-sized domains that are PE-rich and SM-rich (Figure 4.6, top left). When cholesterol is added, it preferentially partitions into SM-rich domains and tends to further exclude PDPE into PUFA-rich domains (Figure 4.6, top right). This partitioning is due to the differential affinity the sterol possesses for PDPE vs. SM, not

because it has exceeded its solubility in PDPE-rich domains. Exclusion of PUFA-containing phospholipid driven by incompatibility with the highly ordered matrix formed by SM and cholesterol is an alternative mechanism that would produce the same effect that was recently proposed by Lindblom and coworkers (46) in a study of lipid diffusion in PC/SM/cholesterol mixtures. Accordingly, the polyunsaturated phospholipid has less contact with the sterol and experiences only a modest increase in order. POPE and SM similarly separate into PE-rich and SM-rich domains in a membrane devoid of sterol (Figure 4.6, bottom left), although probably not to the same extent as with DHA. However, when cholesterol is introduced, the diminished affinity it feels for monounsaturated POPE relative to SM is less pronounced than for PDPE. The sterol mixes into OA-containing PE-rich domains as well as into SM-rich domains (Figure 4.6, bottom right). By virtue of greater proximity, there is then a substantial sterol-associated increase in order for the monounsaturated phospholipid in the mixture. Consistent with this behavior, fast exchange of sterol between two equally populated pools was also inferred from  $^2\text{H}$  NMR spectra recorded for a deuterated analog of cholesterol added to 1-plamitoyl-2-oleoylphosphatidylcholine (POPC)/brain SM (1:1:1 mol) (47). Quantitative estimation of the partitioning of cholesterol between domains, an issue complicated by incomplete de-mixing of SM and PE and their likely redistribution following the introduction of sterol, cannot be made with the mixtures studied here.

### Conclusion

The co-existence of PUFA-rich/cholesterol-poor (non-raft) and SM-rich/cholesterol-rich (raft) domains within plasma membranes has the potential to be the molecular origin, in part, of the multitude of health benefits associated with dietary consumption of fish oils (5). Movement of signaling proteins between these organizationally distinct domains then modulates cellular events via changes in protein conformation. The results of this study establish the lipid driven formation of such domains. When PDPE substitutes for POPE in PE/SM/cholesterol mixtures, the differential in order and membrane thickness between PE-rich and SM-rich domains becomes approximately  $3 \times$  greater.

### Acknowledgements

It is a pleasure to thank K. Beyer for communicating  $^2\text{H}$  NMR data prior to publication. This work was supported in part by grants from the National Institutes of Health (CA 57212 to W.S. and HL 083187 to R.B.)

This chapter was published in Biophysics Journal, 95 (1) 203-14 (2008) as a paper entitled “Docosahexaenoic Acid Enhances Segregation of Lipids between Raft and Non-Raft Domains:  $^2\text{H}$  NMR Study” by Smita P. Soni, Daniel S. LoCascio, Yidong Liu, Justin A. Williams, Robert Bittman, William Stillwell and Stephen R. Wassall.

## References

1. Salem, N., Jr., B. Litman, H. Y. Kim, and K. Gawrisch. 2001. Mechanisms of action of docosahexaenoic acid in the nervous system. *Lipids* 36:945-959.
2. Salem, N., H. Y. Kim, and J. A. Yergey. 1986. Docosahexaenoic Acid: Membrane Function and Metabolism. Academic Press, New York.
3. Stillwell, W., and S. R. Wassall. 2003. Docosahexaenoic acid: membrane properties of a unique fatty acid. *Chem. Phys. Lipids* 126:1-27.
4. Wassall, S. R., M. R. Brzustowicz, S. R. Shaikh, V. Cherezov, M. Caffrey, and W. Stillwell. 2004. Order from disorder, corralling cholesterol with chaotic lipids. The role of polyunsaturated lipids in membrane raft formation. *Chem. Phys. Lipids* 132:79-88.
5. Stillwell, W., S. R. Shaikh, M. Zerouga, R. Siddiqui, and S. R. Wassall. 2005. Docosahexaenoic acid affects cell signaling by altering lipid rafts. *Reprod. Nutr. Dev.* 45:559-579.
6. Huster, D., K. Arnold, and K. Gawrisch. 1998. Influence of docosahexaenoic acid and cholesterol on lateral lipid organization in phospholipid mixtures. *Biochemistry* 37:17299-17308.
7. Mitchell, D. C., and B. J. Litman. 1998. Effect of cholesterol on molecular order and dynamics in highly polyunsaturated phospholipid bilayers. *Biophys. J.* 75:896-908.
8. Singer, S. J., and G. L. Nicolson. 1972. The fluid mosaic model of the structure of cell membranes. *Science* 175:720-731.



9. Jacobson, K., E. D. Sheets, and R. Simson. 1995. Revisiting the fluid mosaic model of membranes. *Science* 268:1441-1442.
10. Simons, K., and E. Ikonen. 1997. Functional rafts in cell membranes. *Nature* 387:569-572.
11. Edidin, M. 2003. The state of lipid rafts: from model membranes to cells. *Annu. Rev. Biophys. Biomol. Struct.* 32:257-283.
12. Brown, D. A., and E. London. 2000. Structure and function of sphingolipid- and cholesterol-rich membrane rafts. *J. Biol. Chem.* 275:17221-17224.
13. Pike, L. J. 2006. Rafts defined: a report on the Keystone symposium on lipid rafts and cell function. *J. Lipid Res.* 17:1597-1598.
14. Simons, K., and R. Ehehalt. 2002. Cholesterol, lipid rafts, and disease. *J. Clin. Invest.* 110:597-603.
15. Simons K., and W. L. Vaz. 2004. Model systems, lipid rafts, and cell membranes. *Annu. Rev. Biophys. Biomol. Struct.* 33:269-95.
16. Bittman, R., C. R. Kasireddy, P. Mattjus, and J. P. Slotte. 1994. Interaction of cholesterol with sphingomyelin monolayers and vesicles. *Biochemistry* 33:11776-11781.
17. Shaikh, S. R., A. C. Dumauual, A. Castillo, D. LoCascio, R. A. Siddiqui, W. Stillwell, and S. R. Wassall. 2004. Oleic and docosahexaenoic acid differentially phase separate from lipid raft molecules: a comparative NMR, DSC, AFM, and detergent extraction study. *Biophys. J.* 87:1752-1766.

18. Gennis, R. B. 1989. *Biomembranes*. Springer-Verlag, New York.
19. Zerouga, M., W. Stillwell, J. Stone, A. Powner, and L. J. Jenki. 1996. Phospholipid class as a determinant in docosahexaenoic acid's effect on tumor cell viability. *Anticancer Res.* 16:2863-2868.
20. Anderson, R. E., and L. Sperling. 1971. Lipids of ocular tissues. VII. Positional distribution of the fatty acids in the phospholipids of bovine retina rod outer segments. *Arch. Biochem. Biophys.* 144:673-677.
21. Shaikh, S. R., V. Cherezov, M. Caffrey, S. P. Soni, D. LoCascio, W. Stillwell, and S. R. Wassall. 2006. Molecular organization of cholesterol in unsaturated phosphatidylethanolamines: X-ray diffraction and solid state <sup>2</sup>H NMR reveal differences with phosphatidylcholines. *J. Amer. Chem. Soc.* 126:5375-5383.
22. Shaikh, S. R., M. R. Brzustowicz, N Gustafson, W. Stillwell, and S. R. Wassall. 2002. Monounsaturated PE does not phase separate from the lipid raft molecules sphingomyelin and cholesterol: role for polyunsaturation? *Biochemistry* 41:10593-10602.
23. Barenholz, Y. 1984. Sphingomyelin-lecithin balance in membrane: composition, structure, and function relationships. *In Physiology of Membrane Fluidity*, Vol. 1. M. Shinitsky, editor, CRC Press, Boca Raton. 131-174.
24. Bittman, R., and C. A. Verbicky. 2000. Methanolysis of sphingomyelin. Toward an epimerization-free methodology for the preparation of D-erythro-sphingosylphosphocholine. *J. Lipid Res.* 41:2089-2093.

25. Nyholm, T., M. Nylund, A. Soderholm, and J. P. Slotte. 2003. Properties of palmitoyl phosphatidylcholine, sphingomyelin, and dihydrosphingomyelin bilayer membranes as reported by different fluorescent reporter molecules. *Biophys. J.* 84:987-997.
26. McCabe, M. A., and S. R. Wassall. 1997. Rapid deconvolution of NMR powder spectra by weighted fast Fourier transformation. *Solid State Nucl. Magn. Reson.* 10:53-61.
27. Davis, J. H., K. R. Jeffery, M. Bloom, M. I. Valic, and T. P. Higgs. 1976. Quadrupolar echo deuteron magnetic resonance spectroscopy in ordered hydrocarbon chains. *Chem. Phys. Lett.* 42:390-394.
28. Davis, J. H. 1983. The description of membrane lipid conformation, order and dynamics by  $^2\text{H}$ -NMR. *Biochim. Biophys. Acta* 737:117-171.
29. Lafleur, M., B. Fine, E. Sternin, P. R. Cullis, and M. Bloom. 1989. Smoothed orientational order profile of lipid bilayers by  $^2\text{H}$ -nuclear magnetic resonance. *Biophys. J.* 56:1037-1041.
30. Mehnert, T., K. Jacob, R. Bittman, and K. Beyer. 2006. Structure and lipid interaction of N-palmitoylsphingomyelin in bilayer membranes as revealed by  $^2\text{H}$ -NMR spectroscopy. *Biophys. J.* 90:939-946.
31. Shaikh, S. R., A. C. Dumauual, L. J. Jencki, and W. Stillwell. 2001. Lipid phase separation in phospholipid bilayers and monolayers modeling the plasma membrane. *Biochim. Biophys. Acta* 1512:317-328.
32. Maulik, P. R., and G. G. Shipley. 1996. N-palmitoyl sphingomyelin bilayers: structure and interaction with cholesterol. *Biochemistry* 35:8025-8034.

33. Engel, A. K., and D. Cowburn. 1981. The origin of multiple quadrupole couplings in the deuterium NMR spectra of the 2 chain of 1,2 dipalmitoyl-sn-glycero-3-phosphorylcholine. *FEBS Lett.* 126:169-171.
34. Seelig, J. 1977. Deuterium magnetic resonance: theory and application to lipid membranes. *Q. Rev. Biophys.* 10:353-418.
35. Stillwell, W., S. R. Shaikh, D. LoCascio, R. A. Siddiqui, J. Seo, R. S. Chapkin, and S. R. Wassall. 2006. Docosahexaenoic Acid. An Influential Membrane-Altering Omega-3 Fatty Acid. *In* *Frontiers in Nutrition Research*. J. D. Huang, editor. Nova Science Publishers, Inc., Hauppauge, New York. 249-271.
36. van Dijk, P. W. 1979. Negatively charged phospholipids and their position in the cholesterol affinity sequence. *Biochim. Biophys. Acta* 555:80-101.
37. Niu, S. L., and B. J. Litman. 2002. Determination of membrane cholesterol partition coefficient using a lipid vesicle-cyclodextrin binary system: effect of phospholipid acyl chain unsaturation and headgroup composition. *Biophys. J.* 83:3408-3415.
38. Filippov, A., G. Orädd, and G. Lindblom. 2006. Sphingomyelin structure influences the lateral diffusion and raft formation in lipid bilayers. *Biophys. J.* 90:2086-2092.
39. Sturtevant, J. M. 1974. Phase transitions of phospholipids. *In* *Quantum Statistical Mechanics in the Natural Sciences*. B. Kursunogla, S. Mintz, and S. Widmayer, editors. Plenum Press, New York. 63-83.

40. Brzustowicz, M. R., V. Cherezov, M. Caffrey, W. Stillwell and S. R. Wassall. 2002. Molecular organization of cholesterol in polyunsaturated membranes: Microdomain formation. *Biophys. J.* 82:285-298.
41. Shaikh, S. R., V. Cherezov, M. Caffrey, W. Stillwell, and S. R. Wassall. 2003. Interaction of cholesterol with a docosahexaenoic acid-containing phosphatidylethanolamine: trigger for microdomain/raft formation? *Biochemistry* 42:12028-12037.
42. Paré, C., and M. Lafleur. 1998. Polymorphism of POPE/cholesterol system: a  $^2\text{H}$  nuclear magnetic resonance and infrared spectroscopic investigation. *Biophys. J.* 74:899-909.
43. Guo, W., V. Kurze, T. Huber, N. H. Afdhak, K. Beyer, and J. A. Hamilton. 2002. A solid-state NMR study of phospholipid-cholesterol interactions: sphingomyelin-cholesterol binary systems. *Biophys. J.* 83:1465-1478.
44. Holte, L. L., S. A. Peter, T. M. Sinnwell, and K. Gawrisch. 1995.  $^2\text{H}$  nuclear magnetic resonance order parameter profiles suggest a change of molecular shape for phosphatidylcholines containing a polyunsaturated acyl chain. *Biophys. J.* 63:2396-2403.
45. Nagle, J. F. 1993. Area/lipid of bilayers from NMR. *Biophys. J.* 64:1476-1481.
46. Filippov, A., G. Orädd, and G. Lindblom. 2007. Domain formation in model membranes studied by pulsed-field gradient-NMR: the role of lipid polyunsaturation. *Biophys. J.* 93:3182-3190.

47. Aussenac, F., M. Tavares, and E. J. Dufourc. 2003. Cholesterol dynamics in membranes of raft composition: a molecular point of view from  $^2\text{H}$  and  $^{31}\text{P}$  solid-state NMR. *Biochemistry* 42:1383-1390.

Table 4.1: Average order parameters  $\bar{S}_{CD}$  derived from  $^2\text{H}$  NMR spectra for POPE/PSM\* (1:1 mol) and PDPE/PSM\* (1:1 mol) in the absence and presence of cholesterol (1:1:1 mol) at 35 °C. Corresponding values for POPE\*/egg SM (1:1 mol) and PDPE\*/egg SM (1:1 mol) are included for comparison.

Membrane Composition	No cholesterol	With cholesterol	
		$\bar{S}_{CD}$	$\Delta\bar{S}_{CD}$
POPE/PSM*	0.237	0.296	0.059
POPE*/egg SM <sup>1</sup>	0.167	0.266	0.099
PDPE/PSM*	0.227	0.291	0.064
PDPE*/egg SM <sup>1</sup>	0.165	0.208	0.043

<sup>1</sup>Values taken from Wassall *et al.* (4)

Figure 4.1:  $^2\text{H}$  NMR spectra for a 50 wt% aqueous dispersion in 50 mM Tris buffer (pH 7.5) of POPE/PSM\*(1:1 mol) (left panel) and POPE/PSM\*/cholesterol (1:1:1 mol) (right panel). Spectra were recorded at (a and e) -23, (b and f) 12, (c and g) 27 and (d and h) 52 °C



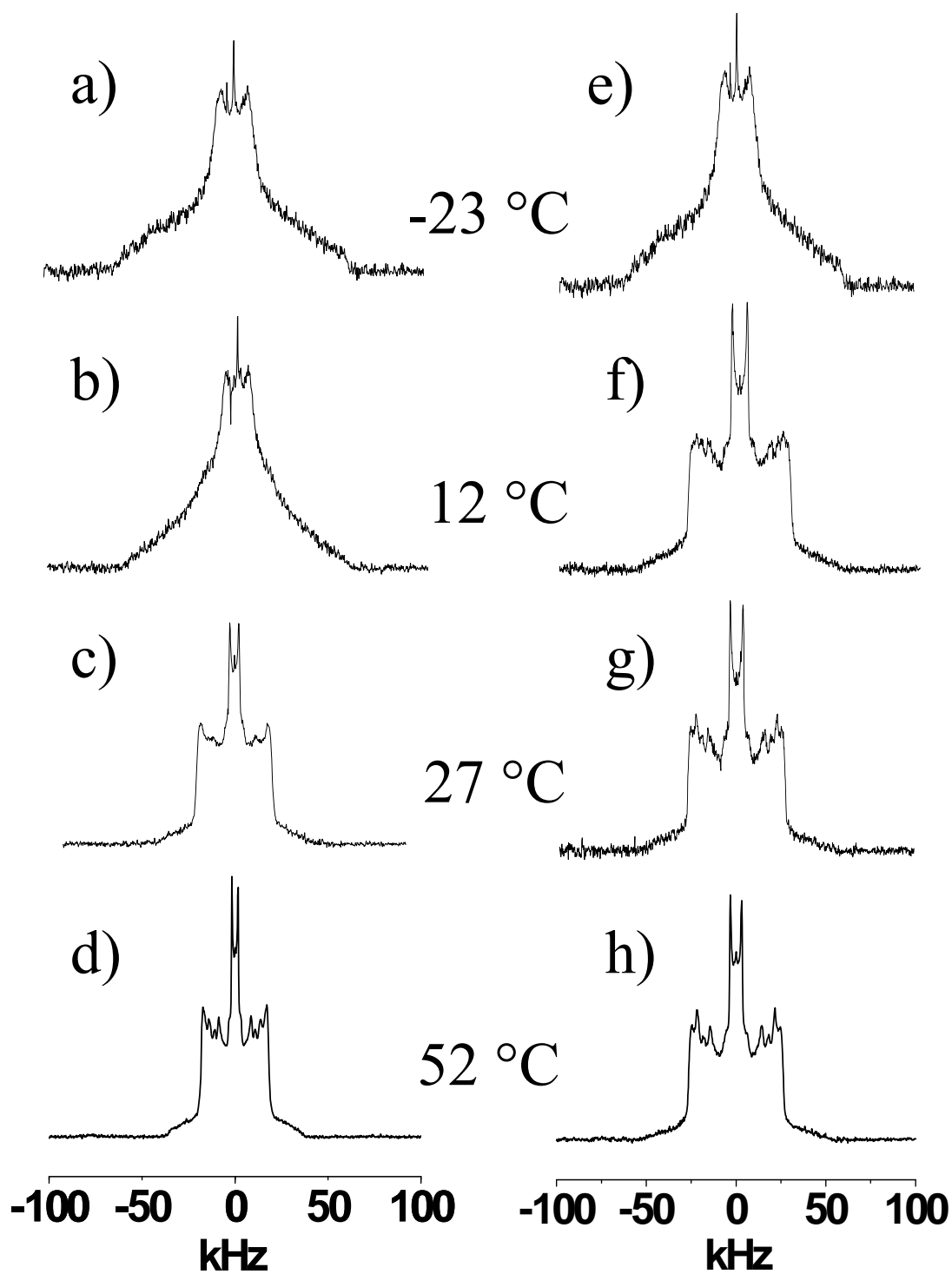


Figure 4.1

Figure 4.2:  $^2\text{H}$  NMR spectra for a 50 wt% aqueous dispersion in 50 mM Tris buffer (pH 7.5) of PDPE/PSM\* (1:1 mol) (left panel) and PDPE/PSM\*/cholesterol (1:1:1 mol) (right panel). Spectra were recorded at (a and e) -23, (b and f) 12, (c and g) 27 and (d and h) 52 °C

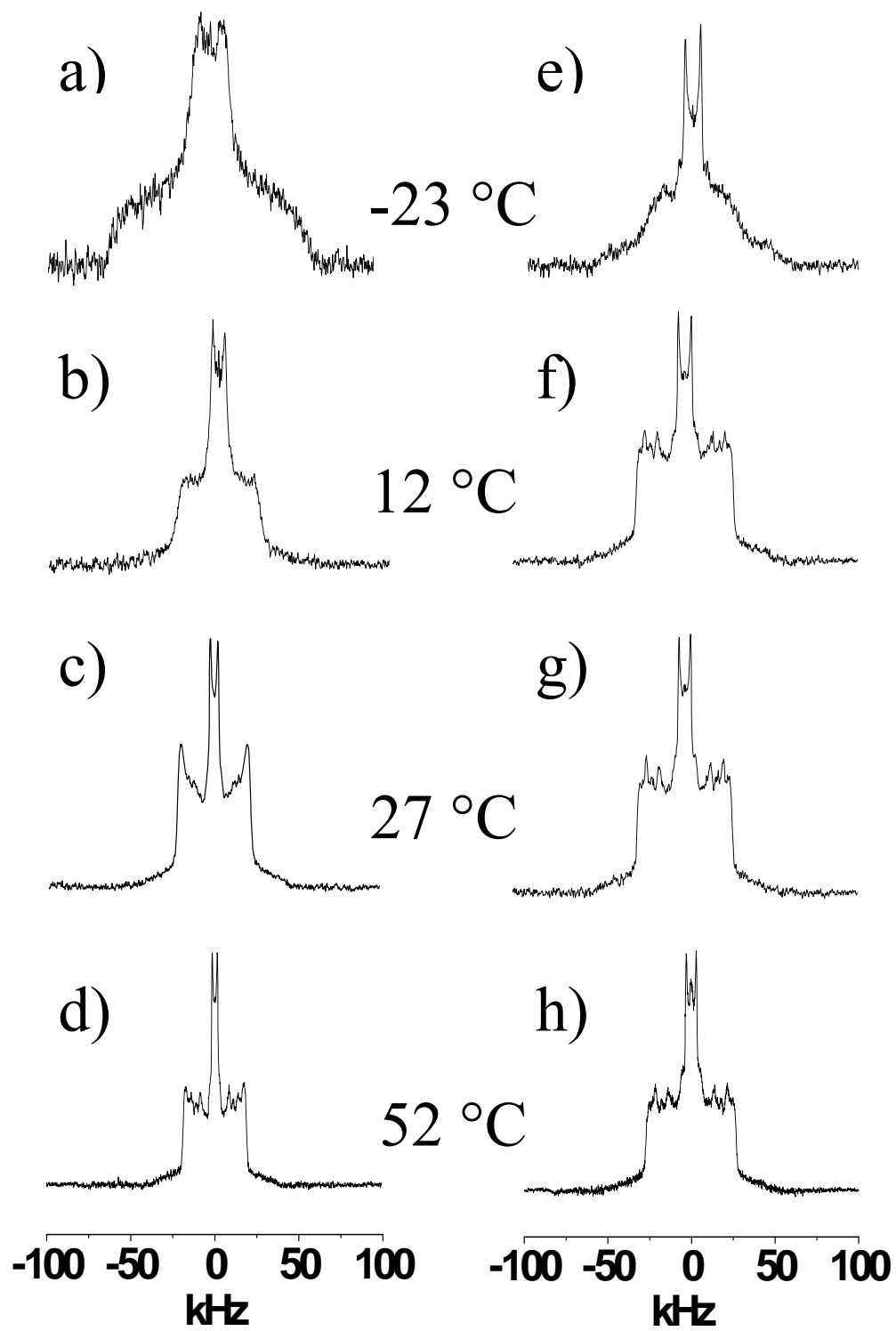


Figure 4.2

Figure 4.3: Variation of the first moment  $M_1$  as a function of temperature for, a) POPE/PSM\* (1:1 mol) in the absence (■) and presence (□) of cholesterol (1:1:1 mol), and, b) POPE/PSM\* (1:1 mol) in the absence (■) and presence (□) of cholesterol (1:1:1 mol).  $M_1$  is plotted logarithmically for clarity and X designates the midpoint of the sharp drop in moment observed when the sterol is absent. DSC cooling scans for, c) POPE/PSM (1:1 mol) and (d) PDPE/PSM (1:1 mol). The scans are inverted so that transitions appear as positive peaks

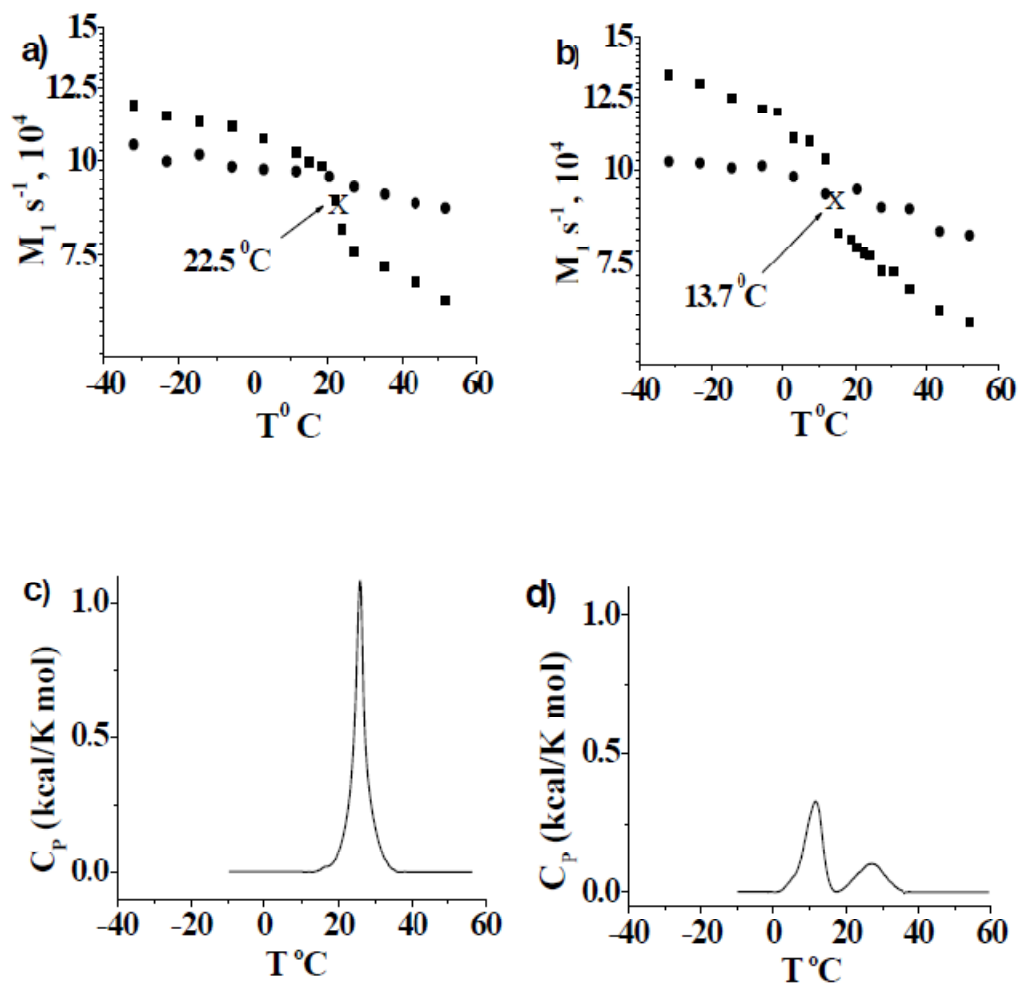


Figure 4.3

Figure 4.4: FFT depaked spectra for POPE/PSM\* (1:1 mol) in the absence, a) and presence, b) of cholesterol (1:1:1 mol), and for PDPE/PSM\* (1:1 mol) in the absence, c) and presence, d) of cholesterol (1:1:1 mol) at 43 °C. The arrows specify assignment of the C2 position

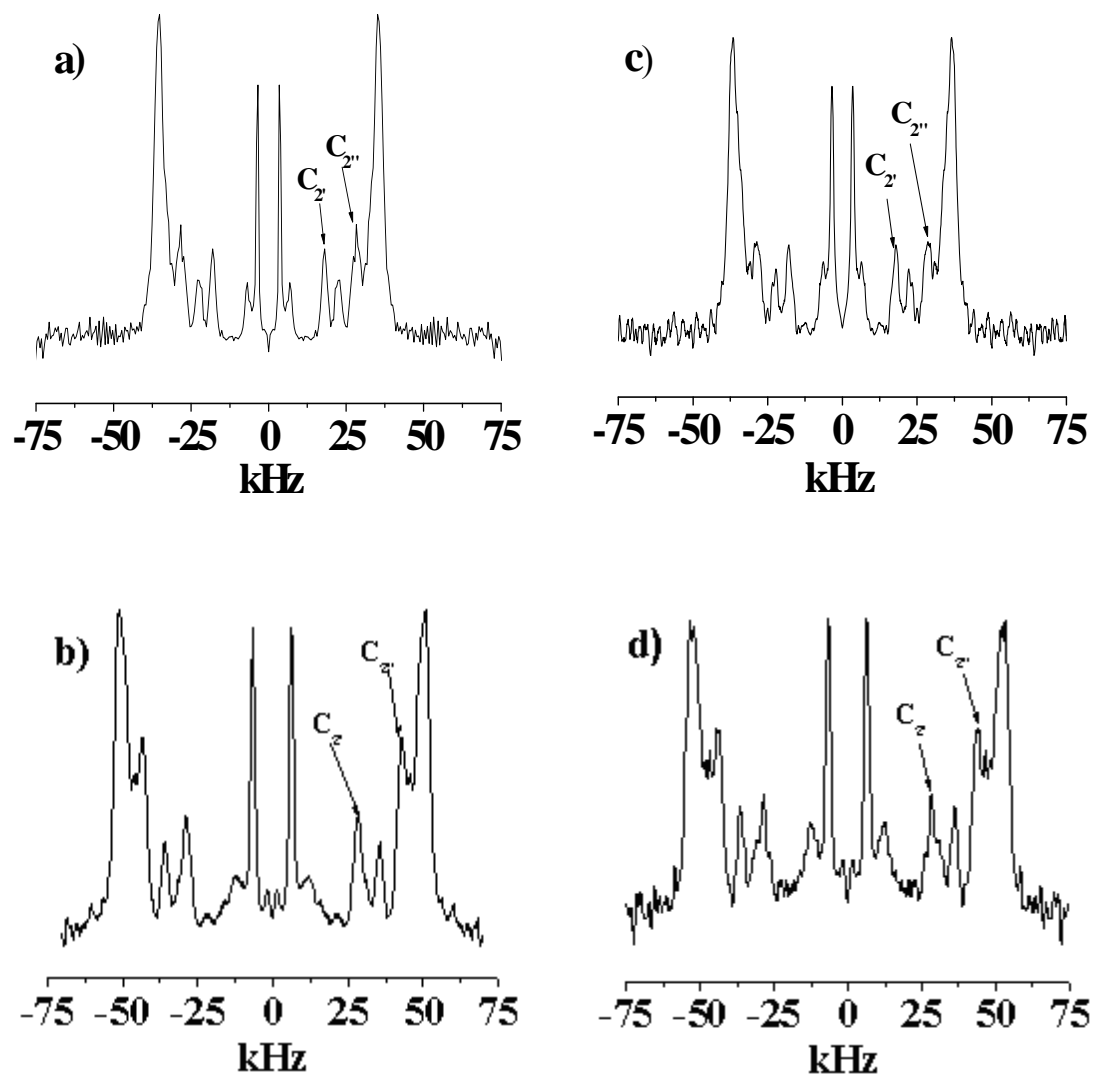


Figure 4.4

Figure 4.5: Order parameter profiles generated from depaked spectra for, a) POPE/PSM\* (1:1 mol) in absence (●) and presence (○) of cholesterol (1:1:1 mol), and for, b) PDPE/PSM\* (1:1 mol) in absence (●) and presence (○) of cholesterol (1:1:1 mol) at 43 °C



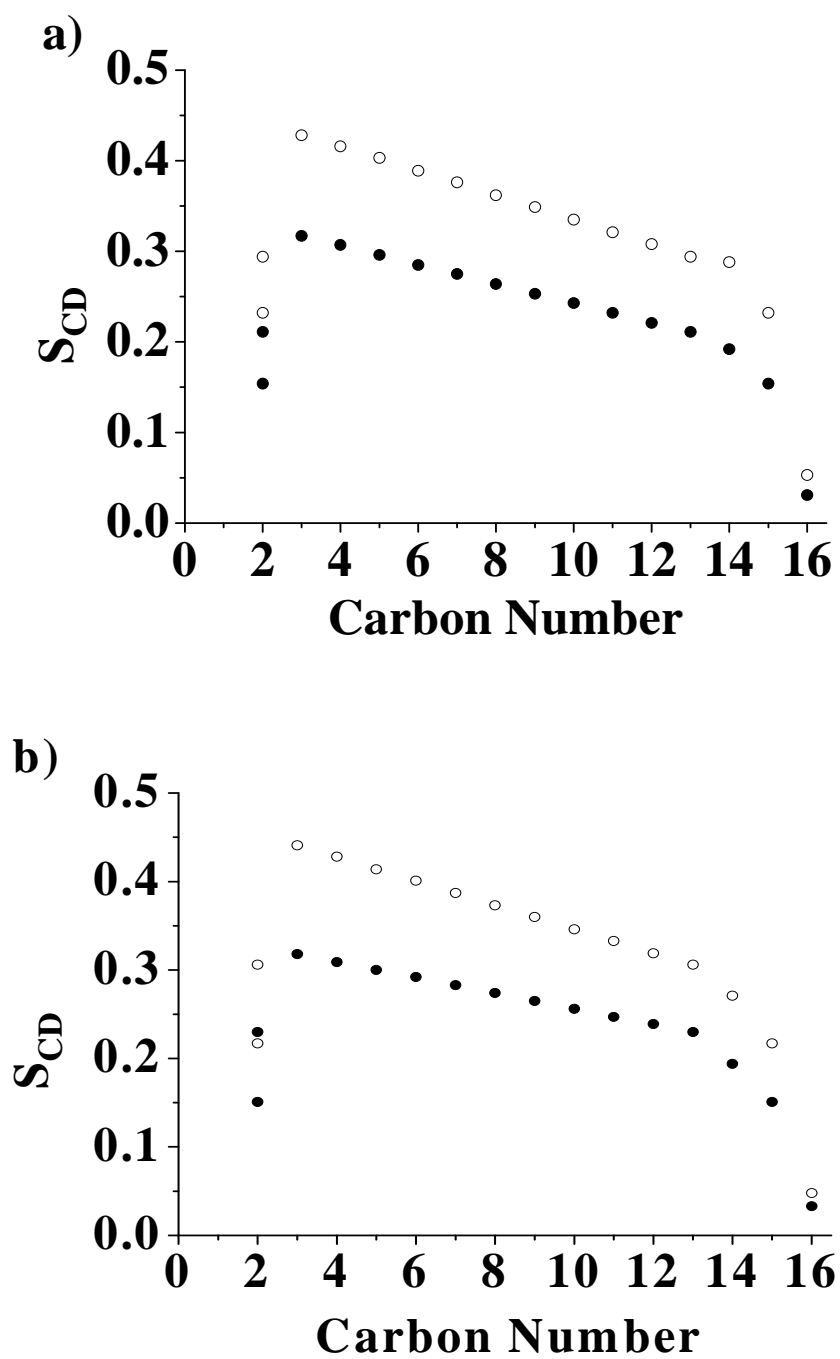


Figure 4.5

Figure 4.6: A cartoon depiction of DHA vs. OA-induced lateral segregation of lipid molecules in PE/SM/cholesterol (1:1:1 mol) membranes. PE-rich and SM-rich domains coexist in PDPE/SM (top left) and POPE/SM (bottom left) membranes in the absence of sterol. Upon addition of cholesterol to PDPE/SM, the sterol is preferentially taken up into SM-rich domains for which it has high affinity and further displaces DHA for which it has low affinity. The formation of DHA-containing PE-rich/cholesterol-poor non-raft and SM-rich/cholesterol-rich raft domains is the result (top right). Upon addition of cholesterol to POPE/SM, in contrast, the sterol incorporates into OA-containing PE-rich, albeit to less extent, as well as SM-rich domains (bottom right). The tremendous aversion of cholesterol for DHA is not possessed by OA

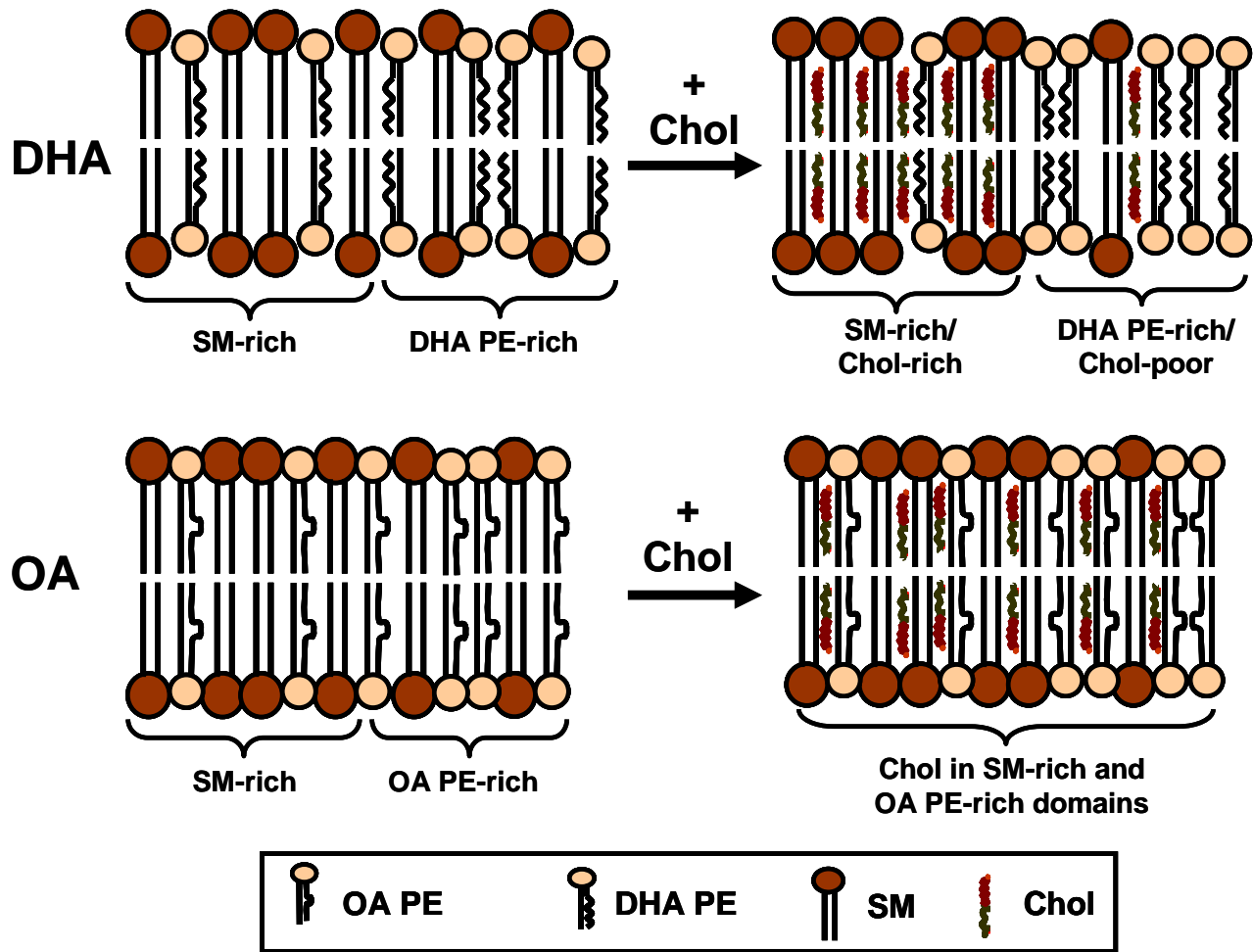


Figure 4.6

## CHAPTER 5: CONCLUSION

Studies of the effect of PUFA and TFA on the properties of lipid membranes were the focus of this thesis. Solid state  $^2\text{H}$  NMR, complemented by DSC and MD simulations, was the primary technique used. The final chapter summarizes the findings and describes work in progress and suggestions for future work that extend the research.

### PUFA

In Chapter 4,  $^2\text{H}$  NMR of  $[\text{}^2\text{H}_{31}]16:0\text{SM}$  ( $[\text{}^2\text{H}_{31}]$ -N-palmitoylsphingomyelin), supplemented by DSC (differential scanning calorimetry), was employed to investigate molecular organization of the sphingolipid in 1:1:1 mol mixtures with 16:0-18:1PE (1-palmitoyl-2-oleoyl-*sn*-glycero-3-phosphoethanolamine) or 16:0-22:6PE (1-palmitoyl-2-docosahexanoyl-*sn*-glycero-3-phosphoethanolamine) and cholesterol (1). 16:0-18:1PE was a control while 16:0-22:6PE represented a PUFA-containing phospholipid. The results were compared to data reported earlier for analogous mixtures of  $[\text{}^2\text{H}_{31}]16:0$ -18:1PE or  $[\text{}^2\text{H}_{31}]16:0$ -22:6PE with egg SM and cholesterol (2). The spectra revealed that both the OA (oleic acid)- and DHA (docosahexaenoic acid)-containing mixtures segregate into SM-rich (higher order) and PE-rich (lower order) domains that are nano-size (<20 nm) irrespective of the presence of cholesterol. Adding cholesterol increases order in both domains, but the differential in the order between SM-rich and PE-rich domains is almost 3x greater with DHA than OA. An explanation for this behavior is that

the cholesterol has poor affinity for DHA (3), which will exclude the sterol from DHA-containing PE-rich domains and DHA from SM-rich/cholesterol-rich domains. We hypothesize that the formation of DHA-rich domains in the plasma membrane may be responsible, in part, for the health benefits produced by dietary fish oils (3, 4).

The diversity of the health problems improved by the consumption of fish oils suggests a general mode of action (3). A likely site of action is the plasma membrane where DHA is taken up into the phospholipids. The model we propose consists of highly disordered PUFA-rich/cholesterol-poor (non-raft) domains forming and coexisting with highly ordered SM-rich/cholesterol-rich rafts in a bulk, predominantly monounsaturated lipid matrix (3, 4). In this arrangement, which was shown schematically in Chapter 1 (Figure 1.1-b), the large difference in order between the domains has the potential to cause changes in conformation that turn on or off signaling proteins when they move from one type of domain to the other. The stimulation of phospholipase D1 (PLD1) activity in human peripheral blood mononuclear cells by DHA, for instance, may occur in this manner (2). PLD1 is excluded from rafts and accumulates in DHA-rich domains where it becomes activated, disrupting signal transduction events (5) and possibly giving rise to the immunosuppression associated with DHA.

The segregation into DHA-rich/sterol-poor and SM-rich/sterol-rich domains implied by our work on 16:0-22:6PE/SM/cholesterol mixture is consistent with the above model. However, although SM-rich/sterol-rich raft-like domains are known to form in mixtures with monounsaturated phospholipids (6), the formation of DHA-rich/sterol-poor domains in mixtures with monounsaturated phospholipids, that is assumed in our model, remains to be demonstrated. To address this issue we propose a  $^2\text{H}$  NMR study of 16:0-

18:1PC/16:0-22:6PE mixtures in the absence and presence of cholesterol. The approach would be the same as was successfully employed in our  $^2\text{H}$  NMR experiments on PE/SM mixtures.  $[\text{}^2\text{H}_{31}]16:0-18:1\text{PC}$  in  $[\text{}^2\text{H}_{31}]16:0-18:1\text{PC}/16:22:6\text{PE}$  and  $[\text{}^2\text{H}_{31}]16:0-22:6\text{PE}$  in  $16:0-18:1\text{PC}/[\text{}^2\text{H}_{31}]16:0-22:6\text{PE}$  will enable each lipid in the mixed membrane to be individually observed and to establish the existence of domains that are organizationally distinct.

### TFA

In Chapter 3 analogs of 1-elaidoyl-2-stearoylphosphatidylcholine (*t*18:1-18:0PC) and 1-oleoyl-2-stearoylphosphatidylcholine (*c*18:1-18:0PC) with a perdeuterated  $[\text{}^2\text{H}_{35}]18:0$  *sn*-2 chain were synthesized and solid state  $^2\text{H}$  NMR, complemented by computer simulations, was employed to compare molecular organization in a model membrane containing elaidic acid (EA) with a single “manmade” *trans* double bond vs. oleic acid (OA) with a single “natural” *cis* double bond (7). Moment analysis of the  $^2\text{H}$  NMR spectra recorded as a function of temperature showed that the chain melting temperature is depressed less for *t*18:1- $[\text{}^2\text{H}_{35}]18:0\text{PC}$  than for *c*18:1- $[\text{}^2\text{H}_{35}]18:0\text{PC}$  relative to saturated 1,2-distearoylphosphatidylcholine ( $18:0-[\text{}^2\text{H}_{35}]18:0\text{PC}$ ). The difference reflects an ability to pack more favorably in the gel state that arises because a *trans* double bond introduces a smaller kink into a chain than a *cis* double bond. Acyl chain order in the liquid crystalline state is comparable in *t*18:1- $[\text{}^2\text{H}_{35}]18:0\text{PC}$  and *c*18:1- $[\text{}^2\text{H}_{35}]18:0\text{PC}$ , and greatly reduced compared to  $18:0-[\text{}^2\text{H}_{35}]18:0\text{PC}$ . The disordering is attributed to a reduced energy barrier for rotation around the C-C single bonds next to a *trans* and *cis* C=C double bond. Thus, while possessing a conformation that somewhat

resembles a saturated chain, *trans* unsaturated EA is disordered like *cis* unsaturated OA. We speculate that EA is a rogue fatty acid that when taken up into a membrane lipid is mistaken for a saturated fatty acid and then locally disrupts molecular organization. If taken up into SM, for example, increased disorder within rafts could adversely impact the function of resident signaling proteins.

To experimentally probe the conformation of the *trans* vs. *cis* unsaturated chain, which will also further validate the MD simulations, we have synthesized  $t[{}^2\text{H}_{33}]18:1-18:0\text{PC}$  (Figure 5.1a) and  $c[{}^2\text{H}_{33}]18:1-18:0\text{PC}$  (Figure 5.1b) with a perdeuterated  $t[{}^2\text{H}_{33}]18:1$  and  $c[{}^2\text{H}_{33}]18:1$  *sn*-1 chain, respectively (Appendix B). This work is still in progress and a preliminary report will be given here. Representative examples from  ${}^2\text{H}$  NMR spectra collected over a range of temperature are shown in Figure 5.2. As with  $t18:1-[]^2\text{H}_{35}]18:0\text{PC}$  and  $c18:1-[]^2\text{H}_{35}]18:0\text{PC}$  that were perdeuterated in the  $[]^2\text{H}_{35}]18:0$  *sn*-2 chain (Figure 3.2), the spectra for both  $t[{}^2\text{H}_{33}]18:1-18:0\text{PC}$  and  $c[{}^2\text{H}_{33}]18:1-18:0\text{PC}$  change from a broad spectrum characteristic of slow anisotropic motion in the gel phase at low temperature (-5 °C, Figure 5.2a and 5.2e) to a spectrum narrowed by fast axial rotation in the liquid crystalline phase at high temperature (45 °C, Figure 5.2d and 5.2h). Looking through the spectra at intermediate temperature similarly confirm that the spectral narrowing that accompanies the melting of the TFA-containing membrane (5 °C, Figure 5.2b; and 20 °C, Figure 5.2c) occurs at higher temperature than in the *cis* fatty acid (CFA)-containing membrane (5 °C, Figure 5.2f; and 20°C, Figure 5.2g).

First moments  $M_1$  calculated from the spectra for  $t[{}^2\text{H}_{33}]18:1-18:0\text{PC}$  (Figure 5.3a, ■) and  $c[{}^2\text{H}_{33}]18:1-18:0\text{PC}$  (Figure. 5.3b, ■) are plotted against temperature in Figure 5.3. The plots include the corresponding data for  $t18:1-[]^2\text{H}_{35}]18:0\text{PC}$  (Figure 5.3a,

□) and  $c18:1-[^2\text{H}_{35}]18:0\text{PC}$  (Figure 5.3b, □). It is immediately obvious that the chain melting behavior detected by the unsaturated *sn*-1 and saturated *sn*-2 chains differ in each case. For the  $t[^2\text{H}_{33}]18:1$  or  $c[^2\text{H}_{33}]18:1$  *sn*-1 chain the moments are lower than for the corresponding  $[^2\text{H}_{35}]18:0$  *sn*-2 chain and the drop in value in the region of the gel to liquid crystalline temperature is less abrupt. The molecular model proposed by Huang and Li (8) to describe chain melting in PC membranes with *sn*-1 saturated/*sn*-2 *cis* monounsaturated chains offers a possible explanation. According to their model, the monounsaturated chain adopts a kinked motif in the gel state like that modeled in our work for the  $t18:1$  chain in  $t18:1-18:0\text{PC}$  and, with a smaller kink, for the  $c18:1$  chain in  $c18:1-18:0\text{PC}$  (Figure 3.6). The kink is assumed to separate a linear segment composed of only *trans* rotamers and a shorter disordered segment containing both *gauche* and *trans* rotamers. Whereas the longer linear segment is involved in intra- and intermolecular van der Waals attractive interactions with neighboring all-*trans* saturated chains in the gel state and contributes to the chain melting process at  $T_m$ , the shorter segment is already partially disordered at  $T < T_m$ .

Although rapid axial rotation in the liquid crystalline phase narrows the spectra observed for  $t[^2\text{H}_{33}]18:1-18:0\text{PC}$  (Figure 5.2d) and  $c[^2\text{H}_{33}]18:1-18:0\text{PC}$  (Figure 5.2h) at 45 °C, they are not expected to have the same shape as the spectra seen under equivalent conditions when the *sn*-2 18:0 chain was perdeuterated (Figure 3.2g and 3.2k). Due to the double bond they consist of a superposition of powder patterns with a very different distribution of order parameter, as reflected in the order parameter profiles generated from MD simulations (Figure 3.5c), and quadrupolar splitting. The average order parameter  $\bar{S}_{CD}$  derived from the first moment  $M_1$  for  $t[^2\text{H}_{33}]18:1-18:0\text{PC}$  and  $c[^2\text{H}_{33}]18:1-$



18:0PC at 45°C are presented in Table 1. They qualitatively agree with the values obtained in the MD simulations that are also listed in the Table. Order in the *t*18:1 and *c*18:1 *sn*-1 chain is lower than in the 18:0 *sn*-2 chain, and the differential is greater for the *cis* chain.

To gain detailed insight into the conformation of the  $t[{}^2\text{H}_{33}]18:1$  and  $c[{}^2\text{H}_{33}]18:1$  chains, the next step will be to construct order parameter profiles from the spectra for  $t[{}^2\text{H}_{33}]18:1-18:0\text{PC}$  and  $c[{}^2\text{H}_{33}]18:1-18:0\text{PC}$ , respectively. This unfinished portion of the work is currently underway. Figure 5.4 shows the depaked spectra that will be used. The depaked spectrum for  $t[{}^2\text{H}_{33}]18:1-18:0\text{PC}$  reveals that the innermost doublet assigned to the terminal methyl is resolvable into two signals with slightly different splitting. Two signals in the innermost pair of peaks are, moreover, apparent under close inspection of the powder pattern spectrum for  $t[{}^2\text{H}_{33}]18:1-18:0\text{PC}$  (Figure 5.5a) shown in Figure 5.5. The same difficulty does not appear to apply to  $c[{}^2\text{H}_{33}]18:1-18:0\text{PC}$  (Figure 5.4b and 5.5b). We are conducting experiments to determine the origin of the two signals from acyl chain migration, where 18:0- $t[{}^2\text{H}_{33}]18:1\text{PC}$  (with the position of the chains switched) as well as  $t[{}^2\text{H}_{33}]18:1-18:0\text{PC}$  is present as the prime candidate. This problem has been noted by others and can lead to a pair of doublets because the motion of chains at the *sn*-1 and -2 positions is not exactly equivalent (9).

Our future plans for TFA research include identifying whether interaction with cholesterol, a membrane lipid, that is intimately involved in the progression of heart disease (10) is modified by the incorporation of a TFA. Employing the previously synthesized deuterated analogs of lipids, we shall compare the effect of cholesterol on molecular organization in model membranes containing EA and OA.

## References

1. Soni, S. P., D. S. LoCascio, Y. Liu, J. A. Williams, R. Bittman, W. Stillwell, and S. R. Wassall. 2008. Docosahexaenoic acid enhances segregation of lipids between : 2H-NMR study. *Biophys J* 95:203-214.
2. Shaikh, S. R., A. C. Dumaul, A. Castillo, D. LoCascio, R. A. Siddiqui, W. Stillwell, and S. R. Wassall. 2004. Oleic and docosahexaenoic acid differentially phase separate from lipid raft molecules: a comparative NMR, DSC, AFM, and detergent extraction study. *Biophys J* 87:1752-1766.
3. Wassall, S. R., and W. Stillwell. 2009. Polyunsaturated fatty acid-cholesterol interactions: domain formation in membranes. *Biochim Biophys Acta* 1788:24-32.
4. Wassall, S. R., and W. Stillwell. 2008. Docosahexaenoic acid domains: the ultimate non-raft membrane domain. *Chem Phys Lipids*.
5. Diaz, O., A. Berquand, M. Dubois, S. Di Agostino, C. Sette, S. Bourgoin, M. Lagarde, G. Nemoz, and A. F. Prigent. 2002. The mechanism of docosahexaenoic acid-induced phospholipase D activation in human lymphocytes involves exclusion of the enzyme from lipid rafts. *J Bio Chem* 277:39368-39378.
6. Veatch, S. L., I. V. Polozov, K. Gawrisch, and S. L. Keller. 2004. Liquid domains in vesicles investigated by NMR and fluorescence microscopy. *Biophys J* 86:2910-2922.
7. Soni, S. P., J. A. Ward, S. E. Sen, S. E. Feller, and S. R. Wassall. 2009. Effect of trans unsaturation on molecular organization in a phospholipid membrane. *Biochemistry* 48:11097-11107.

8. Huang, C., and S. Li. 1999. Calorimetric and molecular mechanics studies of the thermotropic phase behavior of membrane phospholipids. *Biochim Biophys Acta* 1422:273-307.
9. Lafleur, M., M. Bloom, E. F. Eikenberry, S. M. Gruner, Y. Han, and P. R. Cullis. 1996. Correlation between lipid plane curvature and lipid chain order. *Biophys J* 70:2747-2757.
10. Small, D. M. 1988. George Lyman Duff memorial lecture. Progression and regression of atherosclerotic lesions. Insights from lipid physical biochemistry. *Arteriosclerosis* 8:103-129.

Table 5.1: Average order parameter  $\bar{S}_{CD}$  for *t*18:1-18:0PC and 18:1-18:0PC calculated from  $^2\text{H}$  NMR and MD simulation data.

Lipids	<i>sn</i> -1 chain		<i>sn</i> -2 chain	
	$^2\text{H}$ NMR	MD	$^2\text{H}$ NMR	MD
<i>t</i> 18:1-18:0PC	0.111	0.102	0.135	0.148
<i>c</i> 18:1-18:0PC	0.097	0.095	0.128	0.146

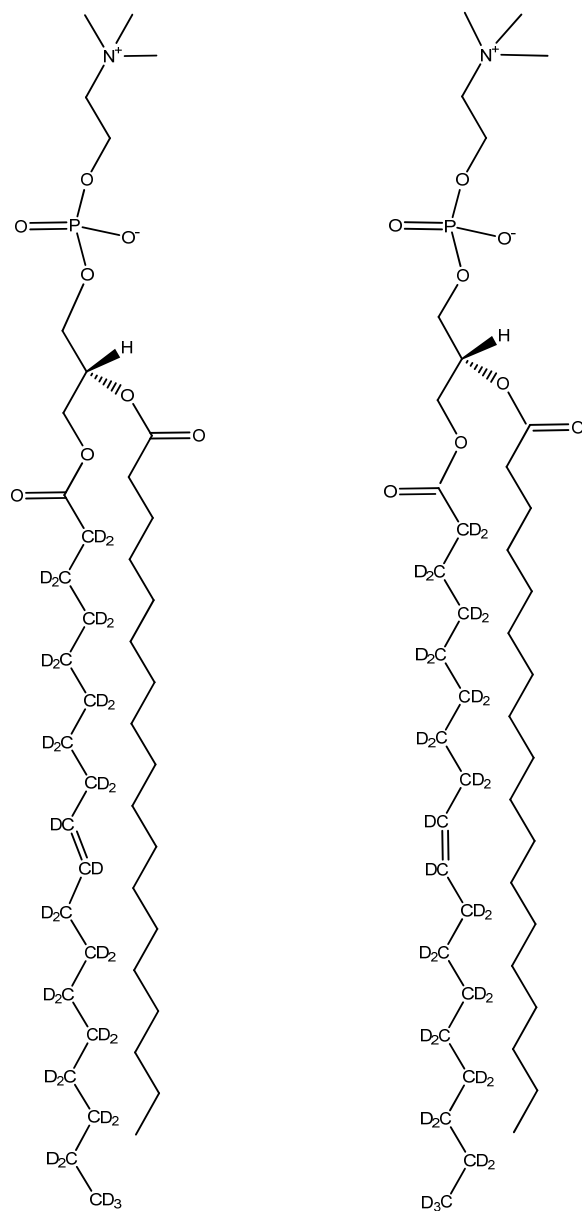
a)  $t[{}^2\text{H}_{33}]18:1-18:0\text{PC}$ b)  $c[{}^2\text{H}_{33}]18:1-18:0\text{PC}$ 

Figure 5.1: Molecular Structure of  $t[{}^2\text{H}_{33}]18:1-18:0\text{PC}$  and  $c[{}^2\text{H}_{33}]18:1-18:0\text{PC}$  with the perdeuterated unsaturated *sn*-1 chain.

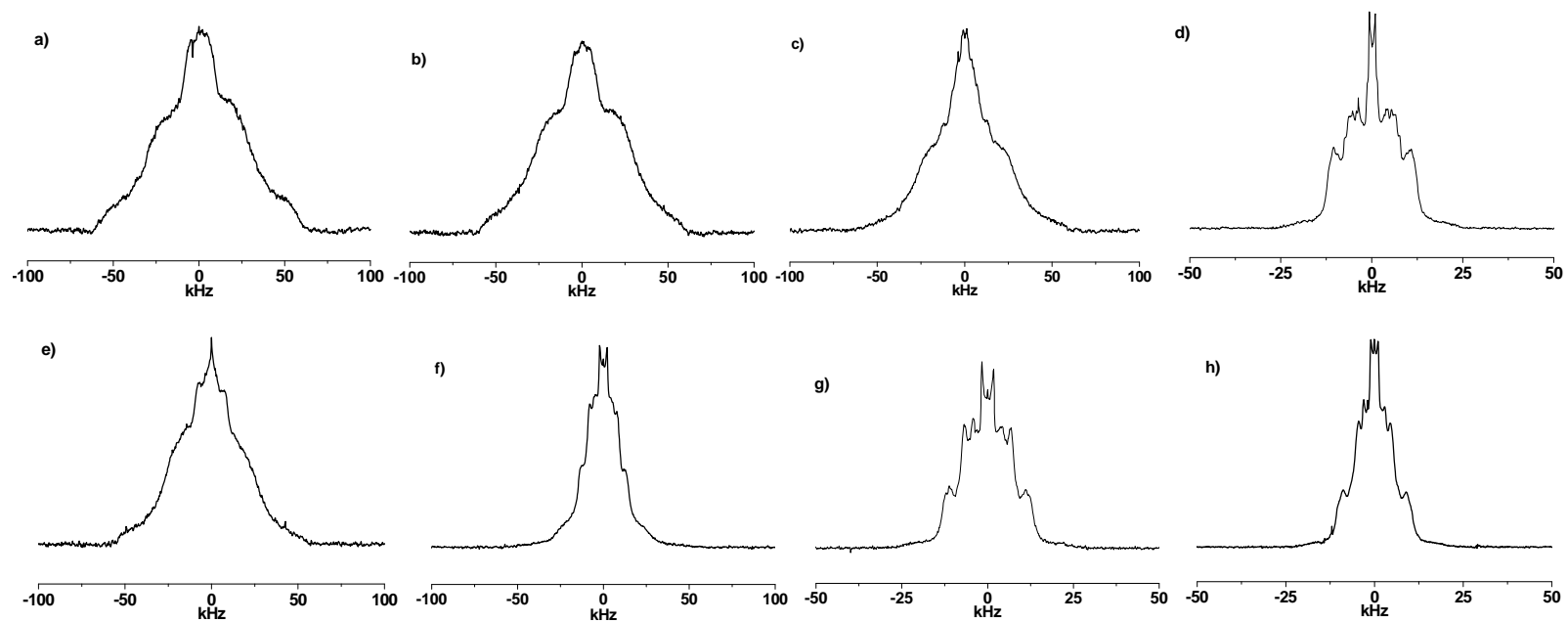


Figure 5.2:  $^2\text{H}$  NMR spectra for 50 wt% aqueous dispersions in 50 mM Tris (pH 7.5) of (a-d)  $t[^2\text{H}_{33}]18:1-18:0\text{PC}$  and (e-h)  $c[^2\text{H}_{33}]18:1-18:0\text{PC}$ . The spectra were recorded at (a and e)  $-5\text{ }^\circ\text{C}$ , (b and f)  $5\text{ }^\circ\text{C}$ , (c and g)  $20\text{ }^\circ\text{C}$  and (d and h)  $45\text{ }^\circ\text{C}$ .

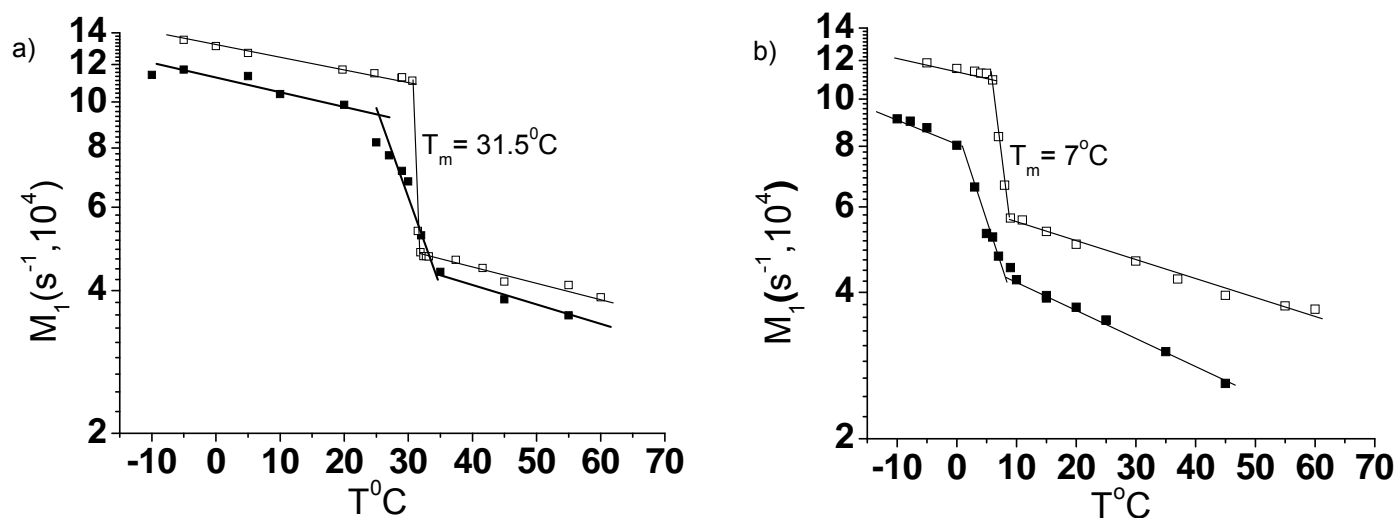


Figure 5.3: Variation of the first moment ( $M_1$ ) as a function of temperature for a)  $t[{}^2\text{H}_{33}]18:1-18:0\text{PC}$  (■) and  $t18:1-{}^2\text{H}_{35}]18:0\text{PC}$  (□) b)  $c[{}^2\text{H}_{33}]18:1-18:0\text{PC}$  (■) and  $c18:1-{}^2\text{H}_{35}]18:0\text{PC}$  (□).  $M_1$  is plotted logarithmically for clarity. The value given is for the temperature of the chain melting transition.  $T_m$  is the midpoint of the sharp drop in moment measure for the  ${}^2\text{H}_{35}]18:0$  *sn*-2 chain.

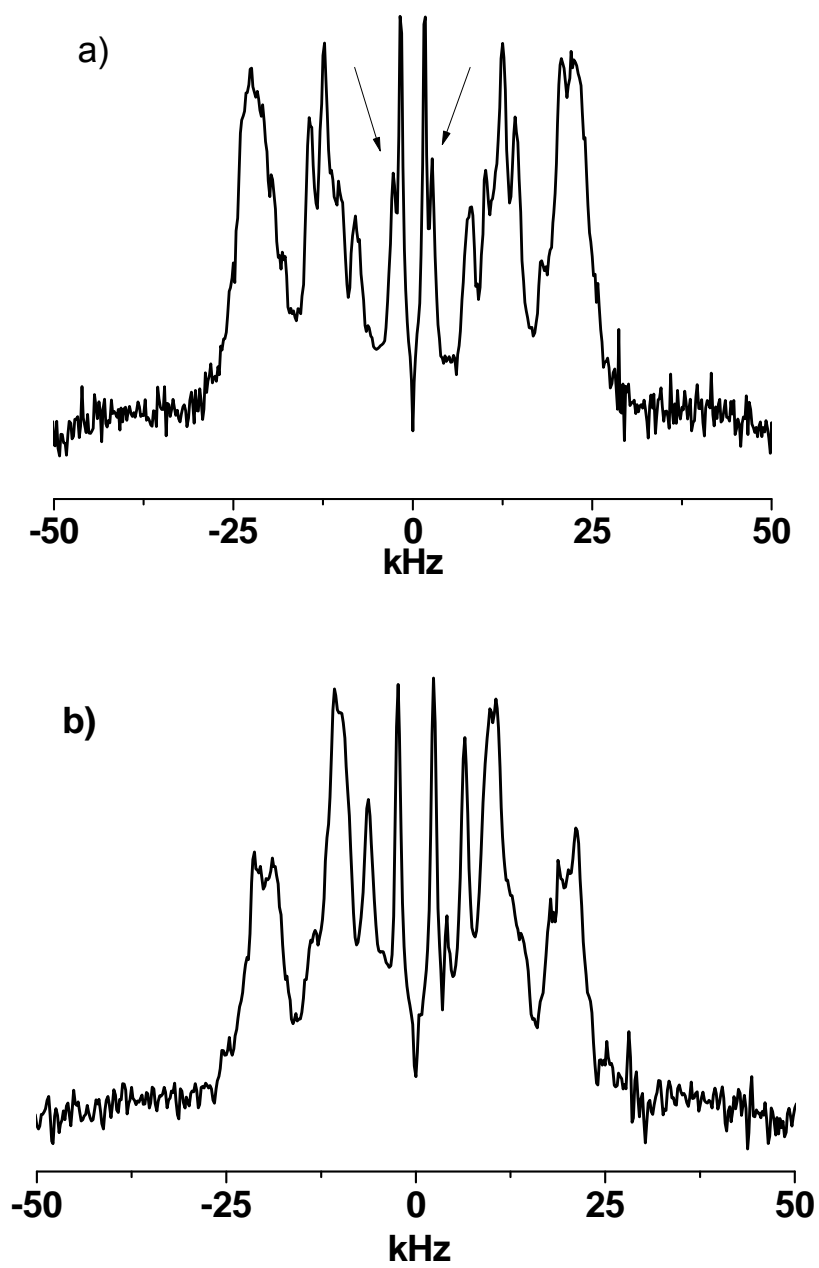


Figure 5.4: FFT depaked spectra derived from the powder pattern spectra at 45 °C b)  $t[{}^2\text{H}_{33}]18:1-18:0\text{PC}$  and b)  $c[{}^2\text{H}_{33}]18:1-18:0\text{PC}$ .



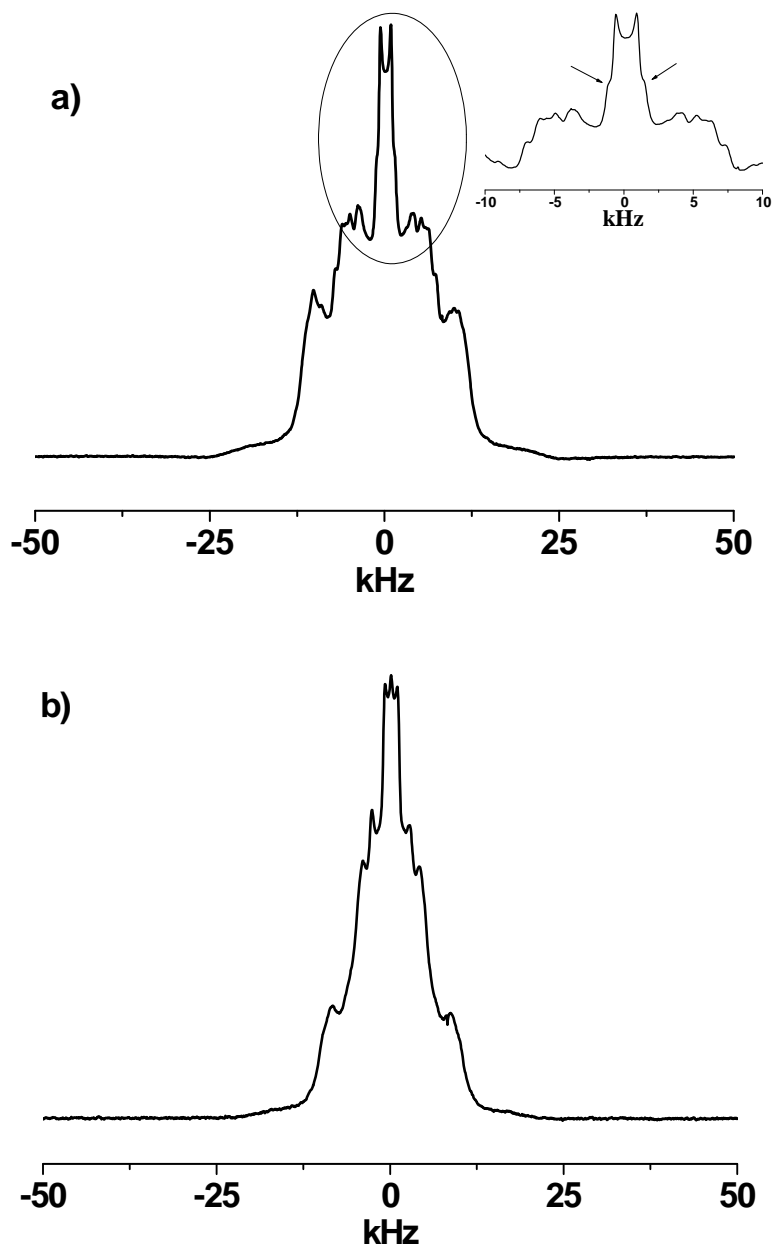


Figure 5.5:  $^2\text{H}$  NMR spectra at  $45\text{ }^\circ\text{C}$  for a)  $t[{}^2\text{H}_{33}]18:1-18:0\text{PC}$  and b)  $c[{}^2\text{H}_{33}]18:1-18:0\text{PC}$

## APPENDICES

Appendix A: Synthesis of per-deuterated saturated chain of phospholipids (1)

1. In a round bottom flask (r.b) add dicyclohexylcarbodiimide (DCC, 0.8mmol) and deuterated stearic acid (0.4mmol) and dissolve in 5mL of freshly distilled CHCl<sub>3</sub>.
2. Stir the reaction with a stirrer-bar in an argon atmosphere at room temperature for 15mins.
3. Add 1-acyl-2-hydroxy-*sn*-glycero-3-phosphocholine (0.2mmol) in the presence of *N,N*-dimethylamniopyridine (DMAP, 0.8mmol).
4. Check the progress of the reaction using TLC every 24 hrs using solvent CHCl<sub>3</sub>/MeOH/H<sub>2</sub>O (58:40:4).
5. Stir the mixture in an argon atmosphere for 72hrs.
6. Residue was separated into products and reactants using flash silica-gel chromatography in CHCl<sub>3</sub>/MeOH/H<sub>2</sub>O (58:40:4) solvent system.
7. 1-Acyl-2-stearoyl-d<sub>35</sub>-*sn*-glycero-3-phosphocholine containing fractions collected and rotary evaporated to give a final yield of 80%.
8. TLC: CHCl<sub>3</sub>/MeOH/H<sub>2</sub>O (58:40:4), R<sub>f</sub> = 0.4.
9. 1-Acyl-2-stearoyl-d<sub>35</sub>-*sn*-glycero-3-phosphocholine was confirmed using <sup>1</sup>H NMR and further purified using HPLC ( High performance liquid chromatography) with a reverse-phase silica C18 column (methanol solvent system).
10. Molecular mass (825.36 for 1-elaidoyl-2-stearoyl-d<sub>35</sub>-*sn*-glycero-3-phosphocholine and 823.34 for 1-oleoyl-2-stearoyl-d<sub>35</sub>-*sn*-glycero-3-phosphocholine) were confirmed using LC-mass spectrometry.

## Reference

1. Sun, M., Y. Deng, E. Batyreva, W. Sha, and R. G. Salomon. 2002. Novel Bioactive Phospholipids: Practical Total Syntheses of Products from the Oxidation of Arachidonic and Linoleic Esters of 2-Lysophosphatidylcholine. *J Org Chem* 67:3575-3584.

Appendix B: Synthesis of perdeuterated unsaturated chain of phospholipid(1)

B.1 Oleoyl Chloride-d<sub>33</sub>

1. In a round bottom flask (r.b) stir a solution of oleic acid-d<sub>34</sub> (0.3164mmol, minimum 98 atom% D) in 2.0mL of benzene.
2. Add oxalyl chloride (1.582mmol) dropwise, with evolution of gas.
3. Stir the mixture for 1hr at room temperature.
4. Rotary evaporate to yield oleoyl chloride as clear oil (100% yield).

B.2 1-Oleoyl-d<sub>33</sub>-2-hydroxy-*sn*-glycero-3-phosphocholine (Oleoyl lyso PC, 18:1LPC)

1. In a r.b, add R-2-3-dihydroxypropyl 2-(trimethylammonio) ethyl phosphate (0.2640mmol), (GPC- not cadmium chloride adduct) and dibutyltin oxide (0.2640mmol).
2. Dissolve in 3.0mL of isopropanol and reflux for an hour.
3. Cool to room temperature and then add trimethylamine (0.03168mmol) and stir for 5mins.
4. Oleoyl chloride-d<sub>33</sub> (0.3165mmol) is then added dropwise in 0.5mL of isopropanol and stirred for 30mins.
5. 10mL of heptane is added and the mixture is filtered.
6. The filtrate is then dried to a white solid in a rotary evaporator.
7. The white solid is dissolved in 20mL of methanol and extracted with heptane (2 x 25mL)

8. Methanol is evaporated to yield Oleoyl lyso PC (85% yield) as a translucent solid.

### B.3 Purification test of Oleoyl lyso PC

1. TLC: 58:40:4 in a solvent solution of CHCl<sub>3</sub>/MeOH/H<sub>2</sub>O for lyso PC, R<sub>f</sub> = 0.11.
2. TLC: 20% ethyl acetate (EtOAc) in hexane for Oleic acid, R<sub>f</sub> = 0.60.
3. <sup>1</sup>H-NMR (CDCl<sub>3</sub>, 500 Mhz) δ 4.335 (1H, CH), 4.077 (2H, CH<sub>2</sub>), 4.125 (1H, CH), 3.935 (2H, CH<sub>2</sub>), 3.668 (2H, CH<sub>2</sub>), 3.344 (9H, CH<sub>3</sub>)

### B.4 Stearic anhydride

1. In an r.b, stearic acid (7.030mmol) and dicyclohexylcarbodiimide (DCC, 3.515mmol) is combined in 20mL of CCl<sub>4</sub> (Carbontetrachloride) and stir for 6hrs.
2. Diethyl ether (20mL) is added to mixture and stirred for 5mins.
3. The mixture is then filtered and dried with MgSO<sub>4</sub> (magnesium sulfate) and evaporated to a white solid.
4. <sup>1</sup>H NMR (CDCl<sub>3</sub>, 500 Mhz) δ 2.456 (4H, CH<sub>2</sub>), 1.670 (4H, CH<sub>2</sub>), 1.268 (56H, CH<sub>2</sub>), 0.895 (6H, CH<sub>3</sub>).

### B.5 1-Oleoyl-d<sub>33</sub>-2-stearoyl-*sn*-glycero-3-phosphocholine (OSPC-d<sub>33</sub>)

1. In a r.b add Oleoyl Lyso PC-d<sub>33</sub> (0.2190mmol) in 13.0mL CHCl<sub>3</sub>, stearic anhydride (2.190mmol) and 4-dimethylaminopyridine (DMAP, 0.2628mmol) and stir continuously at room temperature for 48hrs.

2. Rotary evaporated the mixture and resultant solid is separated by flash silica-gel chromatography, which yields a white solid (27% yield) of OSPC-d<sub>33</sub>, using CHCl<sub>3</sub>/MeOH/H<sub>2</sub>O (58:40:2) solvent system.
3. TLC: using CHCl<sub>3</sub>/MeOH/H<sub>2</sub>O (58:40:2) solvent system, R<sub>f</sub> = 0.23.
4. <sup>1</sup>H NMR (CDCl<sub>3</sub>, 500 Mhz) δ 5.209 (1H, CH), 4.385 (1H, CH), 4.264 (2H, CH<sub>2</sub>), 4.125 (1H, CH), 3.935 (3H, CH<sub>2</sub>), 3.668 (2H, CH<sub>2</sub>), 3.250 (9H, CH<sub>3</sub>), 2.318 (2H, CH<sub>2</sub>), 1.585 (2H, CH<sub>2</sub>), 1.253 (28H, CH<sub>2</sub>), 0.881 (3H, CH<sub>3</sub>).

#### B.6 Elaidic Acid-d<sub>34</sub>

1. Using a Pen Ray photo-lamp, oleic acid-d<sub>34</sub> is isomerized to elaidic acid-d<sub>34</sub> encased in Pyrex test-tube.
2. The apparatus is submerged in a larger test tube containing oleic acid-d<sub>34</sub> (0.3164mmol), diphenyl disulfide (0.037mmol) and 10mL cyclohexane, argon gas is introduced for 15mins.
3. The reaction is stirred for 3 hrs at 0<sup>0</sup>C, protected from ambient light.
4. Solvent is then evaporated to yellow solid and purified using flash silica chromatography using EtOAc-Hexane to elute elaidic acid (81% yield) as light yellow solid.
5. TLC: (80:20) EtOAc-Hexane, R<sub>f</sub>= 0.55 when stained with potassium permanganate.
6. B.5 method was use to synthesise 1-elaidoyl-d<sub>33</sub>-2-stearoyl-*sn*-glycero-3-phosphocholine, (ESPC-d<sub>33</sub>) gave a 43% yield.

## Reference

1. Wang, P., D. H. Blank, and T. A. Spencer. 2004. Synthesis of Benzophenone-Containing Analogues of Phosphatidylcholine. *J Org Chem* 69:2693-2702.



VITA

## VITA

Smita Soni

**Education:**

**PhD:** Physics, 2010, Purdue University, Indianapolis, Indiana. (3.44, Cumulative)

**MS:** Physics, 2003, Purdue University, Indianapolis, Indiana. (3.30, Cumulative).

**BS:** Physics, **with honors** in 2002, Butler University, Indianapolis, Indiana. (3.40, Cumulative, 3.70 Major).

High School: Physics, 12<sup>th</sup> grade, freshman and sophomore year 1996-99 Bhavan's College (First Class), 11<sup>th</sup> grade, Wilson College (First Class), 1995-96. Kindergarten through 10<sup>th</sup> grade, Childers Academy (Distinction), Mumbai, India.

**Awards:**

**SOSGSC & GSO Travel Fellowship:** Representing IUPUI at a Biophysical Society meeting in Boston, MA in March 2009.

**NWAPS Student Travel Award:** 11th Annual Meeting of the Northwest Section of the APS (NWAPS) Vancouver, Canada (2009).

**American Association of Physics Teachers presented Teaching Assistantship award:** IUPUI (2009).

**Outstanding Physics graduate student award:** IUPUI (2008)

**Graduate Student Council Travel Award:** At Purdue University for presenting a poster at a Biophysics society meeting in Long Beach, California in April 2008.

**American Chemical Society Travel fund Award:** For representing IUPUI at the Biophysics society meeting in Salt Lake, Utah. February (2006) and Baltimore, Maryland in March 2007.

**Graduate Student Organization Travel Award:** At Purdue University for presenting a poster at a Biophysics Society meeting in Baltimore, Maryland in April 2004.

**International Student Scholarship award:** At Butler University as an undergraduate for \$4000/per yr, for the duration of 1999-2002.

**Research:**

My research work is focused on the application of solid state  $^2\text{H}$  NMR techniques to the study of molecular organization within membranes. The result of this technique is usually complemented by either DSC and/or MD simulations. The objective is to develop relationships between the structure of biologically important molecules and their physiological function and how in turn it effects on membrane properties.

M.S.Thesis:

The effect of acyl chain unsaturation on phospholipid bilayers: Studies by Solid State  $^2\text{H}$  NMR and MD Simulations

Ph.D Thesis:

The effect of acyl chain unsaturation on phospholipid bilayer

**Published Paper:**

**Smita P. Soni**, Jennifer Runyan, Garrison Birch, Jesse A. Ward, Stephanie E. Sen, Scott E. Feller and Stephen R. Wassall. The effect of *trans* unsaturation on molecular organization in a phospholipid membrane. Accepted- Journal of Biochemistry 2009 Nov 24; 48(46):11097-107.

Saame Raza Shaikh, Daniel LoCascio, **Smita Soni**, Stephen R. Wassall and William Stillwell. Oleic and Docosahexaenoic Acid Containing Phosphatidylethanolamine Differentially Phase Separate from Sphingomyelin. Biochim Biophys Acta. 2009 Nov;1788(11):2421-6.

**Smita P. Soni**, Daniel S. LoCascio, Yidong Liu, Justin A Williams, Robert Bittman, William Stillwell and Stephen R. Wassall. Docosahexaenoic Acid Enhances Segregation of Lipids between Raft and Non-Raft Domains:  $^2\text{H}$  NMR Study.

Biophys J. 2008 Jul;95(1):203-14.

Saame Raza Shaikh, Vadim Cherezov, Martin Caffrey, **Smita P. Soni**, Daniel LoCascio, William Stillwell and Stephen R. Wassall. (2006). Molecular Organization of Cholesterol in Unsaturated Phosphatidylethanolamines: X-ray Diffraction and Solid State  $^2\text{H}$  NMR Reveal Differences with Phosphatidylcholines.

J Am Chem Soc. 2006 Apr 26;128(16):5375-83.

**Platform Presentation:**

**“The effect of *trans* unsaturation on molecular organization in phospholipid bilayers”.** Indiana University, School of Medicine, South Bend, Indiana in October (2009).

**“The effect of acyl chain unsaturation on phospholipid bilayer”.**

Elucida Research-Harvard Medical School, Beverly, Massachusetts in July (2009)

**“The effect of acyl chain unsaturation on phospholipid bilayer”.**

Department of Physics, IUPUI, Indianapolis, Indiana in February (2009)

**“The effect of Trans unsaturation on molecular organization in a phospholipid molecule”.**

124<sup>th</sup> Indiana Academy of Science, Evansville, Indiana in October (2008)

(Nominated for best talk award)

**“The effect of *trans* unsaturation on molecular organization in a phospholipid membrane.”**

123<sup>rd</sup> Indiana Academy of Science, Indianapolis, Indiana in October (2007)

**Poster Presentation:**

**Smita P. Soni**, Jennifer Runyan, Garrison Birch, Jesse A. Ward, Stephanie E. Sen, Scott E. Feller and Stephen R. Wassall, Departments of Physics and Chemistry, IUPUI, Indianapolis, IN, and Department of Chemistry, Wabash College, Crawfordsville, IN.

The effect of Trans unsaturation on molecular organization in a phospholipid membrane.

7<sup>th</sup> European Biophysics Congress, Genoa, Italy, July (2009).

**Smita P. Soni**, Jennifer Runyan, Garrison Birch, Jesse A. Ward, Stephanie E. Sen, Scott E. Feller and Stephen R. Wassall, Departments of Physics and Chemistry, IUPUI, Indianapolis, IN, and Department of Chemistry, Wabash College, Crawfordsville, IN. The effect of Trans unsaturation on molecular organization in a phospholipid membrane. 11th Annual Meeting of the Northwest Section of the APS, Vancouver, BC, Canada, May (2009).

**Smita P. Soni**, Jennifer Runyan, Garrison Birch, Jesse A. Ward, Stephanie E. Sen, Scott E. Feller and Stephen R. Wassall, Departments of Physics and Chemistry, IUPUI, Indianapolis, IN, and Department of Chemistry, Wabash College, Crawfordsville, IN. The effect of Trans unsaturation on molecular organization in a phospholipid membrane. Biophysical Society 53<sup>rd</sup> Annual Conference, Boston, MA in February 2009.

**Smita P. Soni**, Jennifer Runyan, Garrison Birch, Jesse A. Ward, Stephanie E. Sen, Scott E. Feller and Stephen R. Wassall. The effect of Trans unsaturation on molecular organization in a phospholipid molecule. Frontiers in Biological Membranes, symposium by Purdue University and Applied Membrane Sciences (PUBMAS), West Lafayette, Indiana in October 2008.

**Smita P. Soni**, Jennifer Runyan, Garrison Birch, Jesse A. Ward, Stephanie E. Sen, Scott E. Feller and Stephen R. Wassall. Molecular organization in a phospholipid membrane containing *trans* unsaturation. Biophysical Society 52<sup>nd</sup> Annual Conference, Long Beach, California in February 2008.

**Smita P. Soni**, Jennifer Runyan, Jesse A. Ward, Stephanie E. Sen, Scott E. Feller and Stephen R. Wassall. The effect of *trans* unsaturation on molecular organization in a phospholipid membrane.

8<sup>th</sup> Annual Indiana Local Section American Chemical Society Poster session, Eli Lilly and Company, Indianapolis, Indiana in October 2007.

**Smita P. Soni**, Jennifer Runyan , Jesse A. Ward, Stephanie E. Sen, Scott E. Feller and Stephen R. Wassall. *Trans* vs. *Cis* Unsaturation: The Effects on Molecular Organization in a Phospholipid Membrane Studied by Solid State <sup>2</sup>H NMR Spectroscopy and MD Simulations.

Biophysical Society, 51<sup>st</sup> Annual Conference, Baltimore, Maryland in March 2007.

**Smita P. Soni**, Daniel LoCascio, Yidong Liu, Robert Bittman, William Stillwell and Stephen R. Wassall. Solid State <sup>2</sup>H NMR of [<sup>2</sup>H<sub>31</sub>]Palmitoyl Sphingomyelin: II Molecular organization of lipid raft molecules in mixtures with polyunsaturated docosahexaenoic acid-containing phosphatidylethanolamine.

Biophysical Society, 50<sup>th</sup> Annual Conference, Salt Lake, Utah in February 2006.

**Smita P. Soni**, Daniel LoCascio, Yidong Liu, Robert Bittman, William Stillwell and Stephen R. Wassall. Solid state <sup>2</sup>H NMR of [<sup>2</sup>H<sub>31</sub>]Palmitoyl Sphingomyelin: I Molecular organization of lipid raft molecules in mixtures with monounsaturated oleic acid-containing phosphatidylethanolamine.

Biophysical Society, 50<sup>th</sup> Annual Conference, Salt Lake, Utah in February 2006.

**Smita P. Soni**, Daniel LoCascio, Saame Raza Shaikh, Yidong Liu, Robert Bittman, William Stillwell, Stephen R. Wassall. A Role for Docosahexaenoic acid (DHA) in lipid raft separation: A solid state <sup>2</sup>H NMR study of [<sup>2</sup>H<sub>31</sub>]Palmitoyl Sphingomyelin in Phosphatidylethanolamine / Cholesterol mixtures.

Biophysical Society, 49<sup>th</sup> Annual Conference, Long Beach, California in February 2005.

**Smita P. Soni**, Jesse D. Ward, Scott E. Feller and Stephen R. Wassall. Molecular Organization in a *Trans* Unsaturated Membrane.

Biophysical Society, 48<sup>th</sup> Annual Conference, Baltimore, Maryland in March 2004.

**Smita P. Soni**, Jesse D. Ward, Scott E. Feller and Stephen R. Wassall. Molecular Organization in a *Trans* Unsaturated Membrane.

American Chemical Society regional meeting, IUPUI, Indianapolis, Indiana in February 2004.

### **Teaching:**

**High School Summer research mentoring.** From tours of the solid state NMR labs to setting up projects and conducting experiments to reach the goals for the summer, the high school students are great way to brush up on the basics. 2006- present.

**Teaching assistantship at Purdue University, Indiana University.** Mechanics and Heat Electricity Optics (152, 251) and General Physics I and II (201, 202), Fall 2002-2005.

**Nominated for best TA award at Purdue University, Indiana in 2005.**

Organize labs for classes Elementary Physics (PH107, PH108) and Introduction to analytical physics (PH201, PH202), Butler University (2001-02).

### **Work Experience:**

Assisted Dr X. Han, PhD, at Butler University in his programming project in summer of 2001.



**Computer Skills:**

Proficient in MS-office, chem-draw and Origin. Familiar with C, C++ and Fortran.

**Services:**

**International Students Advisor:** Volunteered at the Office of International Affairs in advising students on their concerns and helping to understand the new culture and adjusting to the new environment (2006-2007).

**IUPUI Explore:** Volunteer work to promote the Department of Physics and helping with any queries of the students during the presentation (2005).

**Language:**

Fluent in English, Hindi, Gujarati and Marathi.

**Affiliations:**

Biophysical Society

American Association of Physics Teachers

American Physical Society

American Chemical Society

European Biophysics Congress

Physics Club at IUPUI

Indian Student Organization at IUPUI